

A Study of the  
Full Restricted Three Body Problem  
in the Context of Missions to Binary  
Asteroid Systems

Isabelle Jean

Doctor of Philosophy

Department of Mechanical Engineering

McGill University

Montreal, Quebec

April 2020

A thesis submitted to McGill University  
in partial fulfillment of the requirements of  
the degree of Doctor of Philosophy

©Isabelle Jean, 2020

## ACKNOWLEDGEMENTS

There are many people that made the writing of this thesis come true. First of all, I would like to thank my supervisor Professor Arun Misra for accepting me as a student and believing that I could make it to the point of writing and submitting this thesis. He gave me many opportunities to attend many major conferences and publish in peer reviewed journals. I would also want to thank my co-supervisor, Dr Alfred Ng from the Canadian Space Agency who introduced me to the circular restricted three body problem. He recommended me to Professor Misra and then the adventure began. Without his support to this journey, I would have never started, so not finished either.

Thank you to the students and former students of Professor Misra, Eleonora Botta, Flaviane Cristine Faria, Yu Shi, Angelo Stolfi, Shaziana Kaderali and Shrouiti Dutta who gave me support in many ways. This is not an easy journey and the support of colleagues helped me get through it. Thank you also to the other students in room MD459 for the great conversations and lunch breaks.

I could not complete this section without thanking my family. First, my husband Mathieu Beauregard who supported me from day one in this journey. My three sons, Étienne, Cédric and Rémi who are my inspiration. I wish you could all three of you find your own way to the stars and beyond.

This research was financially supported by the Natural Sciences and Engineering Research Council of Canada (NSERC), the Fonds Québécois de la Recherche

sur la Nature et les Technologies (FQRNT), the Les Vadasz Engineering Fellowship (McGill Engineering Doctoral Award) and the Hydro-Québec Doctoral Award (McGill Engineering Doctoral Award).

## PREFACE

The main contribution of this thesis is to develop a higher order gravitational potential model of the primary bodies of a binary asteroid system and use it to study various aspects of the full restricted three body problem (FRTBP). Various issues such as how the solution of the FRTBP is affected by the solar radiation pressure and by the rotational motion of the primary bodies as well as their non-circular motion around their barycenter, are examined.

Here is a summary of the contributions made in the thesis:

- Analytical expression for the gravitational potential based on a fourth-order Taylor series expansion.
- Equations of motion of the full two body problem and of the full restricted three body problem based on the above mentioned gravitational potential model.
- Design of spacecraft trajectories compatible with the solar radiation pressure (SRP) in the full circular restricted three body problem (FCRTBP).
- Detailed study of the influence of the solar radiation pressure acceleration model on the motion of a spacecraft in the FCRTBP.
- Design of spacecraft trajectories when the shape, rotational motion and non-circular orbital motion of the primary bodies are taken into account, which corresponds to the full restricted three body problem (FRTBP).

- Development of a Lyapunov stability theory-based controller to make it suitable for spacecraft reference trajectories with small discontinuities.
- Calculation of inertia integrals of the fourth order of an ellipsoid and of a polyhedron shape model.

Part of the work presented in this thesis has been published or submitted for publication in the following refereed journals:

1. Jean, I., Misra, A.K., Ng, A., Solar Radiation Pressure-Compatible Trajectories in the Vicinity of a Binary Asteroid, *Journal of Guidance, Control, and Dynamics*, 42 (2019) 1319-1329.
2. Jean, I., Ng, A., Misra, A.K., Impact of solar radiation pressure modelling on orbital dynamics in the vicinity of binary asteroids, *Acta Astronautica*, 165 (2019)167-183.
3. Jean, I., Ng, A., Misra, A.K., Controlled Spacecraft Trajectories in the Full Restricted Three Body Problem, *The Journal of Astronautical Sciences* (under review).

The work has also been presented in several conferences, such as the International Astronautical Congress, the AAS/AIAA Astrodynamics Specialists Conference, the AAS/AIAA Space Flight Mechanics Meeting, the International Space Conference of Pacific-basin Societies (ISCOPS), the Canadian Aeronautics and Space Institute (CASI) Astronautics Conference, the IAA Conference on Dynamics and Control of Space Systems and the Canadian Congress of Applied Mechanics.

The conceptual, computational, analytical and written work presented in this thesis were carried out by Isabelle Jean, with the input and support from her supervisors, Prof. Arun K. Misra and Dr Alfred Ng.

## ABSTRACT

Asteroid missions are now an important component of space exploration and binary asteroids comprise approximately 16% the Near-Earth Asteroids (NEA) population. This fact combined with the planned mission to binary asteroid 65803 Didymos has generated a lot of interest in the study of spacecraft dynamics in the vicinity of binary asteroids. The combination of the effect of the irregular shape and the rotational motion of the primary bodies of the binary asteroid system makes them not only non-linear, but also non-autonomous systems. External perturbations, such as the Solar Radiation Pressure (SRP) play an important role in the motion of a spacecraft in such an environment. The dynamics of a spacecraft in a binary environment with those characteristics is known as the Full Restricted Three Body Problem (FRTBP). This thesis studies different aspects of the FRTBP. First, it details the gravitational potential of a small irregular body and of a binary asteroid system. It is followed by the development of the equations of motion of the Full Two Body Problem (FTBP). Then, the study of the influence of the SRP on the trajectory of a spacecraft in this environment is done. Spacecraft trajectories design techniques taking the SRP acceleration into account are developed. Then, a study of the influence of the SRP acceleration modeling method on the trajectory of a spacecraft is conducted, showing that the attitude of the spacecraft and a detailed model of the SRP acceleration are required to conduct studies of the FCRTBP. The last part of this thesis is the investigation of the motion of a spacecraft when internal

perturbations to the FTBP are included, including the rotational motion of the primary bodies and their non-circular mutual motion. This part of the study develops a technique to design nominal spacecraft trajectories in the FRTBP using a fourth-order gravitational potential model of the two primary bodies. It then compares the control effort required when these reference trajectories are used with that required when reference trajectories built with simpler models are used.

## ABRÉGÉ

Les missions vers les astéroïdes sont maintenant une composante importante de l'exploration spatiale. Les astéroïdes binaires forment environ 16% de la population des astéroïdes proches de la Terre. Ce fait, combiné avec la mission prévue vers l'astéroïde binaire 65083 Didymos a généré beaucoup d'intérêt pour la dynamique des vaisseaux spatiaux opérés près d'astéroïdes binaires. La combinaison de l'effet de la forme irrégulière et de la rotation des corps primaires d'un astéroïde binaire en fait des systèmes non seulement non-linéaires, mais aussi non-autonomes. La pression de radiation solaire (PRS), une perturbation externe au système, joue un rôle important dans la trajectoire d'un vaisseau spatial dans cet environnement. La dynamique d'un vaisseau spatial opéré près d'un astéroïde binaire avec ces caractéristiques est connue sous le nom de problème complet restreint des trois corps (PCRTC). Cette thèse étudie différents aspects du PCRTC. En premier lieu, elle décrit le potentiel gravitationnel d'un petit corps ayant une forme irrégulière, ainsi que celui d'un astéroïde binaire, suivi du développement des équations du mouvement du problème complet des deux corps (PCDC). Ensuite, l'étude de l'influence de la PRS sur la trajectoire d'un vaisseau spatial dans cet environnement est effectuée. Tout d'abord, une technique servant à développer des trajectoires de vaisseaux spatiaux intégrant la PRS est expliquée et démontrée. Par la suite, une étude de l'influence du choix du modèle de l'accélération due à la PRS sur la trajectoire d'un vaisseau spatial est conduite. Cette partie de l'étude a démontré qu'un modèle détaillé de l'accélération due à la PRS est requis pour conduire des études sur le PCRTC. La dernière partie de cette

thèse considère la trajectoire d'un vaisseau spatial lorsque des perturbations interne au PCDC, incluant la rotation des corps primaires et leur orbite non-circulaire autour du centre de masse du système. Cette partie de l'étude utilise une technique pour concevoir des trajectoires de référence dans le PCRTC utilisant un modèle du potentiel gravitationnel des deux corps primaires d'ordre 4. Finalement, une comparaison de l'effort de contrôle nécessaire pour garder un vaisseau spatial sur ces trajectoires et de celui requis lorsque la trajectoire de référence est conçue en utilisant un modèle plus simple est effectuée.

## NOMENCLATURE

- $\mathbf{A}$  = 6x6 matrix of the linearized model of the dynamics of a spacecraft in a binary asteroid system
- $A, B, C$  = semi-axes of the ellipsoids representing the primary bodies in sections 3.1.1 and 4.0.4
- $a$  = semi-major axis of the mutual orbit of the primary bodies of a binary asteroid system
- $a_{SRP}$  = acceleration due to the solar radiation pressure
- $b$  = Sun-Earth distance
- $B$  = mass to area ratio of the spacecraft
- $c$  = speed of light
- $C$  = Jacobi constant for a specific orbit
- $\mathbf{C}_{AB}$  = direction cosine matrix transformation matrix relating the components of a vector expressed in reference frame A to those of the same vector expressed in reference frame B.
- $D$  = distance between a spacecraft and the Sun
- $D_0$  = distance between the Earth and the Sun
- $\mathbf{D}_i$  = arbitrary constant positive definite symmetric matrices used in the calculation of the controller gains
- $dm$  = mass element of a single asteroid

- $dm_i$  = mass element of primary body  $i$  of a binary asteroid
- $d\mathbf{S}$  = vector in the direction normal to the surface  $S$  of the facet of a tetrahedron in a polyhedron shape model
- $dU_{grav}$  = gravitational potential of a mass element
- $\mathbf{D}, \mathbf{E}, \mathbf{F}$  = vertices composing a facet of a tetrahedron in a polyhedron shape model (Appendix B)
- $e$  = eccentricity of the mutual orbit of the primary bodies of a binary asteroid system
- $\mathbf{e}$  = error vector between the state of a reference trajectory and the state of the actual trajectory of a spacecraft
- $\mathbf{e}', \mathbf{e}''$  = first and second differentiation with respect to non-dimensionalized time of the error vector between the state of a reference trajectory and the state of the actual trajectory of a spacecraft
- $\mathbf{F}(t)$  = matrix containing the second derivatives of the gravitational potential with respect to the  $x, y, z$  direction of the synodic reference frame
- $\mathbf{F}(\mathbf{X})$  = constraint vector of the multiple shooting correction algorithm
- $F_{grav_j}$  = gravitational force in the direction of the  $j$  axis of the body fixed reference frame
- $G$  = universal gravitational constant
- $H$  = Hamiltonian of a system
- $h$  = non-dimensionalized angular momentum of a binary asteroid system about its barycenter
- $\mathbf{G}, \mathbf{H}$  = edges of a facet of a tetrahedron in a polyhedron shape model

(Appendix B)

- $g$   $h$  = non-dimensionalized coordinates of edges  $\mathbf{G}$  and  $\mathbf{H}$  (Appendix B)
- $\mathbf{I}$  = inertia matrix of a small body (Appendix B)
- $\mathbf{I}_{n \times n}$  = identity matrix of dimension  $n \times n$
- $I_{jji}$  = second-order principal moment of inertia of primary body  $i$
- $\mathbf{J}(\mathbf{X})$  = matrix of the Jacobian calculated from the state and constraint  
vectors of the multiple shooting correction algorithm
- $J_{jji}$  = second-order inertia integral of primary body  $i$
- $J_{jjji}$  = fourth-order inertia integral of primary body  $i$
- $J_{jjkk_i}$  = coupled fourth-order inertia integral of primary body  $i$
- $l$  = characteristic length of the mutual orbit of the primary bodies of a  
binary asteroid system
- $L$  = Sun luminosity
- $M$  = total mass of a single asteroid or a binary asteroid system
- $M_i$  = mass of primary body  $i$
- $N_i$  = number of tetrahedrons composing the layered mascons model of  
primary body  $i$
- $n$  = mean angular velocity of the mutual orbit of a binary asteroid system
- $\hat{\mathbf{n}}_i$  = unit vector of the direction normal to reflecting surface  $i$  of the  
spacecraft
- $P$  = period of a binary asteroid system or of a periodic trajectory
- $P_{SRP}$  = measure of the pressure exerted by the solar radiation on a spacecraft
- $P_0$  = solar flux at 1 Astronomical Unit(AU)

- $\mathbf{P}(t)$  = time-varying matrix used in the calculation of the control input of the Lyapunov controller
- $\mathbf{Q}$  = constant positive definite symmetric matrix used in the calculation of the control input of the Lyapunov controller
- $q$  = generalized coordinates used in the derivation of the equations of motion in the context of the FTBP
- $R$  = distance between the center of mass of a single asteroid and a spacecraft (sections 2.1 and 2.2)
- $R$  = distance between the centers of mass of the primary bodies of a binary asteroid system (section 3.1)
- $\mathbf{R}$  = position vector of the center of mass of of body 2 with respect to the center of mass of body 1 (section 3.3.2)
- $\mathbf{R}$  = position vector of the center of mass of a polyhedron shape model
- $\mathbf{R}_i$  = position vector of the center of mass of the spacecraft relative to the barycenter of a binary asteroid system
- $R_i$  = distance between the center of mass of the spacecraft relative to the center of mass of primary body  $i$
- $\mathbf{r}_i$  = non-dimensionalized position vector of the center of mass of the spacecraft relative to the center of mass of primary body  $i$
- $\mathbf{r}$  = vector going from the position of the origin of a polyhedron shape model to the center of the facet of a tetrahedron in a polyhedron shape model
- $r$  = non-dimensionalized distance between the centers of mass of the

		primary bodies of a binary asteroid system (section 3.4)
$r_0$	=	characteristic asteroid size of a binary asteroid system
$\mathbf{r}_0$	=	position vector of the spacecraft on a nominal trajectory with respect to the barycenter of a binary asteroid system
$r_s$	=	specular reflectivity parameter of the spacecraft
$r_d$	=	diffuse reflectivity parameter of the spacecraft
$\Delta \mathbf{R}$	=	position vector of the centroid of a tetrahedron of a polyhedron shape model
$\Delta S$	=	surface of a facet of a polyhedron shape model
$T$	=	kinetic energy of a single asteroid or binary asteroid system
$T_0$	=	zeroth-order term of the kinetic energy
$T_2$	=	second-order term of the kinetic energy
$U$	=	effective potential a binary asteroid system
$U_{grav}$	=	gravitational potential a single asteroid or a binary asteroid system
$\mathbf{u}$	=	control input vector
$\hat{\mathbf{u}}$	=	unit vector of the direction going from the Sun to the barycenter of a binary asteroid system
$u$	=	reciprocal of the non-dimensionalized distance between the primary bodies centers of mass
$u_c$	=	reciprocal of the non-dimensionalized distance between the primary bodies centers of mass in the case of circular motion of the primary bodies of a binary asteroid system
$\hat{\mathbf{u}}_R$	=	unit vector along the position vector $\mathbf{R}$ of point P relative to the

- center of mass of the asteroid
- $\hat{u}_{R_j}$  =  $j$  component of the unit vector along the position vector  $\mathbf{R}$  of point P relative to the center of mass of the asteroid expressed in the asteroid body fixed reference frame
- $\Delta V$  = volume of a tetrahedron of a polyhedron shape model
- $V$  = gravitational potential energy of a binary asteroid system (chapters 2 and 3)
- $V$  = Lyapunov function used in the controller algorithm (chapter 6)
- $\mathbf{X}$  = state vector of the multiple shooting correction algorithm
- $X, Y, Z$  = dimensional  $X$ ,  $Y$  and  $Z$  components of the position vector of a spacecraft with respect to the center of mass of an asteroid body expressed in the body fixed reference frame
- $x, y, z$  = non-dimensionalized  $x$ ,  $y$  and  $z$  components of the position vector of a spacecraft with respect to the center of mass of a single asteroid body expressed in the body fixed reference frame
- $x, y, z$  = components of position vector going from the position of the origin of a polyhedron shape model to the center of the facet of a tetrahedron in a polyhedron shape model (Appendix B)
- $x_i, y_i, z_i$  = non-dimensionalized  $x$ ,  $y$  and  $z$  components of the position vector of a spacecraft with respect to the center of mass of primary body  $i$
- $\alpha_i$  = angle between the  $X_i$  axis of the body fixed  $i$  reference frame and the  $X_S$  axis of the synodic reference frame
- $\gamma$  = flight path angle, measured with respect to the  $X_S$  axis of the synodic

- reference frame
- $\delta$  = position vector of a mass element of a single asteroid with respect to its center of mass
- $\delta_j$  =  $j$  component of the position vector of a mass element of a single asteroid with respect to its center of mass expressed in the body fixed reference frame (section 2.1)
- $\delta_i$  = position vector of a mass element of primary body  $i$  relative to its center of mass
- $\epsilon$  = square of the ratio between the characteristic distance  $l$  and the characteristic primary body size  $r_0$  of a binary asteroid system
- $\theta$  = angle of rotation of the synodic reference frame with respect to the inertial reference frame
- $\lambda$  = angle between the plate reference frame and the inertial reference frame
- $\mu$  = mass parameter of a binary asteroid system
- $\rho$  = density of a small irregular body (Appendix B)
- $\rho_{\alpha\alpha i}$  = second-order non-dimensionalized principal moment of inertia of primary body  $i$
- $\rho_{\alpha\alpha\alpha\alpha i}$  = fourth-order non-dimensionalized non-coupled inertia integral of primary body  $i$
- $\rho_{\alpha\alpha\beta\beta i}$  = coupled fourth-order non-dimensionalized inertia integral of primary body  $i$
- $\tau$  = non-dimensionalized time
- $\Phi$  = state transition matrix

- $\psi$  = amplitude of the libration motion of body 2
- $\Omega$  = dimensional angular velocity of a binary asteroid system
- $\omega$  = non-dimensionalized angular velocity of a binary asteroid system
- $\omega'$  = non-dimensionalized angular acceleration of a binary asteroid system
- $\omega_0$  = natural frequency of libration normalized by the mean motion of the mutual orbit of the primary bodies of a binary asteroid system
- $\omega_c$  = non-dimensionalized rotation rate in the FTBP in the case of circular motion of the primary bodies of a binary asteroid system
- $\boldsymbol{\omega}$  = skew-symmetric matrix of the non-dimensionalized angular velocity of the mutual orbit of a binary asteroid system  
(sections 6.1.1 and 6.2.1)
- $\boldsymbol{\omega}_c$  = skew-symmetric matrix of the non-dimensionalized angular velocity of the mutual orbit of a binary asteroid system for circular motion  
(section 4.0.8)
- $\boldsymbol{\omega}'$  = skew-symmetric matrix of the non-dimensionalized angular acceleration of the mutual orbit of a binary asteroid system  
(section 6.1.1)

## ACRONYMS

CRTBP	Circular Restricted Three Body Problem
FCRTBP	Full Circular Restricted Three Body Problem
FRTBP	Full Restricted Three Body Problem
FTBP	Full Two Body Problem
SRP	Solar Radiation Pressure

## TABLE OF CONTENTS

ACKNOWLEDGEMENTS		ii
ABSTRACT		vii
ABRÉGÉ		ix
LIST OF TABLES		xxiv
LIST OF FIGURES		xxv
1	Introduction	1
1.1	Background and Motivation	1
1.2	Literature Review	3
1.2.1	The Circular Restricted Three Body Problem	3
1.2.2	The Full Restricted Three Body Problem (FRTBP)	6
1.2.3	Solar Radiation Pressure (SRP)	11
1.3	Objectives of the Thesis	13
1.4	Outline of the Thesis	14
2	Gravitational Potential of a Small Irregular Body	17
2.1	Fourth-order Taylor Series Expansion of the Gravitational Potential of a Small Irregular Body	18
2.2	Gravitational Force Exerted on a Spacecraft by an Asteroid	22
2.2.1	Validation of the Fourth-order Gravitational Potential Model of a Small Irregular Body	22
2.3	Gravitational Potential of a Binary Asteroid System	25
2.4	Determination of the Gravitational Potential of a Binary Asteroid System Using Layered Mascons	28
2.5	Non-dimensionalization	30
2.6	Summary	34

3	The Full Two Body Problem . . . . .	35
3.1	Equations of Motion of a Binary Asteroid System . . . . .	36
3.1.1	Development of the Equations for Each Generalized Coordinates . . . . .	40
3.2	The Case of Mutual Circular Motion . . . . .	44
3.3	Application to the Binary Asteroid System 65803 Didymos . . . . .	46
3.3.1	Effect of Varying the Constant of Integration $h$ . . . . .	51
3.3.2	Gravitational Potential Energy of a Binary Asteroid System Using a Layered Mascons Model . . . . .	53
3.3.3	Variation of the Gravitational Potential Energy of a Binary Asteroid System due to Uncertainties in its Parameters . . . . .	55
3.4	Summary . . . . .	57
4	Spacecraft Trajectories Compatible with the Solar Radiation Pressure in the FCRTBP . . . . .	59
4.1	Models Used in this Chapter . . . . .	59
4.1.1	Assumptions . . . . .	60
4.1.2	Solar Radiation Pressure Acceleration Model . . . . .	61
4.1.3	Equations of Motion . . . . .	63
4.1.4	Binary Asteroid and Spacecraft Models . . . . .	63
4.2	Designing SRP-compatible Trajectories in the FCRTBP . . . . .	64
4.2.1	Initial Guess for Designing Periodic Orbits in the Classical CRTBP . . . . .	64
4.2.2	Selecting SRP-compatible Orbits . . . . .	67
4.2.3	Qualitative Impact of the SRP on Equilibrium Points and the Jacobi Constant . . . . .	67
4.2.4	Differential-correction Scheme . . . . .	68
4.2.5	Orbits in the Higher-order Gravitational Potential Model and Including the SRP . . . . .	71
4.3	Numerical Results . . . . .	72
4.3.1	Zeroth-order Gravitational Potential Model Orbits . . . . .	73
4.3.2	Fourth-order Gravitational Potential Model Trajectories . . . . .	77
4.3.3	Fourth-order Gravitational Model Trajectories with SRP Acceleration . . . . .	79
4.3.4	Stability Comparison of the Trajectories . . . . .	81
4.3.5	Trajectories with a Different Period . . . . .	83
4.4	Summary . . . . .	84

5	Impact of the Solar Radiation Pressure Acceleration Model on Spacecraft Trajectories in the FCRTBP . . . . .	86
5.1	Description of the Attitude Schemes . . . . .	87
5.1.1	Generic Expressions for the Components of the $\hat{\mathbf{n}}$ Vector Expressed in the Synodic Reference Frame . . . . .	87
5.1.2	Solar Panels Always Perpendicular with the $X_S$ Direction of the Synodic Reference Frame ( $X_S$ attitude scheme) . .	90
5.1.3	Maximum SRP Acceleration (MaxSRP Attitude Scheme) .	91
5.1.4	Minimal SRP Acceleration (MinSRP Attitude Scheme) . .	92
5.1.5	Oscillation of Plate 1, Averaged Around Maximal SRP Acceleration (Oscill MaxSRP Attitude Scheme) . . . . .	92
5.1.6	Oscillation of Plate 1, Averaged Around Minimal SRP Acceleration (Oscill MinSRP Attitude Scheme) . . . . .	93
5.2	Equations of Motion . . . . .	93
5.3	Binary Asteroid and Spacecraft Models . . . . .	93
5.4	Choice of Trajectories Used for the Study . . . . .	94
5.5	Studies Done on Each Attitude Schemes Described in Section 5.1 .	96
5.6	Numerical Results . . . . .	97
5.6.1	Choice of the SRP Model Acceleration to Use . . . . .	97
5.6.2	Acceleration due to SRP throughout one Rotation of the Binary Asteroid System . . . . .	100
5.6.3	Equilibrium Regions throughout one Rotation of the Binary Asteroid System . . . . .	102
5.6.4	Study of the Influence of the Attitude Scheme on the Impact of the SRP Acceleration . . . . .	103
5.7	Summary . . . . .	114
6	The Full Restricted Three Body Problem . . . . .	116
6.1	Equations of Motion . . . . .	117
6.2	Building Nominal Trajectories . . . . .	118
6.2.1	Multiple-shooting Correction Scheme . . . . .	118
6.3	Control System . . . . .	122
6.3.1	Lyapunov Control . . . . .	122
6.3.2	Smoothing the Control Thrust Signal . . . . .	124
6.4	Analysis Procedure Using the 65803 Didymos Binary Asteroid System Model . . . . .	125
6.5	Numerical Results . . . . .	126

6.5.1	Retrograde Trajectory Around Body 2 . . . . .	127
6.5.2	Planar Lyapunov Trajectory . . . . .	129
6.5.3	Vertical Lyapunov Trajectory . . . . .	132
6.5.4	Halo Trajectory . . . . .	134
6.6	Summary . . . . .	137
7	Conclusions . . . . .	139
7.1	Summary of the Findings . . . . .	139
7.2	Suggestions for Future Work . . . . .	142
A	Reference Frames Used in the Thesis . . . . .	144
B	Development of the Expression of the Gravitational Potential of an Asteroid	146
C	Fourth-order Inertia Integrals of an Arbitrarily Shaped Body . . . . .	154
C.1	Fourth-order Inertia Integrals of an Ellipsoid . . . . .	154
C.2	Calculating Inertia Integrals from a Polyhedron Shape Model . . .	156
C.2.1	Second-order Inertia Integrals . . . . .	158
C.2.2	Fourth-order Inertia Integrals . . . . .	163
C.2.3	Validation of the Fourth-order Inertia Integrals Calculated from a Polyhedron Shape Model . . . . .	165
D	Solar Radiation Pressure . . . . .	167
	REFERENCES . . . . .	172

LIST OF TABLES

Table	page
3-1 Didymos system parameters . . . . .	46
3-2 Didymos calculated second-order moments of inertia and fourth-order inertia integrals . . . . .	47
4-1 Dimensions of body 1 and body 2 of the binary asteroid system . . . .	64
4-2 Planar Lyapunov family of orbits around $L_1$ . . . . .	73
4-3 Planar Lyapunov family of orbits around $L_2$ . . . . .	74
4-4 Retrograde orbits around body 2 . . . . .	75
4-5 Initial conditions for periodic trajectories using a fourth-order gravi- tational potential model . . . . .	79
4-6 Initial conditions for periodic trajectories with SRP acceleration, fourth-order gravitational potential model . . . . .	81
4-7 Eigenvalues for $L_1$ planar Lyapunov trajectories and retrograde tra- jectories around body 2 . . . . .	82
5-1 Characteristics of the different surfaces of the spacecraft . . . . .	94
5-2 Description of trajectories analyzed . . . . .	103
5-3 Initial conditions for periodic trajectories . . . . .	111
5-4 Initial conditions for periodic trajectories . . . . .	112
C-1 Fourth-order inertia integrals of an ellipsoid . . . . .	165

LIST OF FIGURES

<u>Figure</u>	<u>page</u>
2-1 Body fixed reference frame . . . . .	18
2-2 Gravitational potential of a mass element at point P . . . . .	19
2-3 Constant Hamiltonian for a unit mass spacecraft orbiting asteroid Eros	24
2-4 Variation of forces acting on spacecraft over one orbit [39] . . . . .	25
2-5 Variation of forces acting on spacecraft over one orbit . . . . .	25
2-6 Geometry of the gravitational potential . . . . .	26
2-7 Graphical representation of the Didymos binary asteroid system using a layered mascons model . . . . .	29
3-1 The full two body problem . . . . .	36
3-2 Distance $R$ between the centers of mass of the primary bodies of the binary asteroid system for ten revolutions of the system . . . . .	49
3-3 Potential energy for ten revolutions of the system . . . . .	50
3-4 Kinetic energy for ten revolutions of the system . . . . .	50
3-5 Total energy for ten revolutions of the system . . . . .	51
3-6 Distance $R$ between the centers of mass of the primary bodies of the binary asteroid system of the binary asteroid system for the constant $h$ set at $h_0$ . . . . .	52
3-7 Distance $R$ between the centers of mass of the primary bodies of the binary asteroid system of the binary asteroid system for the constant $h$ set at $0.999h_0$ . . . . .	52
3-8 Potential energy calculated using the Taylor series expansion and the layered mascons models . . . . .	54

3–9	Difference in the calculation of the gravitational potential energy of the binary asteroid system . . . . .	55
3–10	Potential energy variation for different semi-major axis values . . . . .	56
3–11	Potential energy variation for different eccentricity values . . . . .	57
4–1	Binary asteroid system . . . . .	73
4–2	Planar Lyapunov orbits around $L_1$ and $L_2$ . . . . .	75
4–3	Family of retrograde orbits around body 2 . . . . .	76
4–4	Evolution of families with respect to initial position and $C$ . . . . .	77
4–5	Retrograde trajectories around body 2 of zeroth-order and fourth-order . . . . .	78
4–6	$L_1$ planar Lyapunov trajectories of zeroth-order and fourth-order . . . . .	78
4–7	Retrograde trajectories around body 2 with and without SRP acceleration included in the model . . . . .	80
4–8	$L_1$ planar Lyapunov trajectories with and without SRP acceleration included in the model . . . . .	80
4–9	$L_1$ planar Lyapunov trajectories with and without SRP acceleration included in the model, zoomed on trajectory . . . . .	81
4–10	Lyapunov trajectory with a period of 3.1 . . . . .	83
4–11	Retrograde trajectory around body 2 with a period of 3.1, zoomed on initial position . . . . .	84
5–1	Kinematics between plates reference frame and inertial reference frame . . . . .	88
5–2	Candidate trajectories around primary bodies and the binary asteroid system as a whole . . . . .	95
5–3	Candidate CRTBP trajectories in the vicinity of $L_1$ . . . . .	96
5–4	Position in the $X_S$ direction of the candidate CRTBP trajectories in the vicinity of $L_1$ with respect to the number of revolution of the binary asteroid system . . . . .	96

5-5	SRP acceleration in the $X_S$ direction of the synodic reference frame for different models and parameters over one rotation of the binary asteroid system . . . . .	98
5-6	SRP acceleration in the $Y_S$ direction of the synodic reference frame for different models and parameters over one rotation of the binary asteroid system . . . . .	98
5-7	SRP acceleration in the $X_S$ direction of the synodic reference frame throughout one rotation of the binary asteroid system for the N-plate SRP acceleration model . . . . .	100
5-8	SRP acceleration in the $Y_S$ direction of the synodic reference frame throughout one rotation of the binary asteroid system for the N-plate SRP acceleration model . . . . .	101
5-9	Evolution of the $L_1$ equilibrium region for one rotation of the binary asteroid system . . . . .	102
5-10	Retrograde trajectory around primary body 1 crossing with $X_S$ - $Z_S$ plane . . . . .	105
5-11	Retrograde trajectory around primary body 1 crossing with $X_S$ - $Z_S$ plane zoomed around primary body 1 . . . . .	105
5-12	Direct trajectory around binary asteroid system crossing with $X_S$ - $Z_S$ plane . . . . .	106
5-13	Retrograde trajectory around binary asteroid system crossing with $X_S$ - $Z_S$ plane . . . . .	106
5-14	Retrograde trajectory around binary asteroid system crossing with $X_S$ - $Z_S$ plane zoomed around primary body 2 . . . . .	107
5-15	Retrograde trajectory around primary body 2 crossing with $X_S$ - $Z_S$ plane . . . . .	107
5-16	Retrograde trajectory around primary body 2 crossing with $X_S$ - $Z_S$ plane zoomed around primary body 2 . . . . .	108
5-17	Evolution of the $C$ value for two rotations of the system for a retrograde trajectory around primary body 1 . . . . .	109

5–18	Evolution of the $C$ value for four rotations of the system for a direct trajectory around the binary asteroid system . . . . .	109
5–19	Evolution of the $C$ value for two rotations of the system for a retrograde trajectory around the binary asteroid system . . . . .	110
5–20	Evolution of the $C$ value for two rotations of the system for a retrograde trajectory around primary body 2 . . . . .	110
5–21	Periodic trajectories over ten revolutions of the binary asteroid system shown in the synodic reference frame . . . . .	113
5–22	Evolution of the $C$ value for the periodic trajectories over two revolutions of the binary asteroid system . . . . .	113
6–1	Initial guess trajectories . . . . .	127
6–2	Evolution of the nominal retrograde trajectory around body 2 . . . . .	128
6–3	Real retrograde trajectory around body 2 followed by spacecraft . . . . .	128
6–4	Control thrust for the retrograde trajectory around body 2 . . . . .	128
6–5	Spacecraft retrograde trajectory around body 2 when using low pass filters . . . . .	129
6–6	Control thrust for the retrograde trajectory around body 2 when using low pass filters . . . . .	129
6–7	Evolution of the planar Lyapunov nominal trajectory . . . . .	130
6–8	Real planar Lyapunov trajectory followed by spacecraft . . . . .	130
6–9	Control thrust for the planar Lyapunov trajectory . . . . .	131
6–10	Spacecraft planar Lyapunov trajectory when using low pass filters . . . . .	131
6–11	Control thrust for the planar Lyapunov trajectory when using low pass filters . . . . .	132
6–12	Evolution of the vertical Lyapunov nominal trajectory . . . . .	133
6–13	Real vertical Lyapunov trajectory followed by spacecraft . . . . .	133

6–14	Control thrust for the vertical Lyapunov trajectory . . . . .	133
6–15	Spacecraft vertical Lyapunov trajectory when using low pass filters . .	134
6–16	Control thrust for the vertical Lyapunov trajectory when using low pass filters . . . . .	134
6–17	Evolution of the halo nominal trajectory . . . . .	135
6–18	Real halo trajectory followed by spacecraft . . . . .	136
6–19	Control thrust for the halo trajectory . . . . .	136
6–20	Spacecraft halo trajectory when using low pass filters . . . . .	137
6–21	Control thrust for the halo trajectory when using low pass filters . . .	137
A–1	Reference frames . . . . .	145
C–1	Facet with vertices and edges . . . . .	157
D–1	Geometry used to describe the solar radiation pressure acceleration .	167
D–2	Graphical representation of the $\hat{n}$ vectors involved in the N-plates model . . . . .	171

## CHAPTER 1

### Introduction

#### 1.1 Background and Motivation

Missions to asteroids are now an important component of the space exploration program of major space agencies in the world, with the goal of better understanding the formation of the solar system and learn about their dynamics to be able to react in case of a possible collision with the Earth. Some well-known examples of missions are NEAR Shoemaker (orbited asteroid Eros in 2000) [1], Hayabusa (landed on asteroid Itokawa in 2005) [2], Dawn, (orbited asteroid Vesta in 2011 and dwarf planet Ceres in 2015) [3], Hayabusa 2 (arrived in the vicinity of asteroid Ryugu in June 2018) [4, 5], and OSIRISRex (arrived at asteroid Bennu in December 2018) [6].

Binary asteroid systems compose approximately 16% of near Earth asteroids [7]. They are composed of two asteroids orbiting the barycenter of the system. ESA and NASA are currently in the planning phase of a mission, the Asteroid Impact and Deflection Assessment (AIDA) mission, to the binary asteroid system 65803 Didymos. The NASA component of the mission, the Double Asteroid Redirection Test (DART), is planned to be launched in 2021 and arrive in the vicinity of Didymos in 2022 and the ESA part of the mission, Hera, is planned to be launched in 2023 and arrive close to Didymos in 2026 [8, 9].

The dynamics models used to represent binary asteroid systems have greatly evolved in the past ten years. The first models represented the primary bodies of

the system as a sphere and an ellipsoid [10]. Later, systems with other geometrical shapes were also studied [11]. Now, the models are using information extracted from polyhedron shape models, which show that the main bodies of the binary systems have highly irregular shapes [12, 13].

Since the main body has a angular velocity that is different from the one of the binary asteroid system as a whole and an irregular shape, the gravitational potential of the binary asteroid system does not only depend on the position where it is calculated, but also on time. The observations of the Didymos system also show that the mutual orbit of the primary bodies does not follow a circular motion, but is slightly elliptical [14]. Uncertainties are also part of the Didymos model, like in any model of a system never visited [15]. These uncertainties may impact the calculation of the gravitational potential of the bodies of the binary asteroid system, thus the dynamics of a spacecraft in its vicinity.

All of these perturbations add complexity to the dynamics of a spacecraft in such an environment. The problem where these perturbations are added to the model is known as the Full Restricted Three Body Problem (FRTBP). In the FRTBP, the primary bodies are modeled using a polyhedron shape model. Their individual angular velocities are taken into account, as well as their non-circular motion around their barycenter. The primary bodies have small masses compared to planetary bodies like the Earth, causing external perturbations, like the Solar Radiation Pressure (SRP), to also affect the dynamics of a spacecraft in the FRTBP.

Studying the FRTBP applied to binary asteroid systems, such as Didymos, is enhancing the knowledge of the dynamics of a spacecraft in their vicinity. With the coming AIDA mission, this is of prime interest to the spacecraft dynamics community.

## **1.2 Literature Review**

The simplest way to model the dynamics of a spacecraft in a binary system is through the Circular Restricted Three Body Problem (CRTBP). It is appropriate for systems such as the Earth-Moon or the Sun-Earth systems, but in the case of binary asteroid systems, it is not sufficient to correctly model the system. Perturbations coming from the irregular shape of the primary bodies and their angular velocity, different from the one of the system as a whole modify the Full Two Body Problem (FTBP) which is the foundation of the Full Restricted Three Body Problem (FRTBP). The small gravitational field of the primary bodies of a binary asteroid system causes external perturbations, such as the Solar Radiation Pressure (SRP), to greatly influence the motion of a spacecraft in their vicinity.

This section reviews the CRTBP and then introduces the different perturbations to the CRTBP and how they are integrated into the FRTBP. The last part of the section is dedicated to the design of trajectories in the FRTBP.

### **1.2.1 The Circular Restricted Three Body Problem**

The CRTBP is a special case of the Three-Body Problem (TBP) that was first studied by Isaac Newton in the 17<sup>th</sup> century. It studies the motion of a negligible mass body in a binary system composed of two primary bodies. The CRTBP is restricted by having the third body having a mass considered negligible compared to the primary bodies and by considering the primary bodies as point masses. It is

circular because the mutual orbit of the primary bodies is circular, having a constant angular velocity and a constant distance between the primary bodies. The CRTBP was investigated by Euler and Lagrange in the 18<sup>th</sup> century. Euler first introduced the idea of using a rotating frame to describe the motion of a small body of negligible mass influenced by two massive bodies. In the early 20<sup>th</sup> century, Henry C. Plummer and Forest R. Moulton produced families of periodic orbits near the libration points. Plummer's work was dedicated to the collinear libration points and Moulton's work was about both the collinear and triangular libration points. Victor Szebehely's book, *Theory of Orbits: The Restricted Problem of Three Bodies* published in 1967 [16], summarizes the knowledge about the Restricted Three Body Problem until then [17].

Farquhar was the first to use the term "halo orbits" in his Ph.D. thesis published in 1968 [18]. Hénon also worked on the RTBP orbits in the same timeframe and produced a series of papers on the numerical exploration of the restricted problem, the fifth of which was dedicated to periodic orbits and their stability [19]. In 1973, Farquhar and Kamel published a paper describing an analytical solution for quasi-periodic orbits about the translunar libration point [20]. They proposed a technique to generate solutions for Lissajous orbits and how they evolve when the in-plane and out-of-plane frequencies are set to equal values. In 1979, Breakwell and Brown described the evolution of halo orbits about  $L_1$  and  $L_2$  [21]. They used the half orbit transition matrix to adjust the initial conditions, so that to obtain periodic orbits. In their work, they used a numerical solution, instead of an analytical one like in the work of Farquhar and Kamel.

In 1984, Howell, published two papers related to halo orbits. The first one presented a numerical study of the halo orbits near collinear libration points for mass ratio ( $\mu$ ) values ranging from 0 to 1. She presented a technique to generate periodic halo orbits and to assess their stability using the state transition matrix [22]. In a second paper, published the same year, Howell presented a special case of the halo orbits: almost rectilinear halo orbits. These appear when the orbits get closer to the smallest primary body of the system, creating a bridge between the  $L_1$  and  $L_2$  halo orbits. She presented how to solve the singularities appearing close to the primary body by using a regularization scheme [23].

Many papers describe the families of orbits about the  $L_1$  and  $L_2$  libration points. One of them, written by Howell, presented the different orbit families near libration points, including Lyapunov, Lissajous and halo orbits [24]. Folta et al. [25] presented the station-keeping strategies for different families of orbit about the Earth-Moon libration points, considering the ARTEMIS mission as an application. In this paper, they spent great effort describing the models and characterizing different families of orbits.

Several other studies compare the different possible orbits close to the Moon with the goal of conducting Moon related missions. Grebow et al. [26] studied different families about the Earth-Moon  $L_1$  and  $L_2$  libration points and compared their periods, stability and stationkeeping costs. Later, Whitley and Martinez did similar work, but included lunar orbits, such as low lunar and lunar frozen orbits [27].

Davis and Howell got interested in the long-term evolution of orbits about libration points. Their work was done for the Sun-Saturn system, but could be applied to any system, such as a binary asteroid system. They used Poincaré maps to describe the satellite trajectory status at its next periapsis passage: escape through  $L_1$  or  $L_2$ , stay bounded or impact the smaller primary, based on the position of the current orbit periapsis. They could use their maps to identify passage periapsis between  $L_1$  and  $L_2$  [28, 29].

Doedel et al. developed a bifurcation and continuation software, AUTO, to find periodic orbits about the equilibrium points in the CRTBP [30, 31]. They worked on the periodic orbits that exist for systems with various mass-ratio. They also built maps of the bifurcations that lead to various types of periodic orbits starting from the equilibrium points of the Earth-Moon system.

### **1.2.2 The Full Restricted Three Body Problem (FRTBP)**

This section of the literature review presents various aspects of the FRTBP. It is necessary to model correctly the motion of a primary bodies of the binary asteroid system to then understand the dynamics of a spacecraft in such an environment.

#### **Modeling of The Gravitational Potential of a Small Irregular Body**

The way the gravitational potential of the primary bodies of a binary asteroid system is modeled is based on the models developed for small irregular bodies such as single asteroids. This section presents the evolution of the gravitational models used for single asteroids. Most of them are also presented in Ref. [32].

There are many ways to model the gravitational potential of a small body. Polyhedron shape models of a single asteroid, such as 4769 Castalia [33] and 4179 Toutatis

[34], have been derived from range-Doppler radar images. Werner and Scheeres have developed the expressions for the calculation of the gravitational potential of a small body based on the polyhedron shape model [35]. They have compared it with mascons and spherical harmonics models and concluded that the polyhedron shape model should be used when the spacecraft is located inside the circumscribing sphere of the small body. Scheeres et al. used the shape model of 4179 Toutatis to derive a second-order gravitational potential model of the asteroid to be used when the spacecraft is outside of the circumscribing sphere of the body while the polyhedron shape model itself is required when the spacecraft is inside the circumscribing sphere. They then used the model to study the motion of a spacecraft in the vicinity of the asteroid [36]. Most spacecraft operations, except close approach and landing, are outside of the circumscribing sphere of a small body. Since the polyhedron shape approach is computationally expensive, the spherical harmonics expansion of the gravitational potential is then what has been used for most studies on the subject.

The gravitational potential of a body can be expressed in terms of its inertia integrals. Dobrovolskis developed a simple method to calculate the inertia integrals of the second order of an arbitrarily shaped body using a polyhedron shape model [37]. These values can be used instead of the spherical harmonics to better represent the inertia of the small body.

Wang et al. [38] used a second-order gravitational potential of a triaxial ellipsoid to model an asteroid and study the dynamics of a spacecraft in its vicinity. The model used was based on the second-order spherical harmonics of the small body. Kikuchi et al. [39], on the other hand, used a fourth-order expression of the spherical harmonics

of a triaxial ellipsoid to model the gravitational potential of a small body and study the orbit-attitude and solar radiation pressure coupled motion of a spacecraft in its vicinity.

A layered-mascon model, with the position of the mascons located at the centers of mass of the tetrahedrons composing the polyhedron shape model has been developed by Venditti [40]. Chanut et al. [42] compared the layered-mascon model with the polyhedron shape model developed by Werner and Scheeres [35] and showed that it can model the gravitational potential outside of a small body with precision while being less computationally expensive.

### **The Full Two Body Problem (FTBP)**

Binary asteroid systems require to be treated differently from systems like the Earth-Moon or the Sun-Earth systems. Their primary bodies have irregular shapes that need to be taken into account when calculating their mutual motion, known as the Full Two Body Problem (FTBP).

Bellerose and Scheeres started their study of the FTBP by modeling the primary bodies as an ellipse and a sphere [43]. They used a second-order gravitational potential model of the primary bodies to conduct an analysis of the system while the primary bodies are in relative equilibrium. It was found that this equilibrium state is achievable when one of the principal axes of the ellipsoid is pointing towards the sphere. In their study of the FRTBP, they considered the mutual orbit of the primary bodies to be circular. They also studied the stability of the equilibrium points of the binary system, using the Routh criteria. As in the case of the CRTBP, they found out that only the equilateral points are stable in the FRTBP as well. Scheeres

also explores the FTBP in [44], studying the stability in the planar case. Here again, the model used for the mutual gravitational potential of the primary bodies is of the second order.

Woo and Misra [11] studied the FTBP and the FRTBP for systems composed of bodies with complex geometrical shapes. They combined geometrical shapes to develop methods to calculate the second-order moments of inertia for shapes such as a pear and a peanut. They also used the calculated moments of inertia to study the FTBP, finding conditions for a binary asteroid system to be in relative equilibrium and have its body orbit their barycenter in a circular fashion.

Hou et al. [45] developed the expression for the mutual gravitational potential of a binary system with primary bodies of arbitrary shapes and mass distribution. The expression they developed is based on a sum that is truncated at the order desired and needs to be calculated at each step of a simulation. They used it to study the FTBP, calculating the mutual motion of the primary bodies for binary systems such as 1999 KW4. They suggested that truncating the gravitational potential at the fourth order is sufficient in the study of the FTBP.

Shi et al. [46], on the other hand, developed the equations for the mutual gravitational potential of the primary bodies of a binary asteroid system based on a polyhedron shape model for the first primary body and an ellipsoid for the second primary body. Based on this model of the gravitational potential, they also developed the equations for the gravitational force and torque exerted on each other by the primary bodies of the system.

Naidu and Margot were interested on the rotational motion of the primary bodies in the FTBP. They developed relations between the eccentricity of the mutual orbit of the bodies around their barycenter and the libration motion of the smallest body [47].

### **Trajectories in the Full Restricted Three Body Problem**

In Ref. [10], Bellerose and Scheeres pushed further the analysis of the equilibrium of a binary asteroid system. They also presented a method to find periodic orbits in the Full Two Body Problem (FTBP) in such a system by using the Poincaré map reduction method. Then, the solution of the FTBP was inserted into the FRTBP to compute possible trajectories for a particle in a binary asteroid system. They studied the motion of a spacecraft around the stable equilateral equilibrium points for primary bodies in a circular mutual motion.

Woo and Misra determined trajectories in the full circular restricted three body problem (FCRTBP) [48]. They used a zeroth-order development of the equations of motion to design Lissajous trajectories near the collinear equilibrium points and bounded trajectories near the equilateral equilibrium points. The trajectories near the collinear equilibrium points were controlled using a Lyapunov controller. Their gravitational potential model was based on the second-order moments of inertia of an arbitrarily shaped body.

Li et al. used a grid search and a two-stage multiple-shooting correction scheme to find bounded trajectories in the FCRTBP [49]. They first found periodic motion in a scenario where the angular velocity of the primary bodies of the binary asteroid system is the same as that of the system as a whole using a grid search method.

They then used the two-stage multiple-shooting correction scheme to modify the trajectories so that they would be fitted for the FCRTBP where the angular velocity of the primary bodies would be different from the one of the system as a whole. Those trajectories lasted a few orbits, but they were not periodic. They were also developed based on the 1999 KW4 binary asteroid model, where the primary bodies have a circular motion around their barycenter. They used a Lyapunov controller to keep the spacecraft on the reference trajectories that had been calculated.

Ferrari [50] developed a single-stage multiple-shooting correction scheme that has also been used by Capannolo et al. [12]. They used it to build periodic trajectories using a polyhedron shape model of binary asteroid system 65803 Didymos. The periodic orbits were calculated with the angular velocity of the primary bodies being the same as the angular velocity of the binary asteroid system as a whole and assuming circular mutual motion of the primaries. Initial conditions were then extracted and used in the FCRTBP to understand the nature of similar quasi-periodic trajectories in the FCRTBP.

### **1.2.3 Solar Radiation Pressure (SRP)**

Since the primary bodies of a binary asteroid system are small, their gravitational potential is low. The motion of a spacecraft in their vicinity can then be significantly affected by an external perturbation, such as the SRP. In Ref. [39], it is shown that the attitude-orbital coupling, added with the SRP is an important component of the dynamics of a spacecraft in the vicinity of a single asteroid and it is believed that this will also apply to binary asteroid systems. This section discusses

how the SRP has been modeled and included in the dynamics model of a spacecraft in the vicinity of binary asteroid systems.

Models of the SRP acceleration have been examined in various contexts and environments. McInnes has written a book detailing the theory and models required for solar sailing [51]. This book is an excellent reference for anyone working with the SRP. Farrés et al. [52] described different ways to model the SRP acceleration, from the cannonball model to highly complex models using spherical harmonics or finite elements analysis. Their goal was to compare the complexity of the model and the computing cost of the last two. Misra et al. [53], on the other hand, used an N-plate model, which they called a cuboid in the context of a single asteroid. They studied the combined effect of the SRP and the orbital-attitude coupled dynamics, which cannot be determined properly using a cannonball model.

Other studies on the dynamics of a spacecraft around a single asteroid focussed mainly on the possibilities the SRP offers on the design of trajectories that would not exist without it [54, 55]. Xin et al. [54] found that the SRP enabled to produce new types of motion around single asteroids called forced orbital motion. Giacotti et al. [55], also investigated spacecraft trajectory design taking the SRP into account.

Morrow and Heiligers have, independently, conducted research on the possibilities of having a spacecraft using a solar sail to stay in hovering points in the vicinity of a single asteroid or orbiting it. Because the hovering points and trajectories are further away from the asteroid, these studies neglected the shape of the asteroid in their model [56, 57]. García Yárnoz et al. used a solar sail to compute trajectories in the Sun-Asteroid CRTBP [58]. Here, the shape of the asteroid has been neglected,

but the trajectories found can be an interesting starting point for a study using a more detailed model of a single asteroid.

Heiligers and Scheeres [57] used a solar sail to explore hovering points in the vicinity of a binary asteroid. In their case, the spacecraft does not go to close proximity of the primary bodies of the binary asteroid, so an oblate sphere is used to model them. Dell'Elce et al. [59] have worked on getting the most suitable orbits for a mission such as AIDA. In their study, a fairly simple model of the SRP, the cannonball model, has been used. These studies use trajectories that go to the proximity of the binary asteroid system, such as Distant Retrograde Orbits (DROs).

The possible use of a solar sail for missions in the Earth-Moon system has also been studied [60, 61]. These are interesting starting points for the study of the possibility of new trajectories when the SRP acceleration is taken into account in their design. These analysis were based on a zeroth-order gravitational potential model as it is normally the case for the Earth-Moon system. In the case of a binary asteroid system, the perturbations due to the higher order terms of the gravitational potential are not negligible, making the search for trajectories more complex.

### **1.3 Objectives of the Thesis**

The overall objective of this thesis is to study the dynamics of a spacecraft in the vicinity of a binary asteroid system. In the present case, the full model of the binary asteroid system, including the rotation, realistic shape and mutual motion of its primary bodies, is utilized.

The first objective of the thesis is to develop an analytical expression for a fourth-order gravitational potential model of a binary asteroid system to be used in

this study. It includes the development of the equation of the gravitational potential of an arbitrarily shaped body, keeping all terms up to the fourth order. It also includes the calculation of the required fourth-order inertia integrals.

The second objective of this thesis is to understand the role of the SRP in the motion of a spacecraft in the context of the FCRTBP, where the irregular shape of the primary bodies is taken into account. The individual rotational motion of the primary bodies and their non-circular motion around their barycenter are not taken into account. It also includes the study of the impact of the modeling SRP acceleration and of the attitude scheme of the spacecraft on the FCRTBP.

The third objective is to study the dynamics of a spacecraft in the FRTBP by including the rotations of the primary bodies and their non-circular motion around their barycenter in the model of the binary asteroid system. The design of the nominal spacecraft trajectories based on the FCRTBP is done first. Then a comparison is carried out between the control effort required when the trajectories are designed using the full model of the binary asteroid with that required when a simpler model is used.

#### **1.4 Outline of the Thesis**

Chapter 2 presents the development of the gravitational potential of a small irregular body, such as a single asteroid. An expression for the gravitational potential based on a fourth-order Taylor series expansion is developed first. This is then translated into the gravitational force exerted on a unit mass spacecraft operated in the vicinity of a single asteroid. Then a comparison is made between the results obtained with the Taylor series expansion with those obtained by another team using

a fourth-order spherical harmonics model. This, added with the calculation of the Hamiltonian on a long period of time, validates the model. The model is then applied to a binary asteroid system.

Chapter 3 visits the FTBP. It first explores the development of the equations of motion in the FTBP. The case of circular motion of the primary bodies is then discussed. The equations of motion are applied to the binary asteroid system Didymos 65803. A short study of the sensitivity of the system to the value of the constant of integration of the equation related to the angular velocity of the system shows how complex the FTBP can be.

In chapter 4, a technique to compute periodic trajectories is developed for a spacecraft operated in the FCRTBP and subjected to the SRP. Sets of planar trajectories such as planar Lyapunov orbits around  $L_1$  and retrograde trajectories around body 2 are found for different attitude schemes of the spacecraft.

In chapter 5, a set of trajectories around body 1, body 2 and the around the full binary asteroid system are developed. They are then used in a model of the FCRTBP including the SRP acceleration for different attitude schemes of a spacecraft. The evolution of the uncontrolled trajectories is then studied to understand how the SRP acceleration affects them. It is done for two cases: when the binary asteroid system is at the perihelion of its orbit around the Sun and when the binary asteroid system is at the aphelion of its orbit around the Sun.

The FRTBP is visited in chapter 6. It includes the design and control of spacecraft trajectories in the FRTBP, including a detailed model of the SRP acceleration. In this chapter, the *full* term means that the inertia integrals are calculated based on

a polyhedron shape model of the primary bodies, that the rotational motion of the primary bodies and the shape of their mutual orbit are as described in the literature. The trajectories suitable for the FRTBP are developed based on a multi-shooting correction algorithm. A control system based on the Lyapunov stability theorem is used to compute the control thrust required for different types of orbits and various levels of detail used in the model.

Chapter 7 concludes the thesis. It synthesizes the finding of the study of the FRTBP. It also recommends topics for future work.

## **CHAPTER 2**

### **Gravitational Potential of a Small Irregular Body**

The gravitational potential of a binary asteroid system is modeled based on the gravitational potential of a small irregular body and can be modeled in many different ways. Only a few years ago, the standard model for analytical development of the equations describing the gravitational potential of a small irregular body was in terms of the second-order spherical harmonics. About four years ago, the fourth-order spherical harmonics model of the gravitational potential started to be used. Now, many small irregular bodies are modelled using shape polyhedron models from which it is possible to calculate the gravitational potential using different techniques. One of them is to use the polyhedron shape model to extract the second and fourth-order inertia integrals and use them in a Taylor series expansion of the gravitational potential where the terms are kept up to the fourth order. Reference [45] demonstrated that such a gravitational model of the fourth order is necessary and sufficient to model the mutual motion of the primary bodies of a binary asteroid system. This model of the gravitational potential has the main advantage that it can use the inertia integrals for any shape model to calculate the gravitational forces acting on a spacecraft in the vicinity of the small body or conduct analytical investigations of the effects of the parameters of the system. The model does not require too much computing power, which is desirable during the development phase of a mission where the models of the small irregular body are updated regularly, requiring the analyses

to be repeated. Another novel technique to model the gravitational potential of small irregular bodies has been developed by Venditti et al. [41]. It consists of separating the body into layers of mascons and sum the gravitational potential of each mascon to get the gravitational potential of the body.

## 2.1 Fourth-order Taylor Series Expansion of the Gravitational Potential of a Small Irregular Body

The gravitational potential of an arbitrarily shaped asteroid is first calculated. The calculations are all made in the body fixed reference frame, which has its origin at the center of mass of the asteroid and is aligned with the principal moments of inertia of the asteroid (see Appendix A). The axis of rotation of the asteroid is aligned with its maximum moment of inertia, as shown in Fig. 2-1.

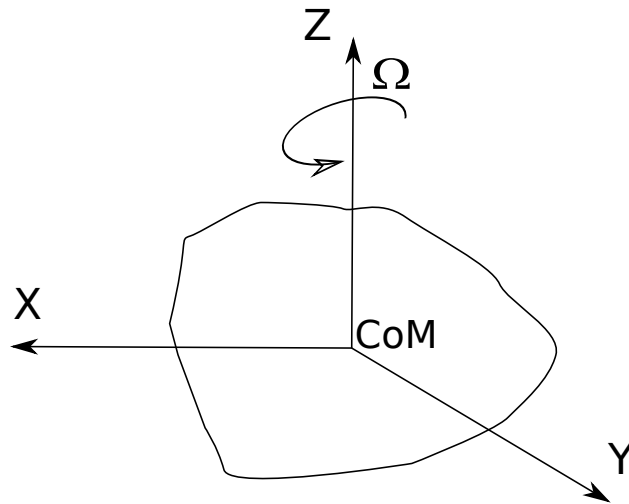


Figure 2-1: Body fixed reference frame

The gravitational potential due to a mass element  $dm$  at a point P at the distance  $|\mathbf{R} - \boldsymbol{\delta}|$  from the of mass element of the asteroid can be written as:

$$dU_{grav} = \frac{G}{|\mathbf{R} - \boldsymbol{\delta}|} dm \quad (2.1)$$

where  $G$  is the universal gravitational constant,  $\boldsymbol{\delta}$  is the position vector of the mass element  $dm$  relative to the center of mass of the asteroid and  $\mathbf{R}$  is the position vector of point P relative to the center of mass of the asteroid, as shown in Fig. 2-2.

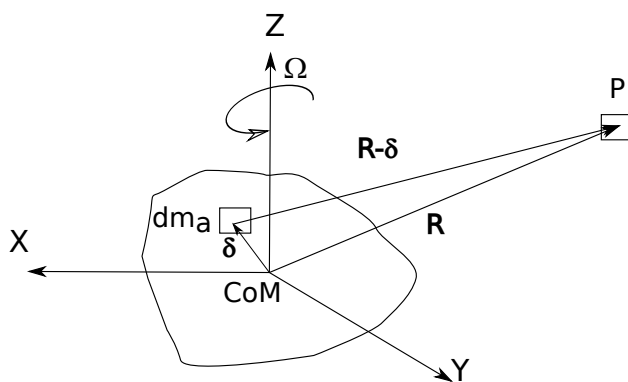


Figure 2-2: Gravitational potential of a mass element at point P

The total gravitational potential of the asteroid at point P is the sum of the gravitational potential generated by all the mass elements of the asteroid:

$$U_{grav} = \int \frac{G}{|\mathbf{R} - \boldsymbol{\delta}|} dm \quad (2.2)$$

Integration of Eq.2.2 requires the expansion of the  $\frac{1}{|\mathbf{R} - \boldsymbol{\delta}|}$  term in a Taylor series, which is described below.

First, it is necessary to rewrite the expression  $\frac{1}{|\mathbf{R}-\boldsymbol{\delta}|}$  as:

$$\begin{aligned}
\frac{1}{|\mathbf{R}-\boldsymbol{\delta}|} &= [(\mathbf{R}-\boldsymbol{\delta}) \cdot (\mathbf{R}-\boldsymbol{\delta})]^{-1/2} \\
&= [R^2 - 2(\mathbf{R} \cdot \boldsymbol{\delta}) + \delta^2]^{-1/2} \\
&= \frac{1}{R} \left[ 1 - \frac{2}{R} (\hat{\mathbf{u}}_{\mathbf{R}} \cdot \boldsymbol{\delta}) + \left( \frac{\delta}{R} \right)^2 \right]^{-1/2}
\end{aligned} \tag{2.3}$$

where  $\hat{\mathbf{u}}_{\mathbf{R}}$  is the unit vector along the position vector  $\mathbf{R}$  of point P relative to the center of mass of the asteroid. The last expression of Eq. 2.3 can be converted into  $(1+x)^{-1/2}$  where  $x = -\frac{2}{R}(\hat{\mathbf{u}}_{\mathbf{R}} \cdot \boldsymbol{\delta}) + \left(\frac{\delta}{R}\right)^2$ , and can be expanded binomially:

$$(1+x)^{-1/2} = 1 - \frac{1}{2}x + \frac{3}{8}x^2 - \frac{5}{16}x^3 + \frac{35}{128}x^4 \dots \tag{2.4}$$

Let us compute each term individually, keeping the terms up to  $O(1/R^4)$ :

$$\begin{aligned}
\frac{1}{2}x &= -\frac{(\hat{\mathbf{u}}_{\mathbf{R}} \cdot \boldsymbol{\delta})}{R} + \frac{1}{2} \left( \frac{\delta}{R} \right)^2 \\
\frac{3}{8}x^2 &= \frac{3}{8} \left( \frac{4}{R^2} (\hat{\mathbf{u}}_{\mathbf{R}} \cdot \boldsymbol{\delta})^2 - \frac{4\delta^2}{R^3} (\hat{\mathbf{u}}_{\mathbf{R}} \cdot \boldsymbol{\delta}) + \frac{\delta^4}{R^4} \right) \\
\frac{5}{16}x^3 &= -\frac{5}{2R^3} (\hat{\mathbf{u}}_{\mathbf{R}} \cdot \boldsymbol{\delta})^3 + \frac{15}{4R^4} \delta^2 (\hat{\mathbf{u}}_{\mathbf{R}} \cdot \boldsymbol{\delta})^2 + O(R^{-5}) \\
\frac{35}{128}x^4 &= \frac{35}{8R^4} (\hat{\mathbf{u}}_{\mathbf{R}} \cdot \boldsymbol{\delta})^4 + O(R^{-5})
\end{aligned} \tag{2.5}$$

Grouping the terms together and inserting them into Eq. 2.1, one obtains the following result:

$$\begin{aligned}
dU_{grav} = G \left\{ \frac{1}{R} - \frac{1}{R^2} (\hat{\mathbf{u}}_R \cdot \boldsymbol{\delta}) + \frac{1}{R^3} \left[ \frac{3}{2} (\hat{\mathbf{u}}_R \cdot \boldsymbol{\delta})^2 - \frac{1}{2} \delta^2 \right] \right. \\
+ \frac{1}{R^4} \left[ -\frac{3}{2} \delta^2 (\hat{\mathbf{u}}_R \cdot \boldsymbol{\delta}) + \frac{5}{2} (\hat{\mathbf{u}}_R \cdot \boldsymbol{\delta})^3 \right] \\
\left. + \frac{1}{R^5} \left[ \frac{3}{8} \delta^4 - \frac{15}{4} \delta^2 (\hat{\mathbf{u}}_R \cdot \boldsymbol{\delta})^2 + \frac{35}{8} (\hat{\mathbf{u}}_R \cdot \boldsymbol{\delta})^4 \right] \right\} \quad (2.6)
\end{aligned}$$

The total gravitational potential of the asteroid being the sum of the gravitational potential exerted by all the mass elements of the asteroid, one needs to integrate each of the terms in Eq. 2.6 over the entire mass distribution of the asteroid. After some algebra, detailed in Appendix B, the final expression for the gravitational potential of an asteroid at a point P, calculated up to the fourth-order, can be written as:

$$\begin{aligned}
U_{grav} = \frac{MG}{R} + \frac{3G}{2R^3} \left[ \frac{1}{3} (I_{xx} + I_{yy} + I_{zz}) - \frac{1}{R^2} (X^2 I_{xx} + Y^2 I_{yy} + Z^2 I_{zz}) \right] \\
+ \frac{G}{8R^5} \left[ \frac{35}{R^4} (X^4 J_{xxxx} + Y^4 J_{yyyy} + Z^4 J_{zzzz}) \right. \\
+ 6 ((XY)^2 J_{xxyy} + (YZ)^2 J_{yyzz} + (XZ)^2 J_{zzxx}) \\
- \frac{30}{R^2} (X^2 J_{xxxx} + Y^2 J_{yyyy} + Z^2 J_{zzzz} + \\
(X^2 + Y^2) J_{xxyy} + (Y^2 + Z^2) J_{yyzz} + (Z^2 + X^2) J_{zzxx}) \\
\left. + 3 (J_{xxxx} + J_{yyyy} + J_{zzzz}) + 6 (J_{xxyy} + J_{yyzz} + J_{zzxx}) \right] \quad (2.7)
\end{aligned}$$

where  $R$  is the distance between point P and the center of mass of the asteroid,  $X$ ,  $Y$ ,  $Z$  are the components of the position vector of point P with respect with the

center of mass of the asteroid, expressed in the asteroid body fixed reference frame,  $I_{xx}$ ,  $I_{yy}$ ,  $I_{zz}$  are the principal moments of inertia of the asteroid and  $J_{xxxx}$ ,  $J_{yyyy}$ ,  $J_{zzzz}$ ,  $J_{xxyy}$ ,  $J_{yyzz}$ ,  $J_{zzxx}$  are fourth-order inertial integrals of the asteroid. Appendix C details methods that can be used to calculate the fourth-order inertial integrals.

## 2.2 Gravitational Force Exerted on a Spacecraft by an Asteroid

The gravitational force exerted on a unit mass spacecraft by an asteroid is the gradient of the gravitational potential calculated in the previous section:

$$\mathbf{F}_{grav} = \frac{\partial U_{grav}}{\partial \mathbf{R}} \quad (2.8)$$

The components of the gravitational force along the asteroid body principal axes are then:

$$\begin{aligned} F_{grav_x} &= \frac{\partial U_{grav}}{\partial x} \\ F_{grav_y} &= \frac{\partial U_{grav}}{\partial y} \\ F_{grav_z} &= \frac{\partial U_{grav}}{\partial z} \end{aligned} \quad (2.9)$$

where  $U_{grav}$  is calculated using Eq. 2.7. The resulting equations can be found in Appendix B.

### 2.2.1 Validation of the Fourth-order Gravitational Potential Model of a Small Irregular Body

Before validating of the gravitational potential model developed in this chapter by comparing with an existing model, it is necessary to ascertain that the simulation results are reliable. This is done by using the principle of the conservation of the Hamiltonian of a dynamical system. It is calculated, in the inertial reference frame

located at the center of mass of the asteroid, using the following expression:

$$H = T_2 - T_0 + V \quad (2.10)$$

where  $T_2$  contains all terms in the kinetic energy that are quadratic in generalized velocities and  $T_0$  contains all terms that are independent of generalized velocities.  $V$  is the potential energy of the system. In the present case, the generalized coordinates used are the components of the position vector expressed in the asteroid body fixed reference frame,  $X$ ,  $Y$  and  $Z$ . Based on this, the equation for the kinetic energy of a unit mass spacecraft in the inertial reference frame is:

$$T = \frac{1}{2} \left[ \left( \dot{X}^2 + \dot{Y}^2 + \dot{Z}^2 \right) + \Omega^2 (X^2 + Y^2 + Z^2) \right] \quad (2.11)$$

where  $\Omega$  is the angular velocity of the asteroid body fixed reference frame,  $X$ ,  $Y$ ,  $Z$  and  $\dot{X}$ ,  $\dot{Y}$ ,  $\dot{Z}$  represent the components of the position and the velocity of the unit mass expressed in the asteroid body fixed reference frame.  $\left( \dot{X}^2 + \dot{Y}^2 + \dot{Z}^2 \right)$  corresponds to  $T_2$  and  $\Omega^2 (X^2 + Y^2 + Z^2)$  corresponds to  $T_0$ .

In the actual system, the only force acting on the spacecraft is the gravitational force, which is a conservative force. By definition, the gravitational potential energy of a unit mass spacecraft is the negative value of the gravitational potential of the asteroid at point P located at the center of mass of the spacecraft:

$$V_{grav} = -U_{grav} \quad (2.12)$$

The Hamiltonian is then:

$$H = \frac{1}{2} \left[ \left( \dot{X}^2 + \dot{Y}^2 + \dot{Z}^2 \right) - \Omega^2 (X^2 + Y^2 + Z^2) \right] - U_{grav} \quad (2.13)$$

A simulation of the motion of a unit mass spacecraft around a model of the single asteroid Eros was run for a simulated duration of three days. As shown in Fig. 2–3, the Hamiltonian was conserved throughout the simulation. This gives us confidence in the dynamics simulation code developed.

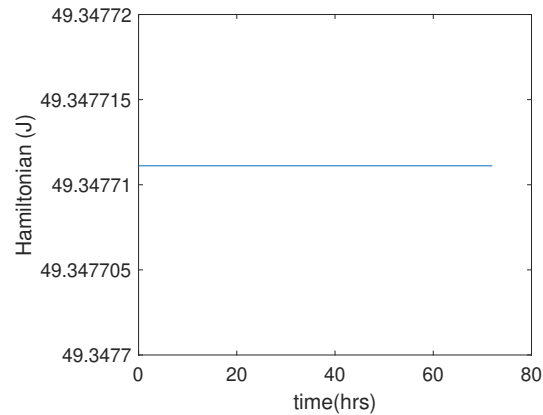


Figure 2–3: Constant Hamiltonian for a unit mass spacecraft orbiting asteroid Eros

Next, the validation of the gravitational model is done by comparing simulation results with those found in Ref. [39], where a model based on spherical harmonics of the fourth order was used. For this exercise, the same spacecraft model and orbit as the ones used in their paper were utilized. The norm of the forces calculated over a full orbit of the spacecraft for each order term of the gravitational potential were compared. They are presented in Figs. 2–4 and 2–5.

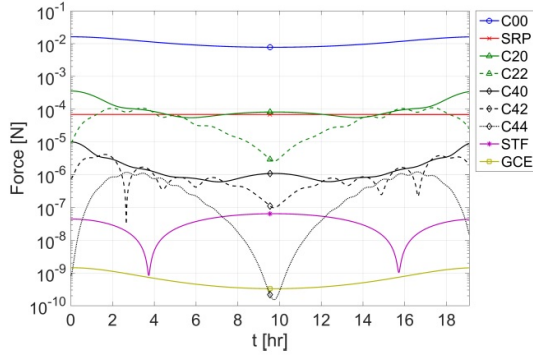


Figure 2–4: Variation of forces acting on spacecraft over one orbit [39]

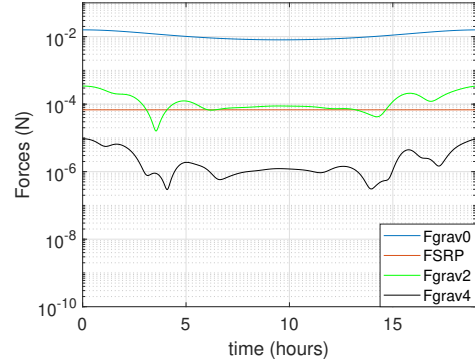


Figure 2–5: Variation of forces acting on spacecraft over one orbit

The forces calculated by the different potential order terms are similar (see Figures 2–4 and 2–5). In these figures, the blue curve represents the force from the zeroth-order term of the gravitational potential, the green ones the force from the second-order terms of the gravitational potential and the black ones the force from the fourth-order terms of the gravitational potential. The force contributions are of the same order of magnitude and follow a similar trend for each of the order terms of the gravitational potential. The main difference is that the individual order terms in the Taylor series cannot be separated into different terms like those for the spherical harmonics. As there are not a lot of available data on the subject, this has been the best possible validation exercise. Both models being an approximation of the gravitational potential, this exercise is mainly qualitative.

### 2.3 Gravitational Potential of a Binary Asteroid System

The gravitational potential of a binary asteroid system is the sum of the gravitational potential of each of the primary bodies. A graphical description of the parameters used in the calculation of the gravitational potential is shown in Fig.2–6.

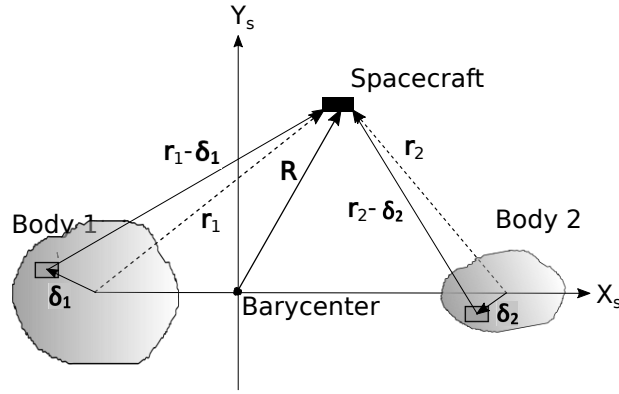


Figure 2–6: Geometry of the gravitational potential

In Fig. 2–6,  $R$  is the position vector of the center of mass of the spacecraft with respect to the barycenter of the binary asteroid system,  $\delta_i$  is the position vector of a mass element of body  $i$  with respect to the center of mass of primary body  $i$ ,  $r_i$  is the position vector of the center of mass of the spacecraft with respect to the center of mass of primary body  $i$  and  $r_i - \delta_i$  is the position vector of the center of mass of the spacecraft with respect to a mass element of body  $i$ .

In the case of a binary asteroid system, the calculations are made in the synodic reference frame, which rotates with the same angular velocity than that of the system as a whole. The primary bodies are orbiting their barycenter, which is located at the origin of the synodic reference frame. Their rotational motion is about the  $Z_S$  axis of the synodic reference frame. Each primary body has its own angular velocity, which can be different from that of the system as a whole. The primary body  $i$  fixed reference frame is then not necessarily aligned with the synodic reference frame. This particularity needs to be taken into account in the calculation of the gravitational potential. The expression for the gravitational potential of primary body  $i$ , expressed

in the synodic reference frame, is as follows. The total gravitational potential is the sum of  $U_{grav1}$  and  $U_{grav2}$ .

$$\begin{aligned}
U_{gravi} = & \frac{GM_i}{R_i} + \frac{3G}{2R_i^3} \left[ \frac{1}{3} (I_{xxi} + I_{yyi} + I_{zz}) - \frac{1}{R^2} (X_i^2 I_{xxi} + Y_i^2 I_{yyi} + Z_i^2 I_{zz}) \right] \\
& + \frac{G}{8R_i^5} \left[ \frac{35}{R_i^4} \left\{ X_i^4 J_{xxxxi} + Y_i^4 J_{yyyyi} + Z_i^4 J_{zzzzi} \right. \right. \\
& \left. \left. + 6 (X_i^2 Y_i^2 J_{xxyyi} + Y_i^2 Z_i^2 J_{yyzzi} + Z_i^2 X_i^2 J_{zzxzi}) \right\} \right. \\
& \left. - \frac{30}{R_i^2} \left\{ X_i^2 J_{xxxxi} + Y_i^2 J_{yyyyi} + Z_i^2 J_{zzzzi} \right. \right. \\
& \left. \left. + (X_i^2 + Y_i^2) J_{xxyyi} + (Y_i^2 + Z_i^2) J_{yyzzi} + (Z_i^2 + X_i^2) J_{zzxzi} \right\} \right. \\
& \left. + 3 (J_{xxxxi} + J_{yyyyi} + J_{zzzzi}) + 6 (J_{xxyyi} + J_{yyzzi} + J_{zzxzi}) \right], i = 1, 2
\end{aligned} \tag{2.14}$$

where  $X_i$ ,  $Y_i$ ,  $Z_i$  are the components of the position vector of the spacecraft with respect to the center of mass of primary body  $i$  in the primary body  $i$ -fixed reference frame and can be calculated using the direction cosine transformation matrix (DCM) relating the components in the primary body  $i$ -fixed reference frame to those in the synodic reference frame ( $C_{biS}$ ):

$$\begin{bmatrix} X_i \\ Y_i \\ Z_i \end{bmatrix} = C_{biS} \begin{bmatrix} X_{S_i} \\ Y_{S_i} \\ Z_{S_i} \end{bmatrix} = \begin{bmatrix} \cos \alpha_i & \sin \alpha_i & 0 \\ -\sin \alpha_i & \cos \alpha_i & 0 \\ 0 & 0 & 1 \end{bmatrix} \begin{bmatrix} X_{S_i} \\ Y_{S_i} \\ Z_{S_i} \end{bmatrix} \tag{2.15}$$

where  $X_{S_i}$ ,  $Y_{S_i}$  and  $Z_{S_i}$  are the components of the position vector of the spacecraft with respect to the center of mass of primary body  $i$  expressed in the synodic reference frame. The  $X_{S_1}$  and  $X_{S_2}$  components are calculated as follows:

$$\begin{aligned} X_{S_1} &= X_S + \mu R \\ X_{S_2} &= X_S - (1 - \mu) R \end{aligned} \tag{2.16}$$

where  $X_S$  is the  $X$  component of the position vector of the center of mass of the spacecraft with respect to the barycenter of the binary asteroid system expressed in the synodic reference frame. The primary bodies of a binary asteroid system are located along the  $X_S$  axis of the synodic reference frame, which means that the  $Y_{S_i}$  and  $Z_{S_i}$  components of the position vector of the spacecraft with respect to the center of mass of primary body  $i$  have the same value than the  $Y_S$  and  $Z_S$  components of the position vector of the center of mass of the spacecraft with respect to the barycenter of the binary asteroid system. The rotation of the primary bodies of the binary asteroid system being only about the  $Z_S$  axis of the synodic reference frame,  $Z_S$  has the same value as  $Z_i$ .

#### **2.4 Determination of the Gravitational Potential of a Binary Asteroid System Using Layered Mascons**

A layered mascons model can be used when a polyhedron shape model of the primary bodies is available and permits to compute the gravitational potential with greater detail than the Taylor series expansion model. The mascons are distributed in the irregular small body via an algorithm developed by Venditti et al. and detailed in Ref. [41]. In this algorithm, the polyhedron shape model is used to build the shape of the body. The body is separated into multiple layers, each of them containing the

same number of tetrahedrons as the number of faces of the polyhedron shape model. A mascon is located at the center of mass of each tetrahedron, building the layered mascon model of the body. This can be applied to the primary bodies of a binary asteroid system. Figure 2–7 shows the final result of the distribution of the mascons in the binary asteroid system 65803 Didymos.

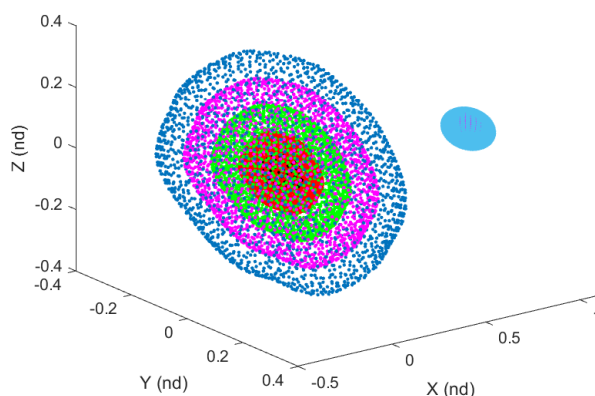


Figure 2–7: Graphical representation of the Didymos binary asteroid system using a layered mascons model

Once the position and the mass of the mascons are known, the total gravitational potential of the binary asteroid system is given by:

$$U_{grav} = \sum_{i=1}^{N_1} \frac{Gdm_{1i}}{|\mathbf{R}_1 - \boldsymbol{\delta}_{1i}|} + \sum_{j=1}^{N_2} \frac{Gdm_{2j}}{|\mathbf{R}_2 - \boldsymbol{\delta}_{2j}|} \quad (2.17)$$

where  $dm_{1i}$  is the mass of tetrahedron  $i$  of body 1,  $dm_{2j}$  is the mass of tetrahedron  $j$  of body 2,  $\boldsymbol{\delta}_{1i}$  is the position vector of the position of the center of mass of tetrahedron  $i$  of body 1 with respect to the center of mass of body 1,  $\boldsymbol{\delta}_{2j}$  is the position vector of the position of the center of mass of tetrahedron  $j$  of body 2 with respect to the

center of mass of body 2,  $N_1$  is the number of tetrahedrons composing body 1 and  $N_2$  is the number of tetrahedrons composing body 2.

The layered mascons method uses much simpler equations than the Taylor series expansion since it is simply adding zeroth-order terms. This method requires more computing power to calculate the gravitational potential than the inertia approach because of the summation that needs to be executed at each step. However, it is much less computationally expensive than the formal polyhedron shape based gravitational potential calculation, while using the detailed shape of the body.

## 2.5 Non-dimensionalization

Non-dimensionalization of the terms in an equation (or expression) is done by removing the units of the variables involved in the problem. Non-dimensionalization simplifies the equations and the calculations by reducing the variation of the values of the variables in the problem, avoiding having very large and very small values in the same calculation. The first step in non-dimensionalization is to choose characteristic parameters of size, distance and rotation rate, as well as a mass parameter.

The characteristic size in this study is the largest semi-axis of the biggest primary body of the binary asteroid system,  $r_0$ . It is used to non-dimensionalize the moments of inertia of the primary bodies of the binary asteroid system. The characteristic length of the mutual orbit of the primary bodies,  $l$ , is the nominal distance between the centers of mass of the primary bodies of a binary asteroid system. It is used to non-dimensionalize distance-related quantities, such as the position of the spacecraft.

The characteristic rotation rate,  $n$ , is the rotation rate of a system with spherical primary bodies of the same masses as the ones of the system and the same distance

separating their centers of mass  $l$ . It is calculated by:

$$n = \left( \frac{G (M_1 + M_2)}{l^3} \right)^{\frac{1}{2}} \quad (2.18)$$

The mass parameter is the ratio of the mass of the smallest primary body to the total mass of the binary asteroid system:

$$\mu = \frac{M_2}{M_1 + M_2} \quad (2.19)$$

These characteristic parameters are used to calculate the non-dimensionalized parameters used in the dynamics model. For example, the non-dimensionalized time is  $\tau = nt$ , the non-dimensionalized position coordinates of the spacecraft are  $x = X/l, y = Y/l, z = Z/l$ , the non-dimensionalized velocities of the spacecraft are  $x' = \dot{X}/nl, y' = \dot{Y}/nl, z' = \dot{Z}/nl$  and the non-dimensionalized accelerations are  $x'' = \ddot{X}/n^2l, y'' = \ddot{Y}/n^2l, z'' = \ddot{Z}/n^2l$ . Note that  $()'$  and  $()''$  denote differentiation with respect to the non-dimensionalized time,  $\tau$ .

Other non-dimensionalized parameters of the binary asteroid system used here are the following:

Non-dimensionalized reciprocal of the distance between the centers of mass of the primary bodies:

$$u = \frac{l}{R} \quad (2.20)$$

Square of the ratio between the characteristic distance  $l$  and the characteristic primary body size  $r_0$  of the binary asteroid system,  $\epsilon$ :

$$\epsilon = \left( \frac{r_0}{l} \right)^2 \quad (2.21)$$

Non-dimensionalized rotation rate of the binary asteroid system:

$$\omega = \frac{\Omega}{n} \quad (2.22)$$

where  $\Omega$  is the dimensional rotation rate of the binary asteroid system.

Non-dimensionalized inertia parameters of the primary bodies:

$$\begin{aligned} \rho_{\alpha\alpha}^2 &= \frac{I_{\alpha\alpha}}{r_0^2 M} \\ \rho_{\alpha\alpha\alpha\alpha}^4 &= \frac{J_{\alpha\alpha\alpha\alpha}}{r_0^4 M} \\ \rho_{\alpha\alpha\beta\beta}^4 &= \frac{J_{\alpha\alpha\beta\beta}}{r_0^4 M} \end{aligned} \quad (2.23)$$

where  $M$  is the total mass of the single asteroid or of the binary asteroid system.

The non-dimensional expression for the gravitational potential of a binary asteroid system is then:

$$\begin{aligned} U_{grav} = \sum_{i=1}^2 \mu_i & \left\{ \frac{1}{r_{i3}} + \frac{3}{2r_{i3}^3} \epsilon \left[ \frac{1}{3} (\rho_{xxi}^2 + \rho_{yyi}^2 + \rho_{zz_i}^2) - \frac{1}{r_{i3}^2} (x_i^2 \rho_{xxi}^2 + y_i^2 \rho_{yyi}^2 + z^2 \rho_{zz_i}^2) \right] \right. \\ & + \frac{1}{8r_{i3}^5} \epsilon^2 \left[ \frac{35}{r_{i3}^4} (x_i^4 \rho_{xxxxi}^4 + y_i^4 \rho_{yyyyi}^4 + z^4 \rho_{zzzz_i}^4 \right. \\ & + 6 ((x_i y_i)^2 \rho_{xxyyi}^4 + (y_i z)^2 \rho_{yyzzi}^4 + (x_i z)^2 \rho_{zzxxi}^4) \\ & - \frac{30}{r_{i3}^2} (x_i^2 \rho_{xxxxi}^4 + y_i^2 \rho_{yyyyi}^4 + z^2 \rho_{zzzz_i}^4 \\ & + (x_i^2 + y_i^2) \rho_{xxyyi}^4 + (y_i^2 + z^2) \rho_{yyzzi}^4 + (z^2 + x_i^2) \rho_{zzxxi}^4) \\ & \left. \left. + 3 (\rho_{xxxxi}^4 + \rho_{yyyyi}^4 + \rho_{zzzz_i}^4) + 6 (\rho_{xxyyi}^4 + \rho_{yyzzi}^4 + \rho_{zzxxi}^4) \right] \right\} \end{aligned} \quad (2.24)$$

where  $\mu_1 = (1 - \mu)$  and  $\mu_2 = \mu$ .



The gravitational forces in the  $Y_s$  and  $Z_s$  directions of the synodic reference frame give similar results. They are omitted here for brevity.

## 2.6 Summary

This chapter has put the fundamentals of the study of the motion of a spacecraft in the vicinity of a small irregular body: the modeling of its gravitational potential. A model using a Taylor series of the fourth order was presented and compared with a model using spherical harmonics of the fourth order. Both models gave similar results. The demonstration of the conservation of the Hamiltonian principle completed the validation of the model. The case of a binary asteroid composed of irregular bodies was then studied. Two ways to model it were discussed: a Taylor series expansion of the fourth order and a layered mascon model. The non-dimensionalization of the variables used in the FRTBP was described. These variables will be used throughout this thesis. The next chapter studies the motion of the primary bodies of a binary asteroid system, the FTBP.

## CHAPTER 3

### The Full Two Body Problem

The FTBP describes the motion of the primary bodies of a binary system. The FRTBP, which describes the motion of the third body, the spacecraft, in that system depends on the mutual motion of the primary bodies. In this chapter, the term "Full" means that the irregular shape of the primary bodies is considered in the binary asteroid model. The individual primary bodies have angular velocities that are different from the angular velocity of the system as a whole and their mutual motion around the barycenter of the system can be non-circular. In the current thesis, the motion of the primary bodies is assumed to be planar, as is the case for the binary asteroid 65803 Didymos. It is also assumed that the primary bodies' axes of rotation coincide with the angular momentum vector of the binary asteroid system as per the description of the system made in Ref. [15]. The biggest body is called body 1 and the smallest body is called body 2. The binary asteroid system is assumed here to be stand alone, which means that external influences, such as the gravitational field of the Sun, are not taken into account. Figure 3-1 illustrates the FTBP with the definition of its parameters  $R$ ,  $\alpha_1$ ,  $\alpha_2$ ,  $\theta$  and the inertial, body 1 fixed, body 2 fixed and synodic reference frames. These are described in more detail in Appendix A.

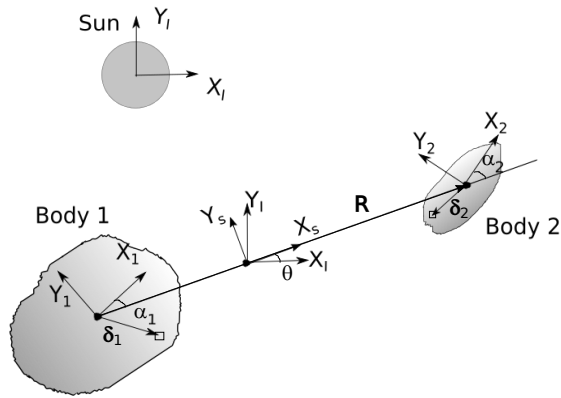


Figure 3-1: The full two body problem

### 3.1 Equations of Motion of a Binary Asteroid System

The equations of motion for the Full Two Body Problem are developed here based on Lagrange's equations. The expression for the gravitational potential is based on Eq. 2.7. Considering that the mass of body 1 is  $M_1$  and the mass of body 2 is  $M_2$ , the potential energy, using a fourth-order gravitational potential model, is given as:

$$\begin{aligned}
V_{1-2} = & -\frac{GM_1M_2}{R} - \frac{3GM_2}{2R^3} \left[ \frac{1}{3} \text{tr} [I_1] - \{\mu_{R,1}\}^T [I_1] \{\mu_{R,1}\} \right] \\
& - \frac{3GM_1}{2R^3} \left[ \frac{1}{3} \text{tr} [I_2] - \{\mu_{R,2}\}^T [I_2] \{\mu_{R,2}\} \right] \\
& - \frac{GM_2}{8R^5} \left[ (35\hat{u}_{Rx,1}^4 - 30\hat{u}_{Rx,1}^2 + 3) J_{xxxx1} + (35\hat{u}_{Ry,1}^4 - 30\hat{u}_{Ry,1}^2 + 3) J_{yyyy1} \right. \\
& + (35\hat{u}_{Rz,1}^4 - 30\hat{u}_{Rz,1}^2 + 3) J_{zzzz1} \\
& + 6(35\hat{u}_{Rx,1}^2\hat{u}_{Ry,1}^2 - 5(\hat{u}_{Rx,1}^2 + \hat{u}_{Ry,1}^2) + 1) J_{xxyy1} \\
& + 6(35\hat{u}_{Ry,1}^2\hat{u}_{Rz,1}^2 - 5(\hat{u}_{Ry,1}^2 + \hat{u}_{Rz,1}^2) + 1) J_{yyzz1} \\
& \left. + 6(35\hat{u}_{Rz,1}^2\hat{u}_{Rx,1}^2 - 5(\hat{u}_{Rz,1}^2 + \hat{u}_{Rx,1}^2) + 1) J_{zzxx1} \right] \\
& - \frac{GM_1}{8R^5} \left[ (35\hat{u}_{Rx,2}^4 - 30\hat{u}_{Rx,2}^2 + 3) J_{xxxx2} + (35\hat{u}_{Ry,2}^4 - 30\hat{u}_{Ry,2}^2 + 3) J_{yyyy2} \right. \\
& + (35\hat{u}_{Rz,2}^4 - 30\hat{u}_{Rz,2}^2 + 3) J_{zzzz2} \\
& + 6(35\hat{u}_{Rx,2}^2\hat{u}_{Ry,2}^2 - 5(\hat{u}_{Rx,2}^2 + \hat{u}_{Ry,2}^2) + 1) J_{xxyy2} \\
& + 6(35\hat{u}_{Ry,2}^2\hat{u}_{Rz,2}^2 - 5(\hat{u}_{Ry,2}^2 + \hat{u}_{Rz,2}^2) + 1) J_{yyzz2} \\
& \left. + 6(35\hat{u}_{Rz,2}^2\hat{u}_{Rx,2}^2 - 5(\hat{u}_{Rz,2}^2 + \hat{u}_{Rx,2}^2) + 1) J_{zzxx2} \right]
\end{aligned} \tag{3.1}$$

To develop the equations of motion (EoM) of the binary system using Lagrange's equations, the following general coordinates are chosen:

- $R$  is the distance between the centers of mass of the bodies
- $\theta$  is the angle between the  $X_S$  axis of the synodic reference frame and the  $X_I$  axis of the inertial reference frame (aligned with the Sun)

- $\alpha_1$  is the angle between the  $X_1$  axis of the body 1 fixed reference frame and the  $X_S$  axis of the synodic reference frame (which is in the direction of the imaginary line joining the centers of mass of the primary bodies)
- $\alpha_2$  is the angle between the  $X_2$  axis of the body 2 fixed reference frame and the  $X_S$  axis of the synodic reference frame

The equation for kinetic energy only uses 2nd order terms:

$$T = \frac{1}{2} \frac{M_1 M_2}{M_1 + M_2} \left( \dot{R}^2 + R^2 \dot{\theta}^2 \right) + \frac{1}{2} I_{zz1} \left( \dot{\theta} + \dot{\alpha}_1 \right)^2 + \frac{1}{2} I_{zz2} \left( \dot{\theta} + \dot{\alpha}_2 \right)^2 \quad (3.2)$$

The generalized coordinates are then:

$$q = \left[ R \quad \theta \quad \alpha_1 \quad \alpha_2 \right] \quad (3.3)$$

The system is considered to have planar motion and the primary bodies are always located on the  $X_S$  axis of the synodic reference frame, so the  $\hat{u}_{Ri,j}$  for the  $i$  direction and  $j$  primary bodies 1 and 2 are:

$$\begin{aligned} \hat{u}_{Rx,1} &= \cos \alpha_1; \hat{u}_{Rx,2} = \cos \alpha_2 \\ \hat{u}_{Ry,1} &= -\sin \alpha_1; \hat{u}_{Ry,2} = -\sin \alpha_2 \\ \hat{u}_{Rz,1} &= \hat{u}_{Rz,2} = 0 \end{aligned} \quad (3.4)$$

With these assumptions, and after some algebra, the gravitational potential energy of the binary asteroid system is:

$$\begin{aligned}
V_{1-2} = & -\frac{GM_1M_2}{R} + \frac{3GM_2}{2R^3} \left[ I_{xx1} \cos^2 \alpha_1 + I_{yy1} \sin^2 \alpha_1 - \frac{1}{3} (I_{xx1} + I_{yy1} + I_{zz1}) \right] \\
& + \frac{3GM_1}{2R^3} \left[ I_{xx2} \cos^2 \alpha_2 + I_{yy2} \sin^2 \alpha_2 - \frac{1}{3} (I_{xx2} + I_{yy2} + I_{zz2}) \right] \\
& - \frac{GM_2}{8R^5} \left[ 35 (\cos^4 \alpha_1 J_{xxxx1} + \sin^4 \alpha_1 J_{yyyy1}) \right. \\
& - 30 (\cos^2 \alpha_1 J_{xxxx1} + \sin^2 \alpha_1 J_{yyyy1}) \\
& + 3 (J_{xxxx1} + J_{yyyy1} + J_{zzz1}) + 210 (\cos^2 \alpha_1 \sin^2 \alpha_1) J_{xxyy1} \\
& \left. - 30 (J_{xxyy1} + \sin^2 \alpha_1 J_{yyzz1} + \cos^2 \alpha_1 J_{zzxx1}) + 6 (J_{xxyy1} + J_{yyzz,1} + J_{zzxx1}) \right] \\
& - \frac{GM_1}{8R^5} \left[ 35 (\cos^4 \alpha_2 J_{xxxx2} + \sin^4 \alpha_2 J_{yyyy2}) \right. \\
& - 30 (\cos^2 \alpha_2 J_{xxxx2} + \sin^2 \alpha_2 J_{yyyy2}) \\
& + 3 (J_{xxxx2} + J_{yyyy2} + J_{zzz2}) + 210 (\cos^2 \alpha_2 \sin^2 \alpha_2) J_{xxyy2} \\
& \left. - 30 (J_{xxyy2} + \sin^2 \alpha_2 J_{yyzz2} + \cos^2 \alpha_2 J_{zzxx2}) + 6 (J_{xxyy2} + J_{yyzz2} + J_{zzxx2}) \right]
\end{aligned} \tag{3.5}$$

The equations of motion are developed based on Lagrange's equations:

$$\frac{d}{dt} \frac{\partial T}{\partial \dot{q}_j} - \frac{\partial T}{\partial q_j} + \frac{\partial V}{\partial q_j} = 0 \tag{3.6}$$

In the coming section, the non-dimensionalization of the equations of motion is done as in section 2.5.

### 3.1.1 Development of the Equations for Each Generalized Coordinates

In this section, the equations for each generalized coordinate are given in details.

#### Equation for the Generalized Coordinate $R$

After some algebra, the equation for the generalized coordinate  $R$  is:

$$\begin{aligned}
\ddot{R} = & R\dot{\theta}^2 - \frac{G(M_1 + M_2)}{R^2} \\
& + \frac{9}{2R^4} \frac{G(M_1 + M_2)}{M_1} \left[ I_{xx1} \cos^2 \alpha_1 + I_{yy1} \sin^2 \alpha_1 - \frac{1}{3} (I_{xx1} + I_{yy1} + I_{zz1}) \right] \\
& + \frac{9}{2R^4} \frac{G(M_1 + M_2)}{M_2} \left[ I_{xx2} \cos^2 \alpha_2 + I_{yy2} \sin^2 \alpha_2 - \frac{1}{3} (I_{xx2} + I_{yy2} + I_{zz2}) \right] \\
& - \frac{5}{8R^6} \frac{G(M_1 + M_2)}{M_1} \left[ 35 (\cos^4 \alpha_1 J_{xxxx,1} + \sin^4 \alpha_1 J_{yyyy,1}) \right. \\
& - 30 (\cos^2 \alpha_1 J_{xxxx,1} + \sin^2 \alpha_1 J_{yyyy,1}) \\
& + 3 (J_{xxx,1} + J_{yyy,1} + J_{zzz,1}) + 210 (\cos^2 \alpha_1 \sin^2 \alpha_1) J_{xxyy,1} \\
& \left. - 30 (J_{xxyy,1} + \sin^2 \alpha_1 J_{yyzz,1} + \cos^2 \alpha_1 J_{zzxx,1}) + 6 (J_{xxyy,1} + J_{yyzz,1} + J_{zzxx,1}) \right] \\
& - \frac{5}{8R^6} \frac{G(M_1 + M_2)}{M_2} \left[ 35 (\cos^4 \alpha_2 J_{xxxx,2} + \sin^4 \alpha_2 J_{yyyy,2}) \right. \\
& - 30 (\cos^2 \alpha_2 J_{xxxx,2} + \sin^2 \alpha_2 J_{yyyy,2}) \\
& + 3 (J_{xxx,2} + J_{yyy,2} + J_{zzz,2}) + 210 (\cos^2 \alpha_2 \sin^2 \alpha_2) J_{xxyy,2} \\
& \left. - 30 (J_{xxyy,2} + \sin^2 \alpha_2 J_{yyzz,2} + \cos^2 \alpha_2 J_{zzxx,2}) + 6 (J_{xxyy,2} + J_{yyzz,2} + J_{zzxx,2}) \right]
\end{aligned} \tag{3.7}$$

After non-dimensionalizing and making a change of variable from  $r$  to  $u$ , the reciprocal of the non-dimensionalized distance between the centers of mass of the primary bodies of the binary asteroid system, and after some algebra, the expression

for  $u''$  is:

$$\begin{aligned}
u'' = & \frac{2u'^2}{u} - u\theta'^2 + u^4 \\
& - \frac{9u^6}{2}\epsilon \left[ \rho_{xx1}^2 \cos^2 \alpha_1 + \rho_{yy1}^2 \sin^2 \alpha_1 - \frac{1}{3} (\rho_{xx1}^2 + \rho_{yy1}^2 + \rho_{zz1}^2) \right] \\
& - \frac{9u^6}{2}\epsilon \left[ \rho_{xx2}^2 \cos^2 \alpha_2 + \rho_{yy2}^2 \sin^2 \alpha_2 - \frac{1}{3} (\rho_{xx2}^2 + \rho_{yy2}^2 + \rho_{zz2}^2) \right] \\
& + \frac{5u^8}{8}\epsilon^2 \left[ 35 (\cos^4 \alpha_1 \rho_{xxxx1}^4 + \sin^4 \alpha_1 \rho_{yyyy1}^4) \right. \\
& - 30 (\cos^2 \alpha_1 \rho_{xxxx1}^4 + \sin^2 \alpha_1 \rho_{yyyy1}^4) \\
& + 3 (\rho_{xxxx1}^4 + \rho_{yyyy1}^4 + \rho_{zzzz1}^4) + 210 (\cos^2 \alpha_1 \sin^2 \alpha_1) \rho_{xxyy1}^4 \\
& \left. - 30 (\rho_{xxyy1}^4 + \sin^2 \alpha_1 \rho_{yyzz1}^4 + \cos^2 \alpha_1 \rho_{zzxx1}^4) + 6 (\rho_{xxyy1}^4 + \rho_{yyzz1}^4 + \rho_{zzxx1}^4) \right] \\
& + \frac{5u^8}{8}\epsilon^2 \left[ 35 (\cos^4 \alpha_2 \rho_{xxxx2}^4 + \sin^4 \alpha_2 \rho_{yyyy2}^4) \right. \\
& - 30 (\cos^2 \alpha_2 \rho_{xxxx2}^4 + \sin^2 \alpha_2 \rho_{yyyy2}^4) \\
& + 3 (\rho_{xxxx2}^4 + \rho_{yyyy2}^4 + \rho_{zzzz2}^4) + 210 (\cos^2 \alpha_2 \sin^2 \alpha_2) \rho_{xxyy2}^4 \\
& \left. - 30 (\rho_{xxyy2}^4 + \sin^2 \alpha_2 \rho_{yyzz2}^4 + \cos^2 \alpha_2 \rho_{zzxx2}^4) + 6 (\rho_{xxyy2}^4 + \rho_{yyzz2}^4 + \rho_{zzxx2}^4) \right]
\end{aligned} \tag{3.8}$$

### Equation for the Generalized Coordinate $\theta$

The equations for the generalized coordinate  $\theta$  reflect the principle of conservation of angular momentum. The dimensional equation:

$$\frac{d}{dt} \frac{\partial T}{\partial \dot{\theta}} = 0 \tag{3.9}$$

represents the conservation of angular momentum, which means that:

$$\frac{\partial T}{\partial \dot{\theta}} = h \quad (3.10)$$

where  $h$  is the constant of integration and is calculated based on the initial conditions of the system. In that case,  $\dot{\theta}$  is calculated using:

$$\dot{\theta} = \frac{M_1 + M_2}{M_1 M_2} \frac{1}{R^2} \left[ h - I_{zz1} (\dot{\theta} + \dot{\alpha}_1) - I_{zz2} (\dot{\theta} + \dot{\alpha}_2) \right] \quad (3.11)$$

The non-dimensionalized version of the equation is:

$$\theta' = \frac{hu^2}{nl^2} + \epsilon u^2 \left( \frac{\rho_{zz1}^2}{\mu} (\theta' + \alpha_1') + \frac{\rho_{zz2}^2}{1 - \mu} (\theta' + \alpha_2') \right) \quad (3.12)$$

### Equations for the Generalized Coordinates $\alpha_1$ and $\alpha_2$

The generalized coordinates  $\alpha_1$  and  $\alpha_2$  are paired with the generalized coordinate  $\theta$  in their equations:

$$\begin{aligned} \ddot{\theta} + \ddot{\alpha}_1 = & \frac{1}{I_{zz1}} \left[ -\frac{3GM_2}{2R^3} \left[ \sin 2\alpha_1 (I_{yy1} - I_{xx1}) \right] \right. \\ & + \frac{GM_2}{8R^5} \left[ (-70 \cos \alpha_1^2 \sin 2\alpha_1 + 30 \sin 2\alpha_1) J_{xxxx1} \right. \\ & + (70 \sin \alpha_1^2 \sin 2\alpha_1 - 30 \sin 2\alpha_1) J_{yyyy1} + 210 (-\sin \alpha_1^2 \sin 2\alpha_1 + \sin 2\alpha_1) J_{xyy1} \\ & \left. \left. + 30 (-\sin 2\alpha_1 J_{yyzz1} + \sin 2\alpha_1 J_{zzxx1}) \right] \right] \end{aligned} \quad (3.13)$$

The equation related to the sum of  $\theta$  and  $\alpha_2$  is:

$$\begin{aligned}
\ddot{\theta} + \ddot{\alpha}_2 = & \frac{1}{I_{zz2}} \left[ -\frac{3GM_1}{2R^3} \left[ \sin 2\alpha_2 (I_{yy2} - I_{xx2}) \right] \right. \\
& + \frac{GM_1}{8R^5} \left[ (-70 \cos \alpha_2^2 \sin 2\alpha_2 + 30 \sin 2\alpha_2) J_{xxxx2} \right. \\
& + (70 \sin \alpha_2^2 \sin 2\alpha_2 - 30 \sin 2\alpha_2) J_{yyyy1} + 210 (-\sin \alpha_2^2 \sin 2\alpha_2 + \sin 2\alpha_2) J_{xxyy2} \\
& \left. \left. + 30 (-\sin 2\alpha_2 J_{yyzz2} + \sin 2\alpha_2 J_{zzxx2}) \right] \right]
\end{aligned} \tag{3.14}$$

Their non-dimensionalized versions are:

$$\begin{aligned}
\theta'' + \alpha_1'' = & \frac{3\mu u^3}{2\rho_{zz1}^2} \left[ -\sin 2\alpha_1 (\rho_{yy1}^2 - \rho_{xx1}^2) \right] \\
& + \frac{\mu u^5 \epsilon}{8\rho_{zz1}^2} \left[ (-70 \cos \alpha_1^2 \sin 2\alpha_1 + 30 \sin 2\alpha_1) \rho_{xxxx1}^4 \right. \\
& + (70 \sin \alpha_1^2 \sin 2\alpha_1 - 30 \sin 2\alpha_1) \rho_{yyyy1}^4 + 210 (-\sin \alpha_1^2 \sin 2\alpha_1 + \sin 2\alpha_1) \rho_{xxyy1}^4 \\
& \left. + 30 (-\sin 2\alpha_1 \rho_{yyzz1}^4 + \sin 2\alpha_1 \rho_{zzxx1}^4) \right]
\end{aligned} \tag{3.15}$$

and

$$\begin{aligned}
\theta'' + \alpha_2'' = & \frac{3\mu u^3}{2\rho_{zz2}^2} \left[ -\sin 2\alpha_2 (\rho_{yy2}^2 - \rho_{xx2}^2) \right] \\
& + \frac{\mu u^5 \epsilon}{8\rho_{zz2}^2} \left[ (-70 \cos \alpha_2^2 \sin 2\alpha_2 + 30 \sin 2\alpha_2) \rho_{xxxx2}^4 \right. \\
& + (70 \sin \alpha_2^2 \sin 2\alpha_2 - 30 \sin 2\alpha_2) \rho_{yyyy2}^4 + 210 (-\sin \alpha_2^2 \sin 2\alpha_2 + \sin 2\alpha_2) \rho_{xxyy2}^4 \\
& \left. + 30 (-\sin 2\alpha_2 \rho_{yyzz2}^4 + \sin 2\alpha_2 \rho_{zzxx2}^4) \right]
\end{aligned} \tag{3.16}$$

## Rotational Motion of the Primary Bodies

While solving the equations of motion of the FTBP, the angular velocity of body 1 is usually set at a value that is constant and chosen based on the measurements made on the chosen system. Body 2 is often assumed to have a mean angular velocity that is the same than that of the binary system as a whole. A libration motion is added to the rotational motion of body 2. As shown in Ref. [47], it is the eccentricity of the mutual orbit of the primary bodies that influences the libration motion of body 2. Even in the case of a system in equilibrium, libration motion still occurs with the same frequency as the mean motion of the mutual motion of the primary bodies of the binary asteroid system. According to Ref. [47], the amplitude  $\psi$  of the libration motion is:

$$\psi = \frac{2e}{\omega_0^2 - 1} \quad (3.17)$$

where  $e$  is the eccentricity of the mutual orbit of the primary bodies around their barycenter, and  $\omega_0$  is the natural frequency of libration motion normalized by the frequency of the mean motion of the mutual orbit. It is given by:

$$\omega_0 = \sqrt{3(B - C)/A} \quad (3.18)$$

where  $A$ ,  $B$  and  $C$  are the semi axes of the ellipsoid representing body 2.

### 3.2 The Case of Mutual Circular Motion

A special case of the FTBP is the case of the primary bodies orbiting their barycenter with a circular motion. It means that the inverse of the distance between their centers of mass ( $u$ ) and the angular velocity of the binary system ( $\omega = \theta'$ ) are constant. Their values will be referred to as  $u_c$  and  $\omega_c$ . To calculate the values for  $u_c$

and  $\omega_c$ , the values of  $\alpha_1$ ,  $\alpha_2$  are set to 0 and  $\alpha'_1$  and  $\alpha'_2$  are set to their mean values.

The system of equations to solve is then:

$$\begin{aligned}
0 = & -u_c \omega_c^2 + u_c^4 \\
& - \frac{3u_c^6}{2} \epsilon \left[ (2\rho_{xx1}^2 - \rho_{yy1}^2 - \rho_{zz1}^2) \right] \\
& - \frac{3u_c^6}{2} \epsilon \left[ (2\rho_{xx2}^2 - \rho_{yy2}^2 - \rho_{zz2}^2) \right] \\
& + \frac{5u_c^8}{8} \epsilon^2 \left[ (8\rho_{xxxx1}^4 + 3\rho_{yyyy1}^4 + 3\rho_{zzz1}^4) - 6(4\rho_{xxyy1}^4 - \rho_{yyzz1}^4 + 4\rho_{zzxx1}^4) \right] \\
& + \frac{5u_c^8}{8} \epsilon^2 \left[ (8\rho_{xxxx2}^4 + 3\rho_{yyyy2}^4 + 3\rho_{zzz2}^4) - 6(4\rho_{xxyy2}^4 - \rho_{yyzz2}^4 + 4\rho_{zzxx2}^4) \right]
\end{aligned} \tag{3.19}$$

and

$$0 = \omega_c - \frac{hu_c^2}{nl^2} - \epsilon u_c^2 \left( \frac{\rho_{zz1}^2}{\mu} (\omega_c + \alpha'_1) + \frac{\rho_{zz2}^2}{1-\mu} (\omega_c + \alpha'_2) \right) \tag{3.20}$$

The equations are solved numerically. The value of the constant of integration  $h$  is calculated based on Eq. 3.12:

$$h_c = \frac{nl^2}{u_c^2} \left( \omega_c - \epsilon u_c^2 \left( \frac{\rho_{zz1}^2 (\theta' + \alpha'_1)}{\mu} + \frac{\rho_{zz2}^2 (\theta' + \alpha'_2)}{1-\mu} \right) \right) \tag{3.21}$$

where  $(\theta' + \alpha'_1)$  and  $(\theta' + \alpha'_2)$  are approximate values of the angular velocity of body 1 and body 2 in the inertial reference frame. Note that the parameters  $u_c$  and  $\omega_c$  are used to adjust the initial conditions of the system when solving the equations of motion of the FTBP and the FRTBP. They represent the ratio between the  $u$  and  $\omega$  values for a binary system composed of spherical bodies and the ones for a binary system composed of non-spherical bodies.

### 3.3 Application to the Binary Asteroid System 65803 Didymos

The NASA/ESA AIDA mission planned to the binary asteroid system 65803 Didymos is one of the motivations for the research presented in this thesis. This is why a model of the binary asteroid system 65803 Didymos is used for numerical applications throughout the document. The equations of motion developed in Section 3.1 are now applied to this specific system. The Didymos system has the parameters presented in Tables 3–1 and 3–2. The values in Table 3–1 are taken from Ref. [15]. The second and fourth-order inertia integrals presented in Table 3–2 are calculated based on the Didymos polyhedron shape model, using the technique presented in Appendix C.2. The polyhedron shape model is used with the authorization from the author of Ref. [63]. For the Didymos binary asteroid system, the calculated values for  $u_c$  and  $\omega_c$  are 0.99368 and 0.99390 respectively.

Table 3–1: Didymos system parameters

<i>Parameter</i>	<i>Body 1</i>	<i>Body 2</i>	<i>System</i>
<i>Eccentricity</i>	<i>N/A</i>	<i>N/A</i>	0.03
<i>Semi – major axis(m)</i>	<i>N/A</i>	<i>N/A</i>	1180
<i>Mass(kg)</i>	$5.2294e + 11$	$4.8631e + 09$	$5.2780e + 11$
<i>Rotation period(hrs)</i>	2.26	11.92 ( <i>assumed</i> )	11.92

Table 3–2: Didymos calculated second-order moments of inertia and fourth-order inertia integrals

<i>Parameter</i>	<i>Body 1</i>	<i>Body 2</i>
$I_{xx} (kg \cdot m^2)$	$3.1348e + 16$	$1.0307e + 13$
$I_{yy} (kg \cdot m^2)$	$3.1920e + 16$	$1.4555e + 13$
$I_{zz} (kg \cdot m^2)$	$3.2790e + 16$	$1.6389e + 13$
$J_{xxxx} (kg \cdot m^4)$	$1.1722e + 21$	$4.6916e + 16$
$J_{yyyy} (kg \cdot m^4)$	$1.0963e + 21$	$1.6236e + 16$
$J_{zzzz} (kg \cdot m^4)$	$9.8672e + 20$	$7.9095e + 15$
$J_{xxyy} (kg \cdot m^4)$	$3.6539e + 20$	$9.1998e + 15$
$J_{yyzz} (kg \cdot m^4)$	$3.2277e + 20$	$3.7774e + 15$
$J_{zzxx} (kg \cdot m^4)$	$3.3555e + 20$	$6.4211e + 15$

The equations of motion of the FTBP are defined using the generalized coordinates  $u$ ,  $\theta$ ,  $\alpha_1$  and  $\alpha_2$ . The initial conditions for the generalized coordinates  $\alpha_1$  and  $\alpha_2$  are set to 0. The initial conditions of the generalized coordinates  $u_0$  and  $\theta'_0$  are calculated based on the Keplerian equations of the two-body problem, using the eccentricity,  $e$ , and the semi-major axis,  $a$ , of the assumed Keplerian mutual orbital motion of the primary bodies around the barycenter of the binary asteroid system.

In the classical two-body problem, where the bodies can be considered as point masses,  $R$  is calculated using:

$$R = \frac{a(1 - e^2)}{1 + e \cos \theta} \quad (3.22)$$

In its non-dimensionalized version, considering the nominal case where  $a = l$ ,  $r$  is:

$$r = \frac{(1 - e^2)}{(1 + e \cos \theta)} \quad (3.23)$$

For a binary system with spherical bodies, the parameter  $u$  could then be calculated using:

$$u = \frac{1}{r} = \frac{(1 + e \cos \theta)}{(1 - e^2)} \quad (3.24)$$

In the case of a binary system with non-spherical bodies, the value of the parameter  $u$  has to be adjusted using the parameter  $u_c$  calculated in section 3.2:

$$u = u_c \frac{1 + e \cos \theta}{1 - e^2} \quad (3.25)$$

Similarly,  $\theta'$  is calculated using:

$$\theta' = \omega = \omega_c \frac{(1 + e \cos \theta)^2}{(1 - e^2)^{3/2}} \quad (3.26)$$

The initial conditions  $u_0$  and  $\theta'_0$  are then the values of Eq. 3.25 and Eq. 3.26 where  $\theta$  is set to  $\theta = 0$ .

The values of  $u_0$  and  $\theta'_0$  are used to calculate the approximation of the value of the constant of integration  $h$  required to solve the equations of motion:

$$h = \frac{nl^2}{u_0^2} \left( \theta'_0 - \epsilon u_0^2 \left( \frac{\rho_{zz1}^2 (\theta' + \alpha'_1)_0}{\mu} + \frac{\rho_{zz2}^2 (\theta' + \alpha'_2)_0}{1 - \mu} \right) \right) \quad (3.27)$$

where  $(\theta' + \alpha'_1)_0$  and  $(\theta' + \alpha'_2)_0$  are the initial angular velocity of the primary bodies calculated in the inertial reference frame.

These parameters were used to simulate the mutual motion of the primary bodies of the system using the equations of motion of the FTBP. The motion of body 2 is

modeled as described in section 3.3, with the semi-axes of body 2 being  $A = 103 m$ ,  $B = 79 m$ , and  $C = 66 m$ . Figure 3–2 shows that the distance between the centers of mass of the binary bodies oscillates between  $1152 m$  and  $1230 m$ . The eccentricity is then  $0.033$ . The averaged distance between the primary bodies is of  $1191 m$ .

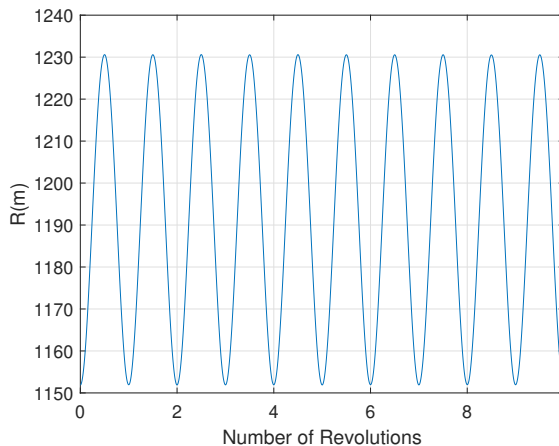


Figure 3–2: Distance  $R$  between the centers of mass of the primary bodies of the binary asteroid system for ten revolutions of the system

The Hamiltonian, in the present case is identical to the total energy of the system:

$$H = T + V \tag{3.28}$$

Figures 3–4 and 3–3 show the kinetic and potential energy over ten revolutions of the binary asteroid system. Figure 3–5 shows the total energy of the system. The actual variation of the energy being approximately  $0.004\%$ , it is considered as constant. This concludes this part of the validation of the equations of the FTBP used in the simulation model.

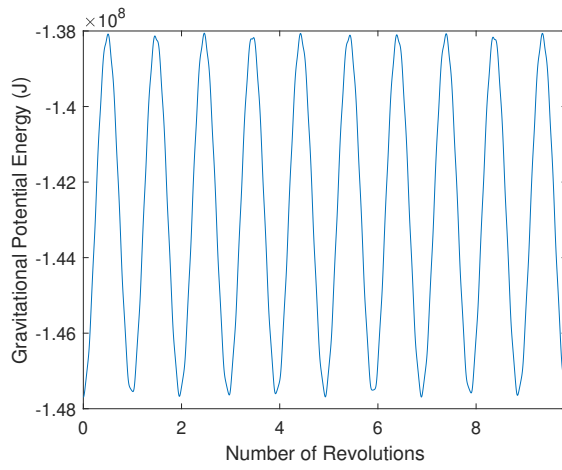


Figure 3-3: Potential energy for ten revolutions of the system

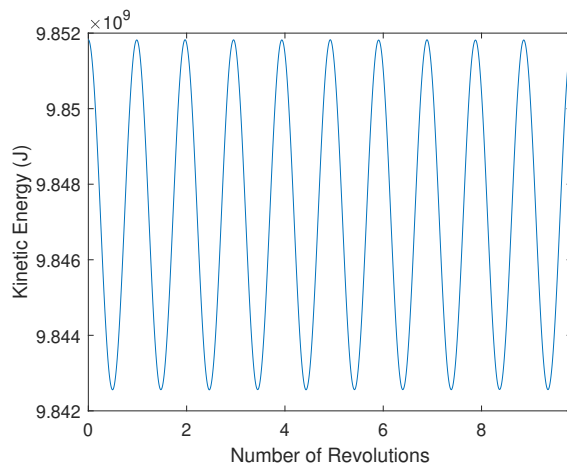


Figure 3-4: Kinetic energy for ten revolutions of the system

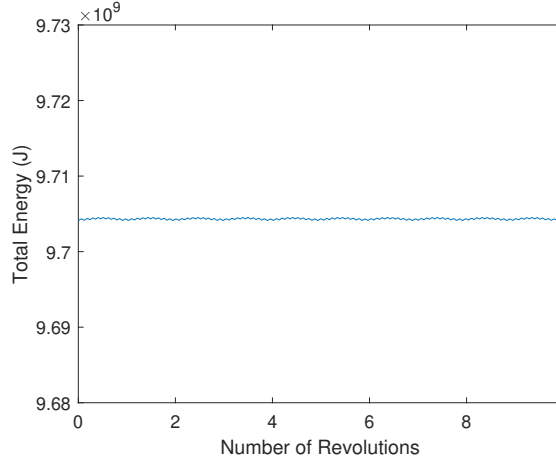


Figure 3-5: Total energy for ten revolutions of the system

### 3.3.1 Effect of Varying the Constant of Integration $h$

The parameter that affects the results presented in Figures 3-2 to 3-5 is the constant of integration  $h$ . Solving the FTBP requires to have an exact value of  $h$  which is obtained by iterating it around the result given by Eq. 3.27. Figure 3-6 shows how the generalized coordinate  $R$  changes throughout 50 revolutions of the binary asteroid system when the constant  $h$  used is the one calculated initially,  $h_0$ . To get the results seen in Fig. 3-2, the constant to use is  $1.00012h_0$ . Figure 3-7 shows the result for a value of  $0.999h_0$ . In these figures, the distance between the centers of mass of the primary bodies changes constantly.

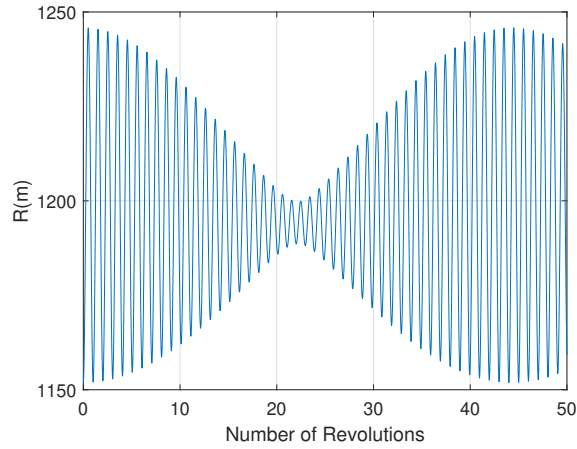


Figure 3–6: Distance  $R$  between the centers of mass of the primary bodies of the binary asteroid system for the constant  $h$  set at  $h_0$

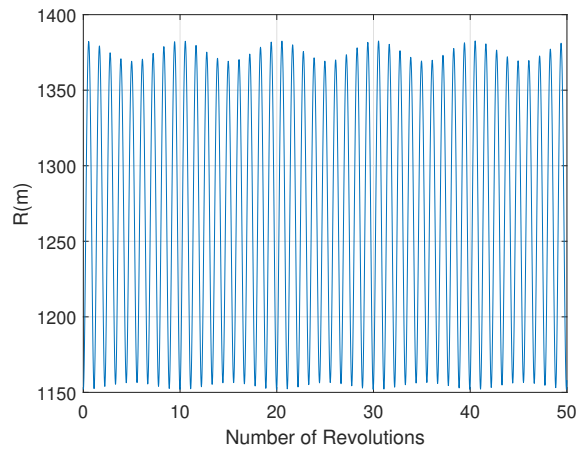


Figure 3–7: Distance  $R$  between the centers of mass of the primary bodies of the binary asteroid system for the constant  $h$  set at  $0.999h_0$

As demonstrated in Ref. [47] the motion of the primary bodies of the binary asteroid system is also highly influenced by the rotational motion of body 2, which is assumed to be librating about the  $X_S$  axis of the synodic reference frame with an

unknown exact amplitude and frequency. The equations of motion of the model of the FTBP are then highly sensitive to these unknowns and to the initial condition of their generalized coordinates.

### 3.3.2 Gravitational Potential Energy of a Binary Asteroid System Using a Layered Mascons Model

The layered mascons model described in section 2.4 can also be used to calculate the gravitational potential energy of a binary asteroid system. In this case, the equation is:

$$V_{12} = - \sum_{i=1}^{N_1} \sum_{j=1}^{N_2} \frac{Gdm_{1i}dm_{2j}}{|\mathbf{R} + \boldsymbol{\delta}_{2j} - \boldsymbol{\delta}_{1i}|} \quad (3.29)$$

This model is used to validate the fourth-order Taylor series expansion model of the gravitational potential energy of the binary asteroid system that is used to calculate the equations of motion of the FTBP.

Figure 3–8 shows how similar are the curves when the potential energy of the system is calculated using a fourth-order Taylor series expansion model vs the layered mascon model over one full orbit of the primary bodies around their barycenter.

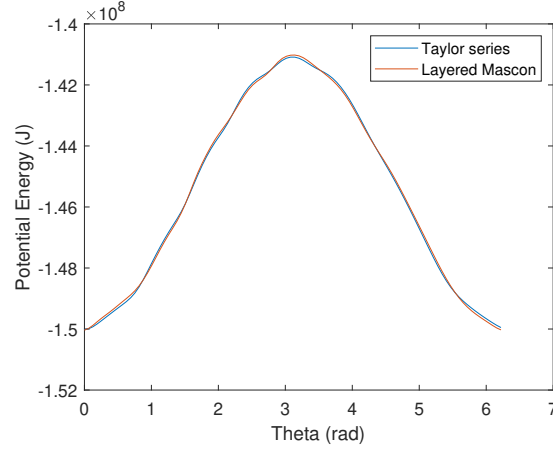


Figure 3–8: Potential energy calculated using the Taylor series expansion and the layered mascons models

To give an order of magnitude of the difference between both models, Fig. 3–9 shows the percentage of difference between the gravitational potential energy calculated with both models. The difference is less than 0.1%, which is not significant. This result shows that both models are equivalent. Because of the lower computational time required when using the fourth-order Taylor series expansion model, this model will be used in the following chapters of this thesis.

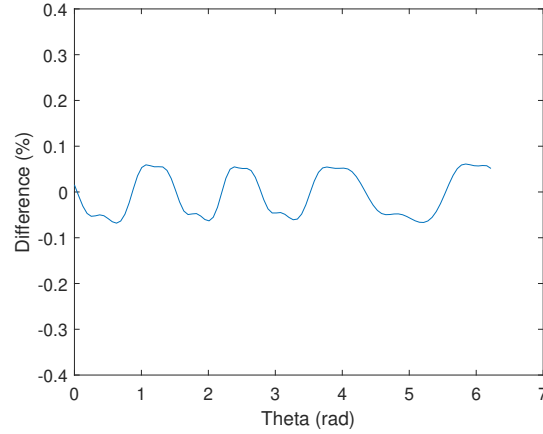


Figure 3-9: Difference in the calculation of the gravitational potential energy of the binary asteroid system

### 3.3.3 Variation of the Gravitational Potential Energy of a Binary Asteroid System due to Uncertainties in its Parameters

The distance between the primary bodies and the eccentricity of the mutual orbit of the primary bodies around the barycenter of the 65803 Didymos binary asteroid are nominally set to 1180  $m$  and 0.03. In fact, there are some uncertainties in the measurements of these values. In Ref. [15], it is stated that the distance between the primary bodies varies between 1160 and 1220  $m$  and the eccentricity has a maximal value of 0.03. In this section, the motion of body 2 is calculated using the equations for Keplerian motion adjusted for irregular bodies. It is estimated as an elliptical motion with an eccentricity  $e$ , angular frequency and reciprocal of the distance between the primary bodies of the system for circular motion of the primary bodies  $\omega_c$  and  $u_c$ , and semi-major axis  $a$ . In the case of an elliptical motion, the value of  $\omega$ ,  $\omega'$  and  $r$  at true anomaly  $\theta$  can be calculated using the following equations:

$$\begin{aligned}
\omega &= \frac{\omega_c (1 + e \cos \theta)^2}{(1 - e^2)^{3/2}} \\
\omega' &= \frac{-2\omega_c \omega (1 + e \cos \theta) (e \sin \theta)}{(1 - e^2)^{3/2}} \\
r &= \frac{(a/l) (1 - e^2)}{u_c (1 + e \cos \theta)}
\end{aligned} \tag{3.30}$$

In this section, the gravitational potential energy of the binary asteroid system is compared for different values of the semi-major axis,  $a$ , and eccentricity,  $e$ , of the orbit of mutual orbit of the primary bodies around the barycenter of the binary asteroid system. The values used are  $a = 1160 \text{ m}$ ,  $a = 1180 \text{ m}$ ,  $a = 1220 \text{ m}$  and  $e = 0.00$ ,  $e = 0.01$ ,  $e = 0.02$ ,  $e = 0.03$ . Figures 3–10 and 3–11 show that the variation of the semi-major axis has a larger impact on the potential energy of the binary asteroid system than the variation of the eccentricity.

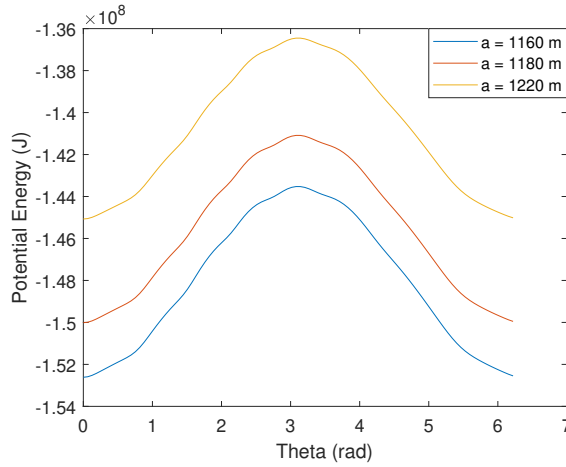


Figure 3–10: Potential energy variation for different semi-major axis values

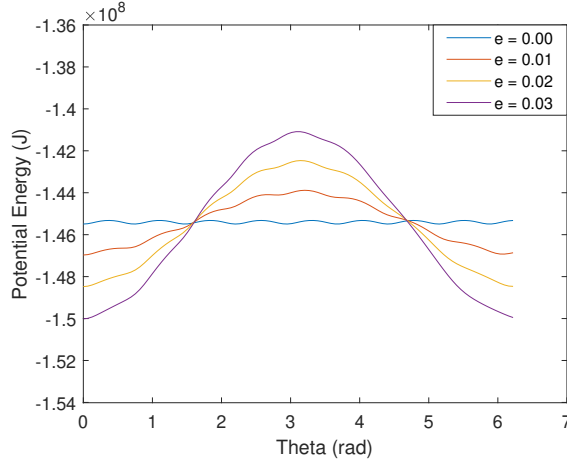


Figure 3–11: Potential energy variation for different eccentricity values

### 3.4 Summary

In this chapter, the motion of the primary bodies of a binary asteroid system, i.e. the FTBP, was studied. The equations of motion were developed based on Lagrange’s equations, using the gravitational potential and the kinetic energy of the system. The case of the circular motion has been described. The theory has then been applied to the binary asteroid system 65803 Didymos, showing that the equations of motion developed represent well the motion of the primary bodies of the system. The conservation of the Hamiltonian principle was demonstrated. The gravitational potential energy of the system has been compared for two type of models: the Taylor series expansion of the fourth order and the layered mascons model. It was shown that both models are equivalent. It was finally shown that the distance between the primary bodies is the parameter of the FTBP that affects the most the variation of the potential energy of the binary asteroid system. In the coming chapters, the effect

of the SRP acceleration on the trajectory of a spacecraft operated in the FCRTBP is studied.

## **CHAPTER 4**

### **Spacecraft Trajectories Compatible with the Solar Radiation Pressure in the FCRTBP**

Asteroids have a small mass compared to planets like the Earth, reducing the gravitational force they can exert on a spacecraft. It means that some external perturbations, like the SRP have a non-negligible impact on the motion of a spacecraft in their vicinity. In Ref. [39], it is shown that the SRP acceleration can have a value that is as large as the second-order terms of the gravitational acceleration. It is believed that these conclusions also apply to binary asteroid systems. This chapter is dedicated to the design of spacecraft trajectories in the vicinity of binary asteroids that are compatible with the SRP acceleration. The SRP is taken into account at the beginning of the design process by integrating it into the equations of motion instead of treating it as a perturbation. In the current study, solar sailing is not a goal of the mission. Since the SRP acceleration is coupled with the attitude of the spacecraft, orbits have been designed using various spacecraft attitude schemes. A stability study has also been conducted on the trajectories designed with and without SRP acceleration included in the model.

#### **4.1 Models Used in this Chapter**

The first section of this chapter details the models used to design the SRP-compatible trajectories. It starts with some assumptions on the dynamical model.

Then, the SRP acceleration model is described, followed by the equations of motion of the spacecraft and the binary asteroid and spacecraft models.

#### 4.1.1 Assumptions

As this chapter is dedicated to the study of the effect of the SRP on the motion of the spacecraft, some simplifications have been made to the model of the binary asteroid system. The full model will be studied in Chapter 6. These simplifications are summarized into the following assumptions:

- (i) The time frame used in the study is short enough to consider the barycenter of the binary asteroid system to be at an approximately fixed position in the inertial reference frame.
- (ii) Because of assumption (i), the distance between the spacecraft and the Sun is considered to be fixed.
- (iii) The primary bodies of the binary asteroid system have a uniform density.
- (iv) The primary bodies of the binary asteroid system move around their barycenter in circular orbits, which means that they are orbiting at a constant rate and the distance between their centers of mass remains constant. This is why the actual problem is defined here as the full circular restricted three body problem (FCRTBP)
- (v) The binary system is in equilibrium, which means that the orientation of primary body 2 with respect to the orientation of primary body 1 is fixed and both bodies rotate at the same rate as the binary asteroid system.

- (vi) The orbital plane of the primary bodies of the binary asteroid system around their barycenter has the same orientation as the orbital plane of the binary asteroid system around the Sun.

#### 4.1.2 Solar Radiation Pressure Acceleration Model

Different types of SRP acceleration models have been used in the literature. References [51, 52] give a good description of most of them. The SRP acceleration models used in this thesis are described in Appendix D. In most of previous studies, simple models, such as the cannonball model has been used. In this chapter, the SRP acceleration is calculated based on a flat plate model. In that case, the  $\hat{\mathbf{n}}$  vector is always  $\hat{\mathbf{n}}_1$  and the  $\hat{\mathbf{n}}_2$  and  $\hat{\mathbf{n}}_3$  vectors are set to  $[0 \ 0 \ 0]^T$ . The spacecraft is considered as only having specular reflectivity, with no absorption. The shadowing of the primary bodies of the binary asteroid system is not taken into account in the calculations. In this case, the acceleration of the spacecraft due to the SRP is given by:

$$\mathbf{a}_{SRP} = \left( \frac{P_{SRP}}{B} \right) (1 + r_s) \langle \hat{\mathbf{u}}, \hat{\mathbf{n}} \rangle^2 \hat{\mathbf{n}} \quad (4.1)$$

Two spacecraft attitude schemes are considered in this chapter. The attitude schemes were chosen to respond to observation of the primary bodies requirements. In the first attitude scheme,  $X_P$  axis pointing of the plates reference frame is always aligned with the direction of the  $X_S$  axis of the synodic reference frame. In this specific attitude scheme, the spacecraft would be observing one of the primary bodies for at least part of its orbit, assuming that the sensor is along the  $X_P$  axis of the plates reference frame. In that case, the  $\hat{\mathbf{n}}$  vector, with its components expressed in

the synodic reference frame, is:

$$\hat{\mathbf{n}} = \text{sign}(\cos\theta) \begin{bmatrix} 1 & 0 & 0 \end{bmatrix}^T \quad (4.2)$$

where  $\text{sign}(\cos\theta)$  is used to signify that when  $\cos\theta$  is negative, i.e. the  $X_S$  direction of the synodic reference frame is in the direction opposite to the direction of the  $X_I$  axis of the inertial reference frame, it is required to inverse the sign of the  $\hat{\mathbf{n}}$  vector. The SRP is then pushing the spacecraft in the negative  $X_S$  direction of the synodic reference frame.

The second spacecraft attitude scheme, flight-path-angle-aligned (FPA-aligned), keeps the  $X_P$  axis of the plates reference frame normal to the direction of flight of the spacecraft. This scheme allows the spacecraft to observe both primary bodies during the course of one orbit for the planar Lyapunov trajectory and body 2 for the retrograde around body 2 trajectory, assuming that the sensor is along the  $X_P$  axis of the plates reference frame. In this case, the  $\hat{\mathbf{n}}$  vector is normal to the direction of flight and is calculated in the synodic reference frame:

$$\hat{\mathbf{n}} = \text{sign}(\cos\theta) \begin{bmatrix} \sin\gamma & \cos\gamma & 0 \end{bmatrix}^T \quad (4.3)$$

$$\gamma = \tan^{-1} \left( \frac{y'}{x'} \right) \quad (4.4)$$

where  $x'$  and  $y'$  are the  $x$  and  $y$  the non-dimensionalized components of the velocity of the spacecraft, expressed in the synodic reference frame. In both cases, the components of the  $\hat{\mathbf{u}}$  vector, expressed in the synodic reference frame, are calculated as

follow:

$$\hat{\mathbf{u}} = \begin{bmatrix} \cos(\theta) & -\sin(\theta) & 0 \end{bmatrix}^T \quad (4.5)$$

### 4.1.3 Equations of Motion

Putting all the previous models together leads to the equations of motion of a spacecraft in the vicinity of a binary asteroid system. In the synodic reference frame, they are given by:

$$\begin{aligned} x'' &= 2\omega_c y' + U_x + a_{SRP_x} \\ y'' &= -2\omega_c x' + U_y + a_{SRP_y} \\ z'' &= U_z + a_{SRP_z} \end{aligned} \quad (4.6)$$

where  $U_i$  is the differentiation with respect to the coordinate  $i$  of the effective potential, which is the sum of the gravitational potential, as calculated in section 2.3, with  $\alpha_1$  and  $\alpha_2$  set to 0, and the potential generated by the centripetal acceleration [61]:

$$U = U_{grav} + \frac{1}{2}\omega_c^2 (x^2 + y^2) \quad (4.7)$$

where  $\omega_c$  is the non-dimensionalized rotation rate of the binary asteroid system for circular motion.

### 4.1.4 Binary Asteroid and Spacecraft Models

Since Didymos is the binary asteroid system targeted by the AIDA mission, a similar system is used here for numerical simulation. The primary bodies are both modelled as tri-axial ellipsoids. The dimensions of the principal semi-axes and primary bodies mass used are given in Table 4-1 [59]. The distance between their

centers of mass is  $l = 1180$  m, the mass ratio parameter is  $\mu = 0.009214$  and the rotation period of the system is 11.9 hours. For the purpose of the SRP acceleration calculation, the system is considered to be at the fixed distance from the Sun of 1  $AU$ . As Didymos has an heliocentric orbit with a semi-major axis of 1.645  $AU$  and an eccentricity of 0.384 [59], this distance is close to its orbit. The spacecraft used in this study is considered purely reflective with a mass to area ratio of 50  $\text{kg}/\text{m}^2$ .

Table 4–1: Dimensions of body 1 and body 2 of the binary asteroid system

<i>Parameter</i>	<i>Body 1</i>	<i>Body 2</i>
$A(m)$	399	103
$B(m)$	392	79
$C(m)$	380	66
$mass(kg)$	$5.22937e + 11$	$4.86315e + 09$

## 4.2 Designing SRP-compatible Trajectories in the FCRTBP

This section presents the technique used to calculate trajectories that are compatible with the SRP in the FCRTBP. After initial guess trajectories are calculated in the CRTBP, SRP-compatible trajectories in the CRTBP are selected. Then, a differential-correction scheme is used to modify them so that they are fitted to the FCRTBP with SRP.

### 4.2.1 Initial Guess for Designing Periodic Orbits in the Classical CRTBP

Planar periodic orbits in the context of the classical CRTBP, where the primary bodies of the system are considered as point masses, serve as the foundation of the search for periodic orbits in the context of a binary asteroid system. Since the

calculations are made in the synodic reference frame, which is rotating, the SRP acceleration is time dependent with a period equal to the one of the binary asteroid system as a whole. To be able to find a periodic orbit in such an environment, it has to have a period that is a rational fraction or a multiplier of the period of the binary asteroid system. Once an orbit with a SRP compatible period is found, it is a candidate to be modified to fit for a higher order gravitational potential model and the SRP acceleration model. The criteria for the orbit to be SRP-compatible are the following:

- (i) The orbit has to exist in the classical CRTBP for the mass ratio of the binary asteroid system targeted.
- (ii) The period of the orbit has to be a rational fraction or a multiplier of the period of the binary asteroid system.

Note that even when these criteria are met, it is always possible that the orbit do not exist in a higher-terms gravitational potential model or in a model including the SRP acceleration.

The first step to find a periodic planar orbit in the classical CRTBP is to determine the value of the Jacobi constant  $C$  for which the periodic orbits exist for different distances from the libration points around which the spacecraft orbits. This is done through a 2-D grid search with the  $X_S$  component of the initial position of the spacecraft in the synodic reference frame and the Jacobi constant  $C$  as parameters. This can also be described as Poincaré mapping with the Poincaré section being the  $Z_S$ - $Y_S$  plane at the required  $X_S$  component of the initial position of the

spacecraft. As demonstrated in Ref.[16], the Jacobian constant  $C$ , can be calculated in the classical CRTBP:

$$C = 2U - (x'^2 + y'^2 + z'^2) \quad (4.8)$$

For the periodic orbit search, the equations of motion of the classical CRTBP are solved numerically for the defined parameters. Here, the search for periodic orbits is limited to planar orbits that are  $X_S$ -axis symmetric. Choosing the initial position of the spacecraft on the  $X_S$  axis of the synodic reference frame and considering only planar motion permits to have the following set of initial conditions:

$$\mathbf{x}_{t_0} = \begin{bmatrix} x_0 & 0 & 0 & 0 & y'_0 & 0 \end{bmatrix}^T \quad (4.9)$$

Note the difference between  $\mathbf{x}_{t_0}$ , which represents the initial state vector, and  $x_0$ , which represents the  $X_S$  component of the initial position of the spacecraft in the synodic reference frame.

The final conditions are the state values when the spacecraft crosses the  $X_S$  axis for the second time, i.e. after a full orbit. The difference between the initial and final conditions is calculated for each of the  $C$  values. A candidate periodic orbit is found when this difference is below a pre-defined threshold. It is then added to a pool of candidate periodic orbits. The candidate periodic orbits are then refined using a differential-correction scheme, described in section 4.2.4. It is then possible to get other members of its family of periodic orbits, which have similar  $C$  values and initial conditions using the same differential-correction method. In the present study, the

$L_2$  and  $L_1$  planar Lyapunov families of periodic orbits, as well as retrograde orbits around body 2 are studied.

#### 4.2.2 Selecting SRP-compatible Orbits

From the candidate orbits found in classical CRTBP, the only ones that are suitable for an SRP-compatible orbits are the ones with a period that is a rational fraction of the rotation period of the binary system studied. This is to make sure that the system, including the SRP, can be considered as time invariant. When this criterion is not met, the trajectory loses its periodicity. For retrograde orbits around body 2, it leads to quasi-periodic orbits, but for Lyapunov orbits, it leads to either escape from the binary asteroid system or impact with one of the primary bodies. In the later case, a higher level of orbit control would be required to maintain it. The period chosen for our study is half of the rotation of the system ( $P/2$ ) which, in non-dimensionalized value, is equivalent to:  $P = \pi/\omega_c$ .

#### 4.2.3 Qualitative Impact of the SRP on Equilibrium Points and the Jacobi Constant

As the force caused by the SRP acceleration is a non-conservative force acting on the spacecraft, there are a few differences in the study of the dynamics of the spacecraft in a binary asteroid system including it. The first aspect to consider is that there are no equilibrium points for the system. In fact, strictly speaking, it would be more appropriate to refer to quasi-equilibrium points in an equilibrium region. It would correspond to the equilibrium points of the classical CRTBP for a system where the SRP acceleration is not taken into consideration.

The second aspect that changes when the SRP acceleration is incorporated into the dynamics model is that there is no constant of integration anymore. The Jacobi

value,  $C$ , is constantly changing when accelerations from non-conservative forces, such as the SRP acceleration are added to the system. The  $C$  constant used here is calculated in the classical CRTBP, using a model without the SRP acceleration.

A quantitative study of these impacts of the SRP acceleration on the dynamics of a spacecraft in the vicinity of a binary asteroid system is done in Chapter 5.

#### 4.2.4 Differential-correction Scheme

Once target initial positions and  $C$  values are found, the orbit is refined using a differential-correction scheme. The differential-correction scheme developed in Refs. [22] and [61] is used here to be able to go from orbits found in the classical CRTBP to orbits that fit models using higher-orders terms of the gravitational potential and the SRP acceleration. Here is a summary of the method presented in Ref. [61]. It applies to a linearized system, where the position vector of the spacecraft relative to the barycenter of the binary asteroid system,  $\mathbf{r}$ , can be replaced by the sum of the position vector of a spacecraft on the reference trajectory relative to the barycenter of the binary asteroid system and the variation of the position of the spacecraft around the reference trajectory:

$$\mathbf{r} = \mathbf{r}_0 + \delta\mathbf{r} \tag{4.10}$$

Linearizing the equations of motion of the system and defining the states of the linearized system as  $\mathbf{x} = \begin{bmatrix} \delta\mathbf{r} & \delta\mathbf{r}' \end{bmatrix}$ , it is possible to define a matrix  $\mathbf{A}$  such that:

$$\mathbf{x}' = \mathbf{A}\mathbf{x} \tag{4.11}$$

In the actual case, the  $\mathbf{A}$  matrix corresponds to the linearized model of the system:

$$\mathbf{A} = \begin{bmatrix} \mathbf{0}_{3 \times 3} & \mathbf{I}_{3 \times 3} \\ -\frac{\partial^2 U}{\partial \mathbf{r}^2} \big|_{\mathbf{r}_0} & \boldsymbol{\omega}_c \end{bmatrix}, \boldsymbol{\omega}_c = \begin{bmatrix} 0 & 2\omega_c & 0 \\ -2\omega_c & 0 & 0 \\ 0 & 0 & 0 \end{bmatrix} \quad (4.12)$$

where  $\mathbf{r}_0$  is the position vector of the spacecraft at the corresponding step of the simulation.

The state transition matrix,  $\boldsymbol{\Phi}(\tau_f; \tau_0)$ , relates the change in the initial state and the state at the final non-dimensionalized time  $\tau_f$  of the simulation:

$$\delta \mathbf{x}(\tau_f) = \boldsymbol{\Phi}(\tau_f; \tau_0) \delta \mathbf{x}(\tau_0) \quad (4.13)$$

and is calculated via numerical integration, with  $\boldsymbol{\Phi}(\tau_0; \tau_0) = I_{6 \times 6}$  as initial condition:

$$\boldsymbol{\Phi}'(\tau_f; \tau_0) = \mathbf{A} \boldsymbol{\Phi}(\tau_f; \tau_0) \quad (4.14)$$

In the present case, the goal is to find the set of initial conditions for which the initial conditions and the final conditions, after one period of the trajectory, would be equal:  $\mathbf{x}(\tau_f) = \mathbf{x}(\tau_0)$ , which means that  $\delta \mathbf{x}(\tau_f)$  would be as close as possible to  $\begin{bmatrix} 0 & 0 & 0 & 0 & 0 & 0 \end{bmatrix}^T$ . The initial and final states are:

$$\mathbf{x}(\tau_0) = \begin{bmatrix} x_0 & 0 & z_0 & 0 & y'_0 & 0 \end{bmatrix}^T, \mathbf{x}(\tau_f) = \begin{bmatrix} x_f & y_f & z_0 & x'_f & y'_f & z'_f \end{bmatrix}^T \quad (4.15)$$

By setting the point where the final states are evaluated to the intersection with the  $X_S$  axis of the synodic reference frame, i.e.  $y_f = 0$ , the final states of the

trajectory are then:

$$\mathbf{x}(\tau_f) = \begin{bmatrix} x_f & 0 & z_f & x'_f & y'_f & z'_f \end{bmatrix}^T \quad (4.16)$$

$\delta\mathbf{x}(\tau_f)$  is then set to:

$$\delta\mathbf{x}(\tau_f) = \begin{bmatrix} (x_0 - x_f) & 0 & (z_0 - z_f) & -x'_f & (y'_0 - y'_f) & -z'_f \end{bmatrix}^T \quad (4.17)$$

As in Ref.[61], the period of the orbit is an important parameter since the SRP acceleration is also taken into consideration there. The final conditions are expanded into a Taylor series of the first order:

$$\delta\mathbf{x}(\tau_f + \delta\tau_f) = \delta\mathbf{x}(\tau_f) + \left. \frac{\partial\mathbf{x}}{\partial\tau} \right|_{\tau=\tau_f} \delta\tau_f \quad (4.18)$$

which is equivalent to:

$$\delta\mathbf{x}(\tau_f + \delta\tau_f) = \mathbf{\Phi}(\tau_f; \tau_0) \delta\mathbf{x}(\tau_0) + \left. \frac{\partial\mathbf{x}}{\partial\tau} \right|_{\tau=\tau_f} \delta\tau_f \quad (4.19)$$

Eq. (4.19) is a system of 6 equations, but only rows 4 and 6 need to be solved:

$$\begin{bmatrix} -x'_f \\ -z'_f \end{bmatrix} = \begin{bmatrix} \phi_{f,41} & \phi_{f,43} & \phi_{f,45} \\ \phi_{f,61} & \phi_{f,63} & \phi_{f,65} \end{bmatrix} \begin{bmatrix} \delta x_0 \\ \delta z_0 \\ \delta y'_0 \end{bmatrix} + \begin{bmatrix} x''_f \\ z''_f \end{bmatrix} \delta\tau_f \quad (4.20)$$

The four unknowns,  $(\delta x_0, \delta z_0, \delta y'_0, \delta\tau_f)$  can be reduced to three when taking into account that the final time,  $(\tau_{f,req})$ , is fixed by the requirement of having a trajectory for which the period is a rational fraction of the period of the rotating binary system:

$$\delta\tau_f = P/k - \tau_f \quad (4.21)$$

where  $P$  is the period of the binary asteroid system and  $k$  is a integer. Row 2 of Eq. (4.19) can be used to solve for the third unknown:

$$\delta y_f = 0 = \phi_{f,21}\delta x_0 + \phi_{f,23}\delta z_0 + \phi_{f,25}\delta y'_0 + y'_f\delta\tau_f \quad (4.22)$$

Solving Eqs. (4.20-4.22) gives the change in the initial conditions that needs to be made to get closer to a periodic trajectory. Executing this algorithm iteratively gives precise initial conditions for periodic trajectories and orbits.

#### 4.2.5 Orbits in the Higher-order Gravitational Potential Model and Including the SRP

Once the SRP-compatible orbits are chosen, a continuation scheme, combined with the differential-correction scheme presented in [61], is applied to make them fit the higher-order gravitational potential model, the FCRTBP. The steps are as follows:

1. Obtain the classical CRTBP orbit.
2. Increase the higher gravitational potential model factor  $f_2$  or  $f_4$ .
3. Apply the differential-correction scheme to get new initial conditions.
4. Repeat steps 2 and 3 until the higher gravitational potential model factor is equal to 1.

The differential-correction algorithm would not converge if the second-order and fourth-order terms were added in their full value. The gravitational potential factor,  $f_2$  and  $f_4$  are numbers between 0 and 1 multiplying the higher order terms, increasing slowly their effect in the model:

$$U = U_0 + f_2U_2 + f_4U_4 \quad (4.23)$$

At the beginning of the algorithm, they are set to 0. They are individually increased by a value of 0.1 each time step 2 is repeated, until they reach the value of 1. The value of  $f_2$  has to reach 1 before  $f_4$  starts to increase.

Each of the parameters of the higher-order gravitational potential model have to be slowly increased by the gravitational potential model factor, including  $u_c$ ,  $\omega_c$  and the values of the accelerations due to the corresponding gravitational potential. The same algorithm applies to the trajectories found here to add the SRP to the model. It has to be done for each attitude scheme individually to get SRP-compatible trajectories.

### 4.3 Numerical Results

The techniques described in this chapter have made possible the design of periodic trajectories in the context of the FCRTBP for binary asteroid systems including the SRP acceleration. The results that were conclusive were based on planar  $L_1$  Lyapunov orbits and retrograde orbits around body 2. As stated earlier, the criterion of the period of the trajectory has to be followed and reduces the number of trajectories that can be brought from the classical CRTBP families of periodic orbits around libration points to trajectories based on the fourth-order gravitational potential model and the SRP acceleration.

The results focus on trajectories around body 2 of the system illustrated in Fig. 4–1. The figures presented later in the chapter will focus on the dynamics of the spacecraft close to primary body 2 of the system, so only the data between  $x_S$ (non-dimensionalized) = 0.7 and 1.3 are presented. This is to ensure that the results can be seen clearly.

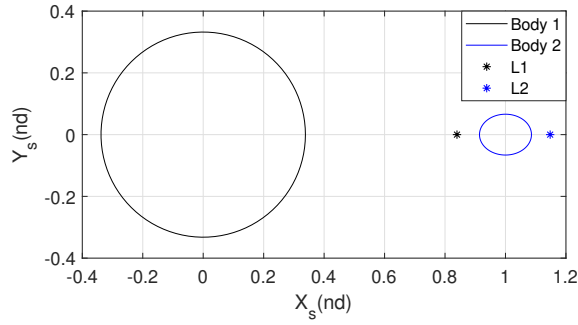


Figure 4-1: Binary asteroid system

### 4.3.1 Zeroth-order Gravitational Potential Model Orbits

The first orbit families designed are the planar Lyapunov families of orbits around both  $L_1$  and  $L_2$  libration points of the classical CRTBP. In Fig. 4-2, the families are shown around primary body 2 of the system. The orbits were "grown" from the libration points until their limits would intersect with primary body 2. The constant  $C$ , initial conditions and period of all of them are presented in Tables 4-2 and 4-3.

Table 4-2: Planar Lyapunov family of orbits around  $L_1$

$C$	$x_0$	$period$
3.13920	0.83485	2.83709
3.12742	0.83172	2.899722
3.11371	0.82860	2.981758
3.09835	0.82531	3.088008
3.09145	0.82381	3.141593

Table 4-3: Planar Lyapunov family of orbits around  $L_2$

$C$	$x_0$	$period$
3.15288	1.13293	3.34751
3.15056	1.12548	3.35680
3.14687	1.11754	3.37149
3.14242	1.10966	3.39110
3.13706	1.10084	3.41955
3.13437	1.09628	3.43730

In Fig. 4-2, the ellipse in the center represents primary body 2 of the system, whereas the stars (\*) represent the  $L_1$  and  $L_2$  libration points, calculated in the classical CRTBP. Tables 4-2 and 4-3 show that in the case of the  $L_2$  planar Lyapunov family, it was not possible to get an orbit with a period that is a rational fraction of the non-dimensionalized rotation period of the system ( $2\pi$  for the classical CRTBP). In the case of the  $L_1$  planar Lyapunov family, only one orbit fits the criterion, which is the one with a  $C$  value of 3.09145 and a period of  $\pi$ . It is represented with a thick purple curve in Fig. 4-2. This orbit was then selected to be modified, so that it would exist in a higher-order gravitational potential model that would also include the SRP acceleration.

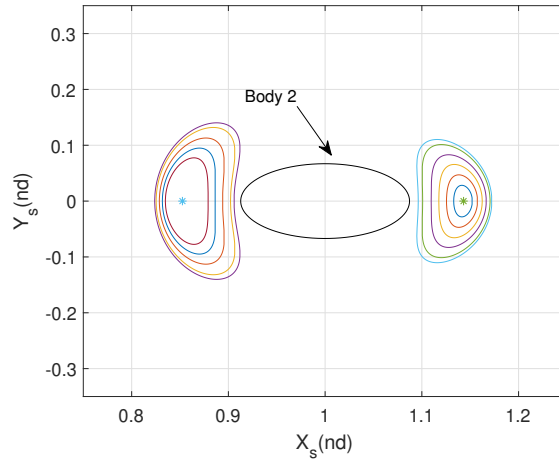


Figure 4–2: Planar Lyapunov orbits around  $L_1$  and  $L_2$

A family of retrograde orbits around body 2 has also been designed. The resulting initial conditions for periodic orbital motion can be seen in Table 4–4, with the resulting trajectories in Fig. 4–3. In this case, a trajectory with a period of  $\pi$  was found for a  $C$  value of 2.94978.

Table 4–4: Retrograde orbits around body 2

$C$	$x_0$	$period$
2.95926	1.14712	2.85000
2.95427	1.15443	3.00000
2.94978	1.16144	3.14159
2.94503	1.16926	3.29678
2.93900	1.17961	3.49658
2.93175	1.19311	3.74634
2.92426	1.20744	3.99600

In Fig. 4–3, the stars represents the  $L_1$  and  $L_2$  libration points. The external orbit is the original one and the orbit represented by a thick red curve is the one with the required period. The ellipse in the center is the surface of the primary body 2 of the system.

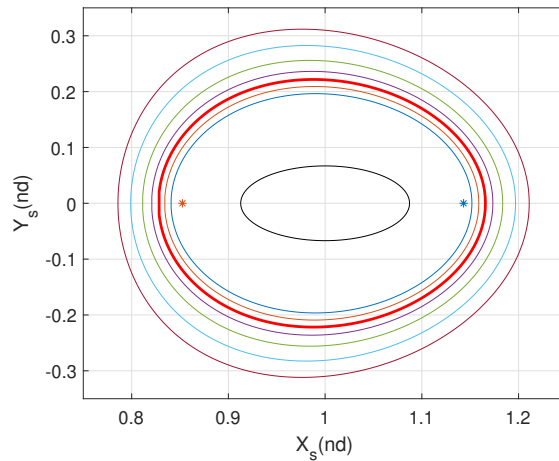


Figure 4–3: Family of retrograde orbits around body 2

It is possible to graphically represent the evolution of the three families of orbits on a plot. In Fig. 4–4, the lines show the evolution of the family as a function of the  $X_S$  component of the initial position in the synodic reference frame and the Jacobi constant  $C$ . The stars indicate when a trajectory has a period of  $\pi$ . The  $L_2$  Lyapunov orbits family does not contain an orbit with a value of  $\pi$ , so it will not be used further in this study.

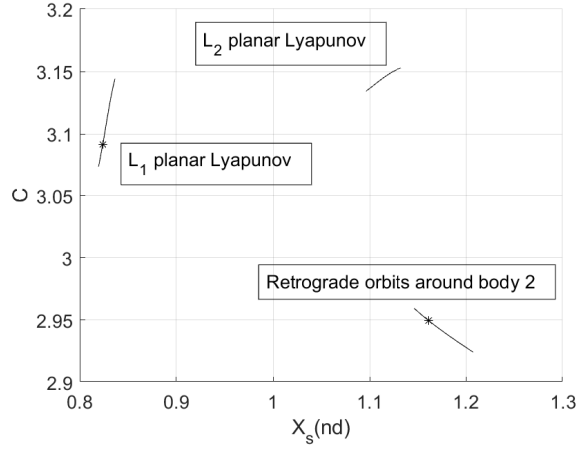


Figure 4-4: Evolution of families with respect to initial position and  $C$

### 4.3.2 Fourth-order Gravitational Potential Model Trajectories

Once the orbits with proper periods were selected, both for the planar Lyapunov orbit and the retrograde orbit around body 2, the differential-correction scheme, combined with the continuation scheme, was applied to get trajectories based on a fourth-order gravitational potential model. The initial conditions for each of them can be found in Table 4-5. Note here that the period of the trajectory is not equal to  $\pi$ , but equal to  $\pi/\omega_c$ , since the rotation period of a binary asteroid system with non-spherical bodies is:  $2\pi/\omega_c$ . In Fig. 4-5 and 4-6, the difference between trajectories modeled with a zeroth and a fourth-order gravitational potential model is visible.

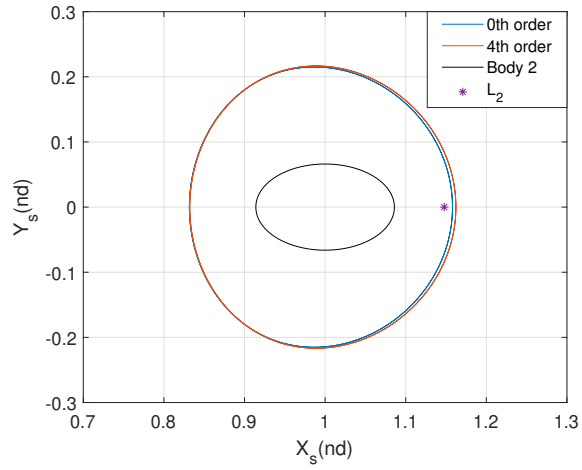


Figure 4-5: Retrograde trajectories around body 2 of zeroth-order and fourth-order

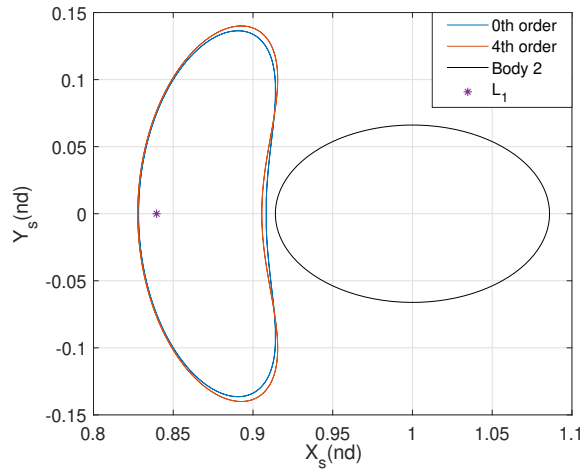


Figure 4-6:  $L_1$  planar Lyapunov trajectories of zeroth-order and fourth-order

Table 4–5: Initial conditions for periodic trajectories using a fourth-order gravitational potential model

<i>Trajectory type</i>	$x_0$	$y'_0$	<i>Period</i>
<i>L<sub>1</sub> planar Lyapunov</i>	0.82335	0.29592	3.14466
<i>Retrograde around body 2</i>	1.16576	−0.45787	3.14466

### 4.3.3 Fourth-order Gravitational Model Trajectories with SRP Acceleration

As stated earlier, two different spacecraft attitude schemes have been considered here. They were chosen because of their practical significance in a mission where the spacecraft would be oriented in such a way that it would be observing one or both primary bodies of the system. The first attitude scheme,  $X_S$  axis pointing, has the  $X_P$  axis of the plates reference frame always aligned with the positive  $X_S$  axis of the synodic reference frame, so the spacecraft would be observing primary body 2 of the system for the entire planar Lyapunov trajectory and part of the retrograde around body 2 trajectory. In the second one, FPA-aligned, the spacecraft rotates during its trajectory, so that the  $X_P$  axis of the plates reference frame is perpendicular to its velocity vector. This scheme allows the spacecraft to observe both primary bodies during the course of one orbit for the planar Lyapunov trajectory and body 2 for the retrograde around body 2 trajectory. The trajectories designed with the SRP acceleration included in the model are periodic after a full rotation of the system about its barycenter. This periodicity is achieved by choosing trajectories with a period that is a rational fraction of the rotation period of the system,  $\pi/\omega_c$ . In this case, both trajectories that were tested with the SRP acceleration included in the

model had a period of half the one of the system, so they go back to their initial conditions after two "orbits". This can be observed in Figs. 4–7, 4–8 and 4–9. Note that Fig. 4–9 is Fig. 4–8 zoomed on the trajectory to show the effect of the SRP on it. The initial conditions for each of these trajectories are in Table 4–6.

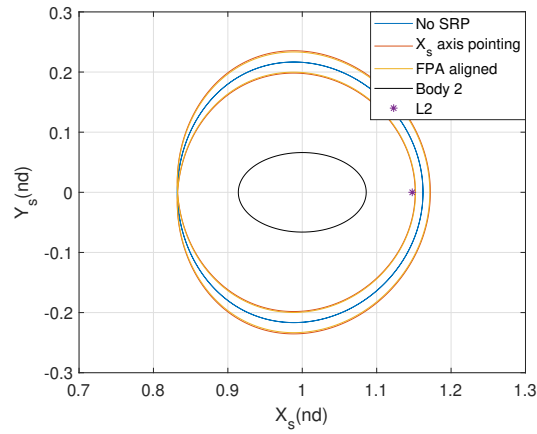


Figure 4–7: Retrograde trajectories around body 2 with and without SRP acceleration included in the model

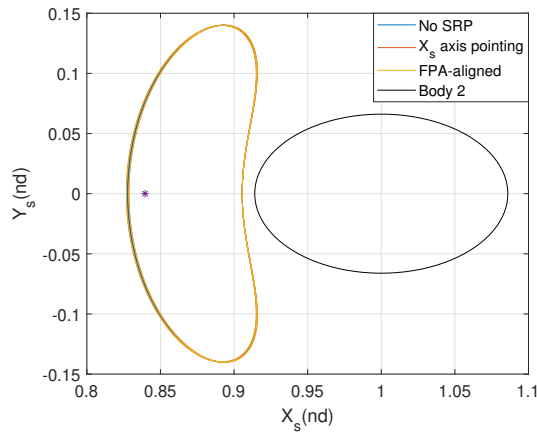


Figure 4–8:  $L_1$  planar Lyapunov trajectories with and without SRP acceleration included in the model

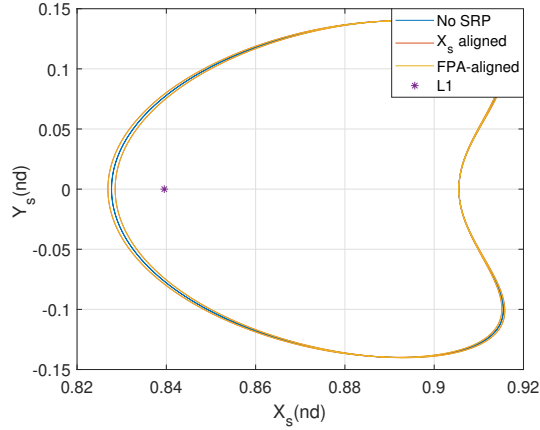


Figure 4–9:  $L_1$  planar Lyapunov trajectories with and without SRP acceleration included in the model, zoomed on trajectory

Table 4–6: Initial conditions for periodic trajectories with SRP acceleration, fourth-order gravitational potential model

<i>Trajectory</i>	<i>Spacecraft attitude scheme</i>	$x_0$	$y'_0$	<i>Period</i>
<i><math>L_1</math> planar Lyapunov</i>	<i><math>X_S</math> axis pointing</i>	0.82254	0.29525	3.14466
<i><math>L_1</math> planar Lyapunov</i>	<i>FPA-aligned</i>	0.82281	0.29598	3.14466
<i>Retrograde around body 2</i>	<i><math>X_S</math> axis pointing</i>	1.17569	-0.46343	3.14466
<i>Retrograde around body 2</i>	<i>FPA-aligned</i>	1.17727	-0.46203	3.14466

#### 4.3.4 Stability Comparison of the Trajectories

A monodromy matrix has been computed for each of the trajectories described previously. It has been calculated over a full rotation of the binary asteroid system, so that the trajectories including the SRP acceleration could complete their cycle. For a periodic orbit to be stable, all of the eigenvalues of its monodromy matrix have to lay on a unit circle, i.e. have a norm value of 1. In the present cases, the

only trajectory satisfying this condition is the retrograde trajectory around body 2 when calculated with the primary bodies represented as point masses. The planar Lyapunov orbits around the  $L_1$  and  $L_2$  libration points, on their side, are known to be unstable [61]. It is not possible for a spacecraft to stay on these trajectories without active control. The evolution of the eigenvalues, as shown in Table 4–7, show that much of the instability is gained when the trajectories are based on a higher-order gravitational potential model, meaning that the shape of the primary bodies is taken into account. SRP has some impact, but it is not as important as the shape of the primary bodies.

Table 4–7: Eigenvalues for  $L_1$  planar Lyapunov trajectories and retrograde trajectories around body 2

<i>Trajectory</i>	<i>Gravity model</i>	<i>Attitude scheme</i>	<i>Norm of max. eigenvalue</i>
<i><math>L_1</math> planar Lyapunov</i>	$0^{th}$	<i>no SRP</i>	1.20203e6
<i><math>L_1</math> planar Lyapunov</i>	$4^{th}$	<i>no SRP</i>	1.27607e6
<i><math>L_1</math> planar Lyapunov</i>	$4^{th}$	<i><math>X_S</math> axis pointing</i>	1.27595e6
<i><math>L_1</math> planar Lyapunov</i>	$4^{th}$	<i>FPA-aligned</i>	1.27625e6
<i>Retrograde around body 2</i>	$0^{th}$	<i>no SRP</i>	1
<i>Retrograde around body 2</i>	$4^{th}$	<i>no SRP</i>	13.20294
<i>Retrograde around body 2</i>	$4^{th}$	<i><math>X_S</math> axis pointing</i>	13.55095
<i>Retrograde around body 2</i>	$4^{th}$	<i>FPA-aligned</i>	13.55739

### 4.3.5 Trajectories with a Different Period

Trajectories with a slightly different period (3.1, instead of 3.144663) were also tested. For the  $L_1$  planar Lyapunov type trajectory, with the FPA-aligned attitude scheme, Fig. 4–10 show that the spacecraft would definitively leave the trajectory before the end of the rotation of the binary asteroid system.

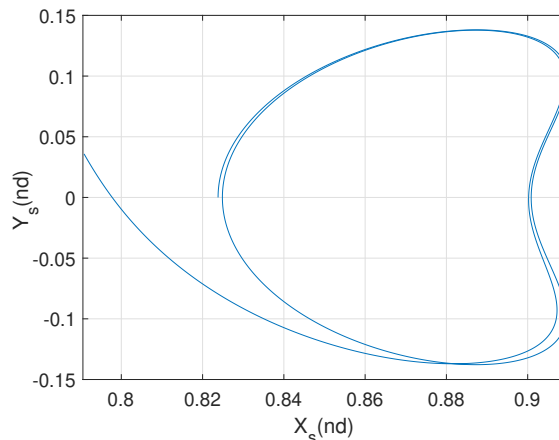


Figure 4–10: Lyapunov trajectory with a period of 3.1

In the case of the retrograde trajectory around body 2, the difference is not as clearly visible if not zooming in the initial and final position region. When zoomed in, as in Fig. 4–11, it is possible to see that the trajectory does not close. The impact of the difference in the period is more clear when considering the maximum eigenvalue of the monodromy matrix, as it goes from 13.557391 for a trajectory with a period of half the one of the system (3.144663) to 37.118950 for a trajectory with a period of 3.1. It shows that for an orbit with a period that is slightly different than an optimal one, the SRP acceleration has a great impact on its stability.

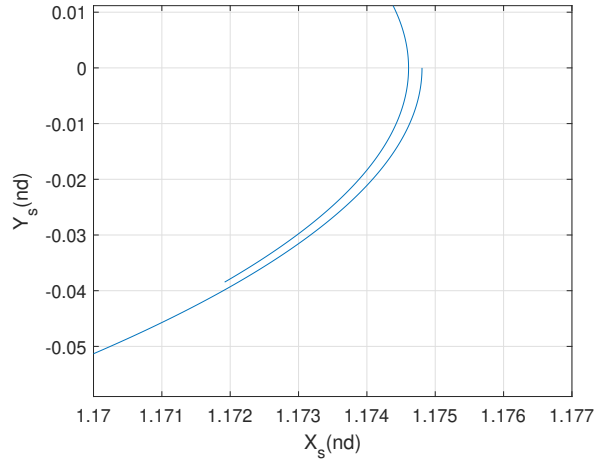


Figure 4–11: Retrograde trajectory around body 2 with a period of 3.1, zoomed on initial position

#### 4.4 Summary

In the present chapter, planar periodic trajectories of a spacecraft in the vicinity of a binary asteroid system using a fourth-order Taylor series expansion gravitational potential model and the SRP acceleration were designed in the FCRTBP. It was found that it is possible to obtain such trajectories when the period criterion of the chosen trajectories from the classical CRTBP is met. It has to be noted that the planar Lyapunov orbits are unstable and cannot be maintained for significant periods of time without control. These trajectories show little difference in their stability when compared to trajectories without the SRP acceleration included in the model. It means that when the trajectory is carefully designed, its stability is not significantly influenced by the SRP itself, which is not the case when the period of the orbit is slightly different from an optimal one. The difference in stability between the classical CRTBP trajectories and the ones in the FCRTBP including

the SRP acceleration comes mainly from the non-sphericity of the primary bodies of the binary asteroid system. The next chapter is studying the attitude-SRP coupling by looking at how non-controlled spacecraft trajectories are influenced by the SRP acceleration model and the spacecraft attitude scheme of the spacecraft used.

## CHAPTER 5

### **Impact of the Solar Radiation Pressure Acceleration Model on Spacecraft Trajectories in the FCRTBP**

As previously stated, the SRP acceleration may not be negligible when calculating the motion of a spacecraft in the vicinity of a binary asteroid. This chapter studies how the choice of the SRP acceleration model influences the strength of the SRP acceleration acting on the spacecraft. It compares the results between when the binary asteroid is at perihelion and at aphelion of its orbit around the Sun. Since the SRP acceleration is coupled with the attitude of the spacecraft, this chapter also studies how it is possible to take advantage of the choice of the nominal attitude of the spacecraft so that the SRP affects the spacecraft dynamics in a desirable manner. Finally, a special case of retrograde orbits around body 2 is studied.

As in the previous chapter, some simplifications to the model of the binary asteroid system are made to put the focus of the study on the effect of the SRP acceleration. The same assumptions as in chapter 4 are made here, except that, in this case, two positions in the orbit of the binary asteroid system around the Sun are considered: at perihelion and at aphelion. For each case, the time frame used in the study is short enough to consider the barycenter of the binary asteroid system to be at an approximately fixed position in the inertial reference frame.

The gravitational potential model used is the one with Taylor series expansion described in section 2.3. The SRP acceleration models are summarized in Appendix

D, with the generic equation being Eq. D.1. In this chapter, the SRP acceleration models that are studied are: the cannonball, the flat plate, the multi-body flat plate and the N-plates models. Various attitude schemes for the spacecraft are examined. The effect of different optical parameters of the spacecraft on the SRP acceleration is investigated using the flat plate model.

## 5.1 Description of the Attitude Schemes

The direction and norm of the SRP acceleration in the synodic reference frame are highly dependent on the orientation of the spacecraft with respect to the direction of the  $\hat{\mathbf{u}}$  vector. In this chapter, five different attitude schemes are examined, with their impact on various types of trajectories. Note that all the  $\hat{\mathbf{n}}_i$  are described for the different attitude schemes. In the case of the use of a flat plate or multi-body flat plate model, the  $\hat{\mathbf{n}}$  vector to use is  $\hat{\mathbf{n}}_1$ . In the case of the cannonball, the attitude of the spacecraft has no effect on the SRP acceleration.

### 5.1.1 Generic Expressions for the Components of the $\hat{\mathbf{n}}$ Vector Expressed in the Synodic Reference Frame

The components of the  $\hat{\mathbf{n}}_i$  vectors in the synodic reference frame are calculated from their equivalent in the inertial reference frame. The general procedure is developed here and will be applied to the calculation of the expressions for each attitude scheme.

Figure 5–1 shows the relationship between the plates reference frame and the inertial reference frame. It also shows how the  $\hat{\mathbf{u}}$  vector is always aligned with the  $X_I$  axis of the inertial reference frame.

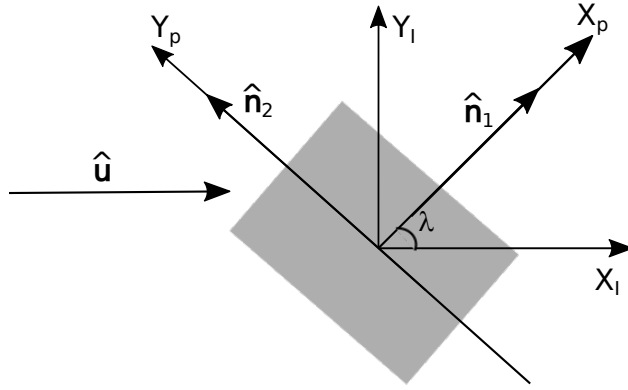


Figure 5–1: Kinematics between plates reference frame and inertial reference frame

The plates reference frame, for the planar case, rotates around the  $Z_I$  axis of the inertial reference frame with an angle  $\lambda$ , giving the direction cosine matrix:

$$\mathbf{C}_{IP} = \begin{bmatrix} \cos\lambda & -\sin\lambda & 0 \\ \sin\lambda & \cos\lambda & 0 \\ 0 & 0 & 1 \end{bmatrix} \quad (5.1)$$

where  $\mathbf{C}_{IP}$  is the direction cosine matrix describing the orientation of the inertial reference frame relative to the plates reference frame.

The expressions of the components of the  $\hat{\mathbf{n}}_i$  vectors in the plate reference frame are:

$$\begin{aligned} \hat{\mathbf{n}}_{1P} &= \begin{bmatrix} 1 & 0 & 0 \end{bmatrix}^T \\ \hat{\mathbf{n}}_{2P} &= \begin{bmatrix} 0 & 1 & 0 \end{bmatrix}^T \\ \hat{\mathbf{n}}_{3P} &= \begin{bmatrix} 0 & 0 & 1 \end{bmatrix}^T \end{aligned} \quad (5.2)$$

The expressions of the components of each of the  $\hat{\mathbf{n}}_i$  vectors in the inertial reference frame are then:

$$\begin{aligned}\hat{\mathbf{n}}_{1_I} &= \begin{bmatrix} \cos\lambda & \sin\lambda & 0 \end{bmatrix}^T \\ \hat{\mathbf{n}}_{2_I} &= \begin{bmatrix} -\sin\lambda & \cos\lambda & 0 \end{bmatrix}^T \\ \hat{\mathbf{n}}_{3_I} &= \begin{bmatrix} 0 & 0 & 1 \end{bmatrix}^T\end{aligned}\tag{5.3}$$

The first component of the  $\hat{\mathbf{n}}_i$  vectors expressed in the inertial reference frame always needs to be positive, so that it is in the same direction as the  $\hat{\mathbf{u}}$  vector (SRP cannot produce an acceleration in a direction opposite to the  $\hat{\mathbf{u}}$  vector). To assure that, the components of the  $\hat{\mathbf{n}}_i$  vectors need to be multiplied by the sign of their first component.

Once the components of the  $\hat{\mathbf{n}}_i$  vectors are calculated in the inertial reference frame, they need to be put in the synodic reference frame for simulation purposes. This is done by a rotation of an angle  $\theta$  around the  $Z_I$  axis of the inertial reference frame. This time, the rotation being from the inertial reference frame to the synodic reference frame, the direction cosine matrix is transposed:

$$\mathbf{C}_{SI} = \begin{bmatrix} \cos\theta & \sin\theta & 0 \\ -\sin\theta & \cos\theta & 0 \\ 0 & 0 & 1 \end{bmatrix}\tag{5.4}$$

where  $\mathbf{C}_{SI}$  is the direction cosine matrix describing the orientation of the synodic reference frame relative to the inertial reference frame.

The direction cosine matrix describing the orientation of the synodic reference frame relative to the plates reference frame is then given by:

$$\mathbf{C}_{SP} = \mathbf{C}_{SI}\mathbf{C}_{IP} = \begin{bmatrix} c\theta c\lambda + s\theta s\lambda & s\theta c\lambda - c\theta s\lambda & 0 \\ c\theta s\lambda - s\theta c\lambda & s\theta s\lambda + c\theta c\lambda & 0 \\ 0 & 0 & 1 \end{bmatrix} \quad (5.5)$$

where  $c$  stands for cosine and  $s$  for sine.

In all cases the unit vector  $\hat{\mathbf{u}}$ , with components expressed in the synodic reference frame, is given by:

$$\hat{\mathbf{u}}_S = \begin{bmatrix} \cos\theta & -\sin\theta & 0 \end{bmatrix}^T \quad (5.6)$$

The generic expressions for the  $\hat{\mathbf{n}}_i$  vectors in the synodic reference frame are then given by:

$$\begin{aligned} \hat{\mathbf{n}}_{1_S} &= \text{sign}(c\lambda) \begin{bmatrix} c\theta c\lambda + s\theta s\lambda & c\theta s\lambda - s\theta c\lambda & 0 \end{bmatrix}^T \\ \hat{\mathbf{n}}_{2_S} &= \text{sign}(-s\lambda) \begin{bmatrix} s\theta c\lambda - c\theta s\lambda & s\theta s\lambda + c\theta c\lambda & 0 \end{bmatrix}^T \\ \hat{\mathbf{n}}_{3_S} &= \begin{bmatrix} 0 & 0 & 1 \end{bmatrix}^T \end{aligned} \quad (5.7)$$

Note that in the attitude schemes described in this study, the  $\hat{\mathbf{n}}_3$  vector has no effect on the SRP acceleration as:  $\langle \hat{\mathbf{u}}, \hat{\mathbf{n}}_3 \rangle = 0$  for all the schemes presented.

### 5.1.2 Solar Panels Always Perpendicular with the $X_S$ Direction of the Synodic Reference Frame ( $X_S$ attitude scheme)

In this attitude scheme, the  $X_P$  axis of the plates reference frame is always aligned with the  $X_S$  axis of the synodic reference frame. In that case  $\lambda = \theta$  in Eq. 5.7. This results in the following expressions for the  $\hat{\mathbf{n}}_i$  vectors expressed in the

synodic reference frame:

$$\begin{aligned}
 \hat{\mathbf{n}}_{1s} &= \begin{bmatrix} 1 & 0 & 0 \end{bmatrix}^T \\
 \hat{\mathbf{n}}_{2s} &= \begin{bmatrix} 0 & 1 & 0 \end{bmatrix}^T \\
 \hat{\mathbf{n}}_{3s} &= \begin{bmatrix} 0 & 0 & 1 \end{bmatrix}^T
 \end{aligned} \tag{5.8}$$

### 5.1.3 Maximum SRP Acceleration (MaxSRP Attitude Scheme)

For the case of the *MaxSRP* attitude scheme, plate 1 is perpendicular to the  $\hat{\mathbf{n}}_1$  vector. Its surface includes the solar panels of the spacecraft, so it is the plate with the largest surface. It is then the plate that contributes the most to the SRP acceleration. In this scheme, vector  $\hat{\mathbf{n}}_1$  is always parallel to the  $\hat{\mathbf{u}}$  vector, making the SRP acceleration maximal, which results in the  $\lambda$  angle being 0 in Eq. 5.7. In this case, the expressions for the components of the  $\hat{\mathbf{n}}_i$  vectors in the synodic reference frame are:

$$\begin{aligned}
 \hat{\mathbf{n}}_{1s} &= \begin{bmatrix} \cos\theta & -\sin\theta & 0 \end{bmatrix}^T \\
 \hat{\mathbf{n}}_{2s} &= \begin{bmatrix} \sin\theta & \cos\theta & 0 \end{bmatrix}^T \\
 \hat{\mathbf{n}}_{3s} &= \begin{bmatrix} 0 & 0 & 1 \end{bmatrix}^T
 \end{aligned} \tag{5.9}$$

Note that in this scheme, the  $\hat{\mathbf{n}}_2$  vector has no effect on the SRP acceleration as:

$$\langle \hat{\mathbf{u}}, \hat{\mathbf{n}}_2 \rangle = 0.$$

#### 5.1.4 Minimal SRP Acceleration (MinSRP Attitude Scheme)

The SRP acceleration is minimal when the dot product of the  $\hat{\mathbf{n}}_1$  vector and the  $\hat{\mathbf{u}}$  vector is minimized, which means that the  $\hat{\mathbf{u}}$  and the  $\hat{\mathbf{n}}_1$  vectors are perpendicular, making the dot product of the two vectors null. This is made possible by having the  $\lambda$  angle set to  $\pi/2$  in Eq. 5.7. The other surfaces of the spacecraft are still contributing to the SRP acceleration, so it is not canceled. The expressions of the components of the  $\hat{\mathbf{n}}_i$  vectors in the synodic reference frame are then:

$$\begin{aligned}\hat{\mathbf{n}}_{1S} &= \begin{bmatrix} \sin\theta & \cos\theta & 0 \end{bmatrix}^T \\ \hat{\mathbf{n}}_{2S} &= - \begin{bmatrix} -\cos\theta & \sin\theta & 0 \end{bmatrix}^T \\ \hat{\mathbf{n}}_{3S} &= \begin{bmatrix} 0 & 0 & 1 \end{bmatrix}^T\end{aligned}\tag{5.10}$$

#### 5.1.5 Oscillation of Plate 1, Averaged Around Maximal SRP Acceleration (Oscill MaxSRP Attitude Scheme)

To maximize the energy produced by the solar panels, while reducing the impact of the SRP, it was decided to consider a scheme where the spacecraft would oscillate around the maximum SRP acceleration attitude scheme with an amplitude of 45 degrees and a rate that is the same as the rotation rate of the binary asteroid system.

In this case the oscillation angle,  $\lambda$ , in radians, is calculated using:

$$\lambda = \frac{\pi}{4} \sin\theta\tag{5.11}$$

and the expressions of the components of the  $\hat{\mathbf{n}}_i$  vectors in the synodic reference frame are as per Eq. 5.7.

### 5.1.6 Oscillation of Plate 1, Averaged Around Minimal SRP Acceleration (Oscill MinSRP Attitude Scheme)

As the solar panels would never face the Sun if the spacecraft would always be in a minimal SRP acceleration attitude scheme, it was decided to add an attitude scheme where the spacecraft would oscillate around the minimal SRP acceleration attitude scheme with an amplitude of 45 degrees and a rate that is the same as the rotation rate of the binary asteroid system. This is to make sure that the solar panels are exposed to the radiation from the Sun. In this case the oscillation angle,  $\lambda$ , in radians, is calculated using:

$$\lambda = \frac{\pi}{4} \sin\theta + \frac{\pi}{2} \quad (5.12)$$

The expressions of the components of the  $\hat{\mathbf{n}}_i$  vectors in the synodic reference frame are then identical to Eq. 5.7.

## 5.2 Equations of Motion

The equations of motion used for this chapter are the same as described in section 4.1.3. The gravitational potential model is also calculated as in section 2.3.

## 5.3 Binary Asteroid and Spacecraft Models

The binary asteroid model used is the same as in chapter 4. For the purpose of the SRP acceleration calculation, two cases are studied: at perihelion and at aphelion of the orbit of the 65803 Didymos binary asteroid system around the Sun, which are at 1.013 AU and at 2.276 AU from the Sun respectively [64].

The spacecraft has the same optical properties as the ones presented in [52]. Its optical properties and mass to area ratio are different for each surface, as shown in Table 5-1.

Table 5–1: Characteristics of the different surfaces of the spacecraft

<i>Surface</i>	<i>% of surface</i>	<i>B</i>	<i>Spec ref</i>	<i>Dif ref</i>
1 – <i>solar panel</i>	76	50	0.249	0.044
1 – <i>bus</i>	24	50	0.06	0
2 – <i>bus</i>	100	296.17	0.06	0
3 – <i>bus</i>	100	217.77	0.06	0

In Table 5–1, surface 1 is composed of the solar panels and the satellite bus. Since the total of the specular reflectivity, the diffusive reflectivity and the absorptivity is 1, only two of the optical properties, specular and diffusive reflectivity here, need to be given.

#### 5.4 Choice of Trajectories Used for the Study

A range of types of trajectories have been tested using a model that is not taking the SRP acceleration into account before conducting this study. Figure 5–2 shows the planar trajectories around the primary bodies and the whole system, and Fig. 5–3 shows trajectories part of the CRTBP in the vicinity of  $L_1$ . The planar trajectories used in this study were designed using a combination of Poincaré mapping and a differential-correction scheme, as described in section 4.2.4. In the case of the spatial trajectories tested, the initial guesses required for the differential-correction scheme were provided by using the AUTO numerical continuation and bifurcation software [31]. Figure 5–4 shows the position in the  $X_S$  direction of the spacecraft for the planar Lyapunov, vertical Lyapunov and halo orbits with respect to the number of revolutions of the binary asteroid system. It shows that they do not stay bounded

when not controlled. In the case of the planar Lyapunov orbit, the end of the data shows when the spacecraft impacts body 2 of the binary asteroid system. This is why they are not taken into account further in this chapter. The orbits chosen for the analysis are then the planar orbits orbiting either around the individual primary bodies or the entire system. The chosen trajectories are: retrograde around body 1, retrograde about body 2, retrograde around the entire system and direct around the entire system, which are all planar trajectories. Each spacecraft attitude scheme is applied to all of the chosen base orbits, giving an extended portrait of the effects and the possibilities given by the SRP acceleration.

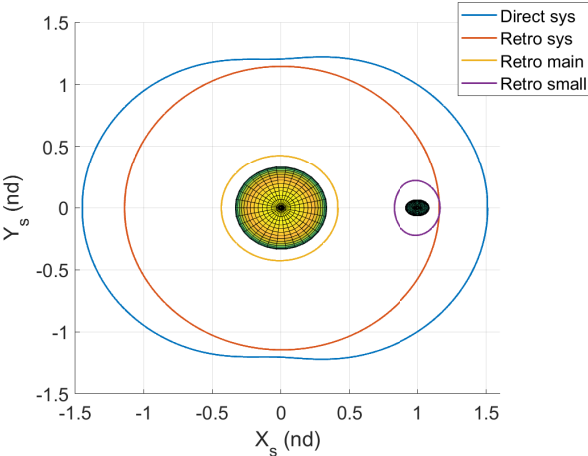


Figure 5–2: Candidate trajectories around primary bodies and the binary asteroid system as a whole

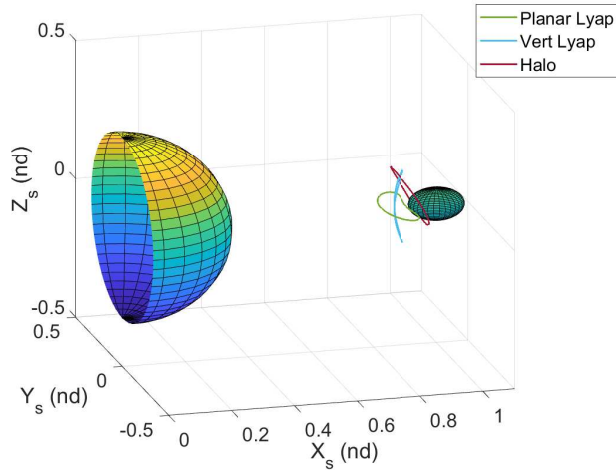


Figure 5–3: Candidate CRTBP trajectories in the vicinity of  $L_1$

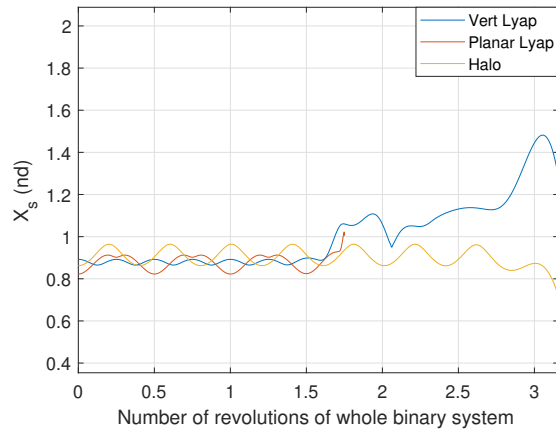


Figure 5–4: Position in the  $X_S$  direction of the candidate CRTBP trajectories in the vicinity of  $L_1$  with respect to the number of revolution of the binary asteroid system

## 5.5 Studies Done on Each Attitude Schemes Described in Section 5.1

Various studies are conducted for each of the attitude schemes described in section 5.1. The studies include calculating the variation of the  $C$  value and the position where the spacecraft crosses the  $X_S$ - $Z_S$  plane of the synodic frame. This is

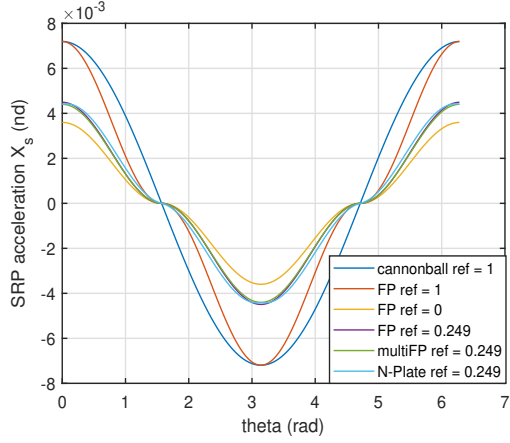
done throughout 10 to 20 rotations of the binary asteroid system to give a reasonable overview of the behavior of the spacecraft under the influence of the SRP. A study of the variation of the SRP acceleration and of the equilibrium regions over 1 rotation of the binary asteroid system is also done. The analyses are done for both when the binary asteroid system is at perihelion and when it is at aphelion of its orbit around the Sun.

## 5.6 Numerical Results

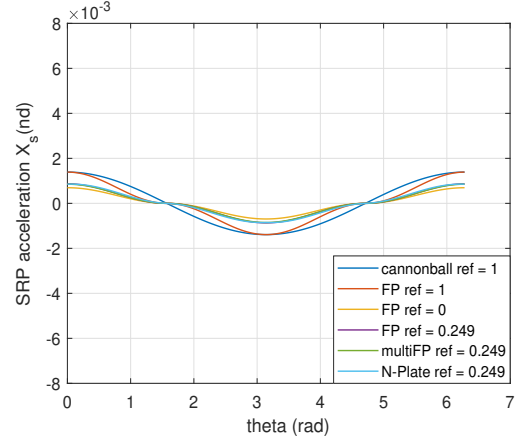
The numerical results section is separated into three parts. First, the choice of the SRP acceleration model used for the analysis is explained. Secondly, analysis of the influence of the attitude scheme on the impact of the SRP acceleration is done for different planar orbits. Last, the same analysis is done for the special case of retrograde trajectories around primary body 2 that were designed specifically for each of the attitude schemes.

### 5.6.1 Choice of the SRP Model Acceleration to Use

The SRP acceleration was numerically calculated throughout one rotation of the binary asteroid system for the  $X_S$  attitude scheme. In Ref. [51], the case of a non-perfectly reflecting solar sail is addressed. Here, the reflectivity was varied in the case of the flat plate model. In the present study, the spacecraft that is targeted has a much lower specular reflectivity coefficient since it is not designed with solar sailing in mind. The spacecraft has solar panels which are mainly absorptive. The effect of using the real optical properties is then more visible. Figures 5-5 and 5-6 show how the SRP acceleration changes over one rotation of the binary asteroid system for the different cases and distances between the binary asteroid system and the Sun.

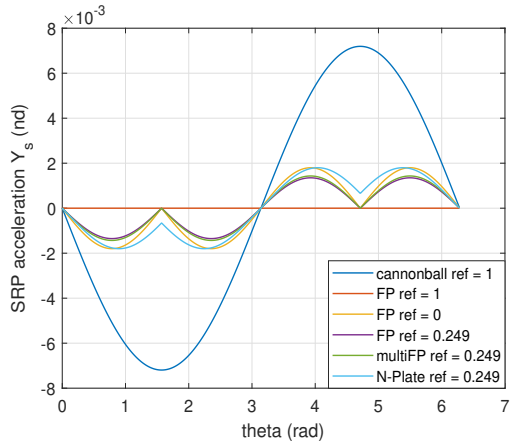


(a) Binary asteroid system at perihelion of its orbit around the Sun

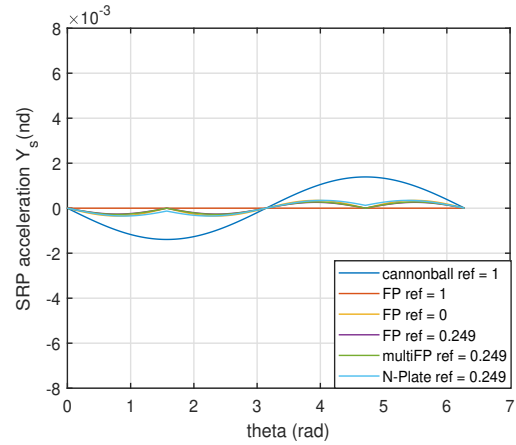


(b) Binary asteroid system at aphelion of its orbit around the Sun

Figure 5–5: SRP acceleration in the  $X_S$  direction of the synodic reference frame for different models and parameters over one rotation of the binary asteroid system



(a) Binary asteroid system at perihelion of its orbit around the Sun



(b) Binary asteroid system at aphelion of its orbit around the Sun

Figure 5–6: SRP acceleration in the  $Y_S$  direction of the synodic reference frame for different models and parameters over one rotation of the binary asteroid system

In Fig. 5-5 and 5-6, the cases studied are the flat plate model with specular reflectivity (ref) of 0, 1 and 0.249, the multi-body flat plate model (multiFP) with a reflectivity of 0.249, the N-plate model (N-Plate) with a reflectivity of 0.249 and the cannonball model with a reflectivity of 1.

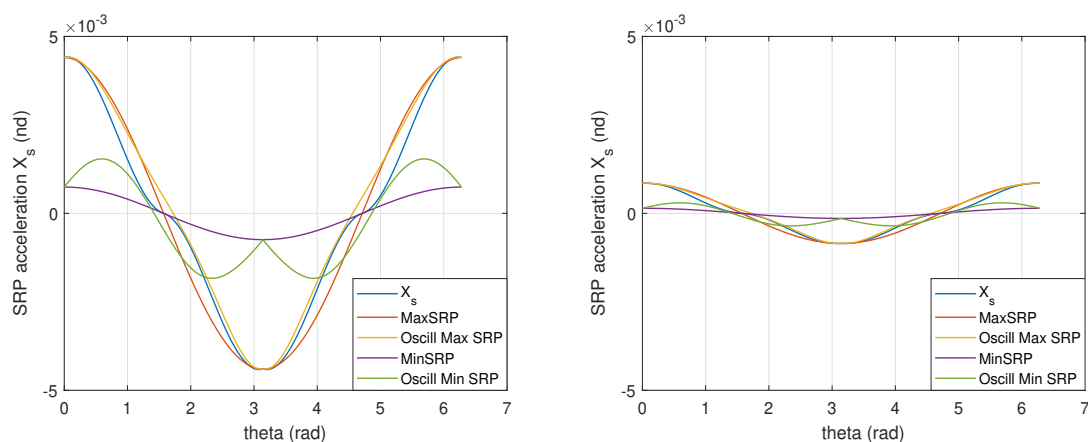
As can be found in Ref. [51] and Ref. [52], there is a loss of the detail when the specular reflectivity is set to 1, since it does not show the SRP acceleration in the  $Y_S$  direction of the synodic reference frame. Since the absorptivity produces an acceleration in the direction of the  $\hat{\mathbf{u}}$  vector, the spacecraft has an acceleration in a direction that is different than if its surface is considered purely reflective. This explains the choice of using realistic reflectivity and absorptivity values in the calculation of the SRP acceleration.

Similarly to the results in Ref. [52], there are other details that appear when the more complex N-plate model is used, especially in the  $Y_S$  direction of the synodic reference frame. When the attitude scheme of the spacecraft becomes more complex, these details become even more important. Since the model is not highly computationally intensive and the details available could make a difference in the results, it is used throughout the rest of the analyses in this chapter.

As expected, the difference is less noticeable when the binary asteroid system is at aphelion than at perihelion of its orbit around the Sun. As there is still a difference in the acceleration due to the SRP for the different models of the SRP acceleration, both distances are included in the other analysis.

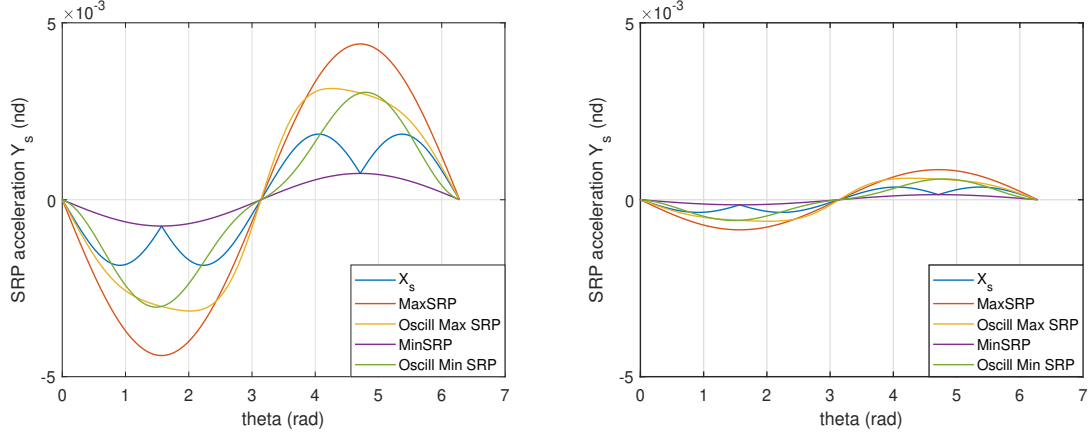
### 5.6.2 Acceleration due to SRP throughout one Rotation of the Binary Asteroid System

As the binary system is rotating, the direction of the  $\hat{u}$  vector changes direction in the synodic reference frame. It creates variations in the acceleration of the spacecraft due to the SRP in the synodic reference frame. It is similar to what is observed when the azimuth of a spacecraft located at the Sun-Earth  $L_2$  is varied [52]. This variation depends on the attitude of the spacecraft with respect to the inertial reference frame and not on its position, since it is considered as being at a constant distance with respect to the Sun. Figures 5–7 and 5–8 show how this acceleration varies in the synodic reference frame throughout the rotation of the binary asteroid system for the different attitude schemes studied here.



(a) Binary asteroid system at perihelion of its orbit around the Sun for the N-plate SRP acceleration model  
 (b) Binary asteroid system at aphelion of its orbit around the Sun for the N-plate SRP acceleration model

Figure 5–7: SRP acceleration in the  $X_S$  direction of the synodic reference frame throughout one rotation of the binary asteroid system for the N-plate SRP acceleration model



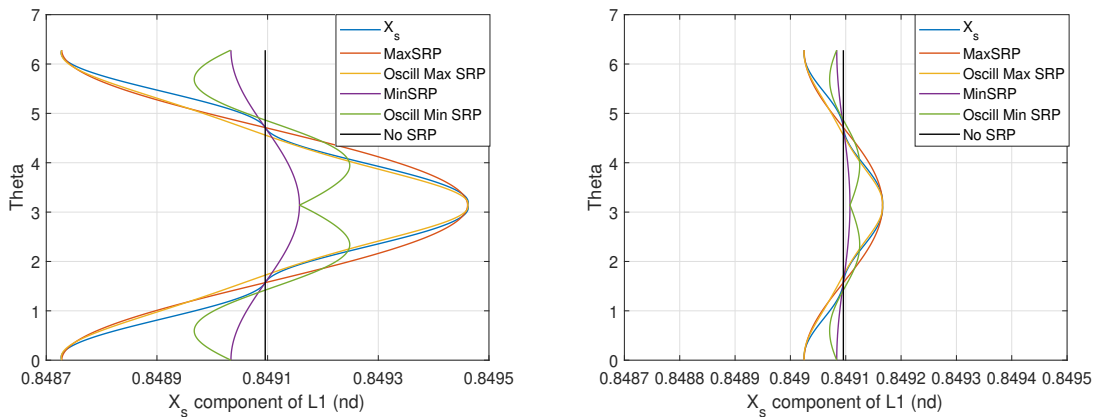
(a) Binary asteroid system at perihelion of its orbit around the Sun for the N-plate SRP acceleration model  
 (b) Binary asteroid system at aphelion of its orbit around the Sun for the N-plate SRP acceleration model

Figure 5–8: SRP acceleration in the  $Y_s$  direction of the synodic reference frame throughout one rotation of the binary asteroid system for the N-plate SRP acceleration model

It is this variation of the SRP acceleration over one revolution of the binary asteroid system that makes the system time-variant (non-autonomous). As the motion of the spacecraft is calculated in the synodic reference frame, it does not have an acceleration that is constant for a specific position, except if the trajectory has a specific period. This is what is observed in the coming parts of the study as the trajectories that were periodic when the SRP acceleration was not taken into account are highly modified by the SRP. Figures 5–7 and 5–8 also show the difference in the variation of the SRP acceleration when the binary asteroid system is at perihelion and when it is at aphelion of its orbit around the Sun.

### 5.6.3 Equilibrium Regions throughout one Rotation of the Binary Asteroid System

As the SRP acceleration changes while the binary asteroid system is rotating, the position of the equilibrium points is also changing. Since they change position, it is more appropriate to refer to them as equilibrium regions. Figure 5–9 shows the variation of the value of the  $L_1$  equilibrium point for 1 rotation of the binary asteroid system for all the different attitude schemes. The area covered by the curves represents the equilibrium region for  $L_1$ . As one can notice, the curves have a shape similar to the one of the variation of the SRP acceleration in the  $X_S$  direction of the synodic reference frame, see Fig. 5–7.



(a) Binary asteroid system at perihelion of its orbit around the Sun (b) Binary asteroid system at aphelion of its orbit around the Sun

Figure 5–9: Evolution of the  $L_1$  equilibrium region for one rotation of the binary asteroid system

#### 5.6.4 Study of the Influence of the Attitude Scheme on the Impact of the SRP Acceleration

Here, planar trajectories around body 1, body 2 and around the entire system are analyzed. For each of the trajectories, the attitude schemes described in section 5.1 are applied. The data that is looked at is as follow: the evolution of the  $C$  value and the value of the  $X_S$  coordinate at the  $X_S$ - $Z_S$  plane crossing. These give both a quantitative and qualitative overview of the evolution of the trajectories.

Table 5-2 shows the initial conditions, i.e. initial position  $x_0$  and velocity  $vy_0$ , in the synodic reference frame and the  $C$  value of the analyzed trajectories before the SRP acceleration is added to the model. *Retro main* is the retrograde trajectory around primary body 1, *Retro small* is the retrograde trajectory around primary body 2, *Retro sys* is the retrograde trajectory around the entire binary asteroid system and *Direct sys* is the direct trajectory around the entire binary asteroid system. The trajectories can also be seen in Fig. 5-2.

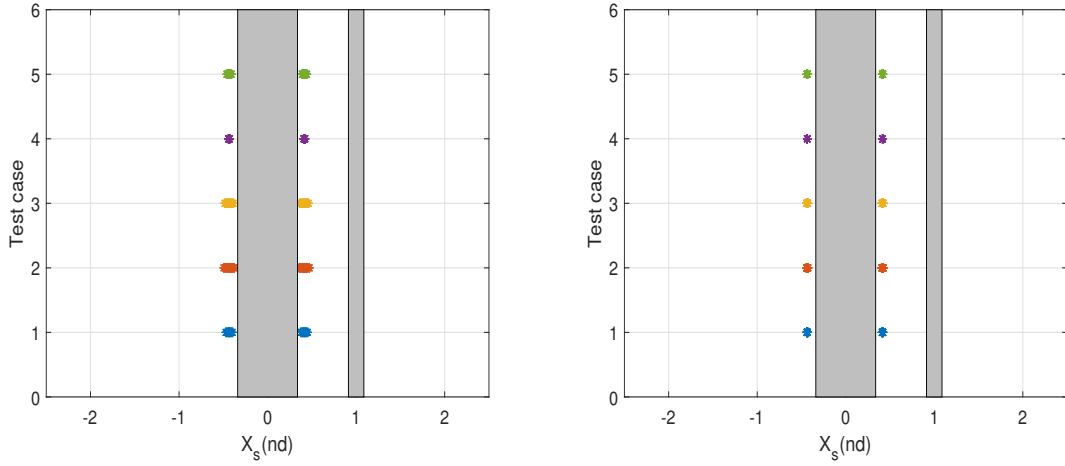
Table 5-2: Description of trajectories analyzed

<i>Trajectory</i>	$x_0$	$vy_0$	$C$
<i>Retro main</i>	0.41600	-1.96446	1.02825
<i>Retro small</i>	1.16501	-0.45776	2.94431
<i>Retro sys</i>	1.15929	-2.11045	-1.30116
<i>Direct sys</i>	1.50997	-0.75521	3.04700

### Crossing of the $X_S$ - $Z_S$ Plane

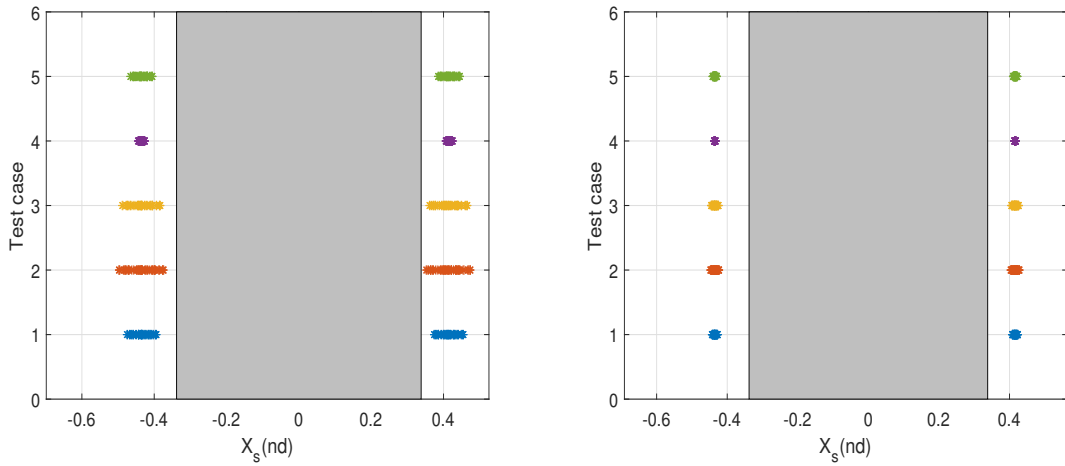
Figures 5–10 to 5–16 show the values of the  $X_S$  component of the position vector of the spacecraft at the crossing of the trajectories with the  $X_S$ - $Z_S$  plane. The dark regions are the space taken by the primary bodies. If a cloud of dots crosses one of the dark regions, the spacecraft has impacted one of the primary bodies. The simulations are done over a duration of ten revolutions of the binary asteroid system except for the case of the direct trajectory around the binary asteroid system where the simulation time was doubled because of its long period. For each figure, test case 1 is for the  $X_S$  attitude scheme, test case 2 is for the *MaxSRP* attitude scheme, test case 3 is for the *Oscill MaxSRP*, test case 4 is for the *MinSRP* attitude scheme and test case 5 is for the *Oscill MinSRP* attitude scheme. When the binary asteroid system is at the perihelion of its orbit around the Sun, the trajectories using the *MaxSRP* and *Oscill MaxSRP* attitude schemes have a greater risk of impacting one of the primary body. The *MinSRP* attitude scheme prevents impacts with a primary body. The trajectories where the *Oscill MinSRP* attitude scheme is used also seem to be safe. When the  $X_S$  attitude scheme is used, the safety of the trajectory is more dependent on the trajectory. As expected, changing the attitude scheme of the spacecraft can change the issue of a mission from unsafe for the spacecraft to safe.

On the other hand, the impact of the attitude of the spacecraft on the trajectories is not as obvious when the binary asteroid system is at the aphelion of its orbit around the Sun. In that case, the attitude scheme of the spacecraft does not influence the safety of the mission.



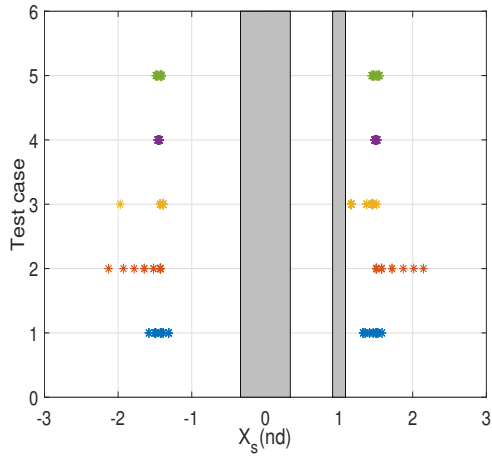
(a) Binary asteroid system at perihelion of its orbit around the Sun  
 (b) Binary asteroid system at aphelion of its orbit around the Sun

Figure 5–10: Retrograde trajectory around primary body 1 crossing with  $X_S$ - $Z_S$  plane

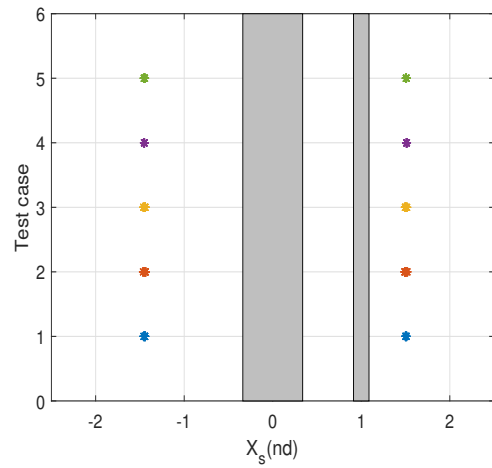


(a) Binary asteroid system at perihelion of its orbit around the Sun  
 (b) Binary asteroid system at aphelion of its orbit around the Sun

Figure 5–11: Retrograde trajectory around primary body 1 crossing with  $X_S$ - $Z_S$  plane zoomed around primary body 1

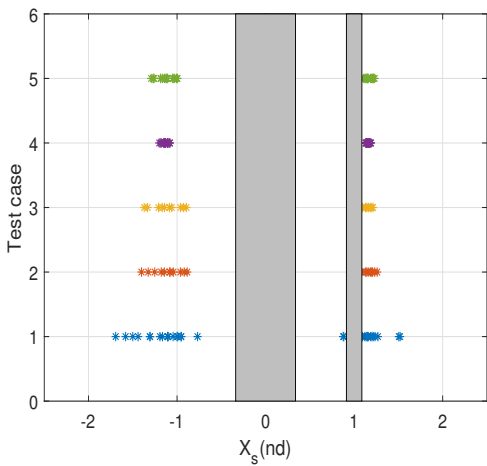


(a) Binary asteroid system at perihelion of its orbit around the Sun

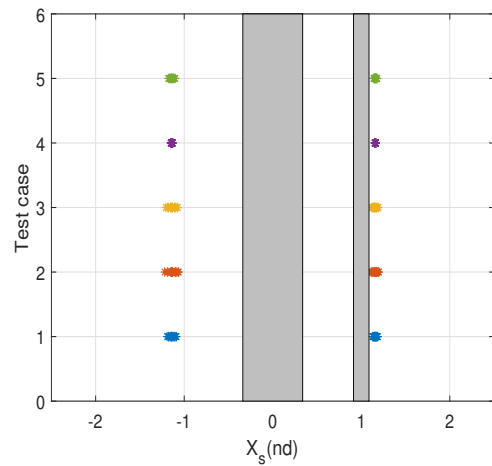


(b) Binary asteroid system at aphelion of its orbit around the Sun

Figure 5–12: Direct trajectory around binary asteroid system crossing with  $X_S$ - $Z_S$  plane

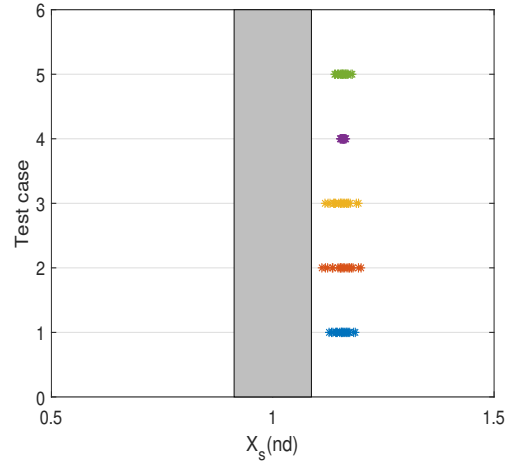
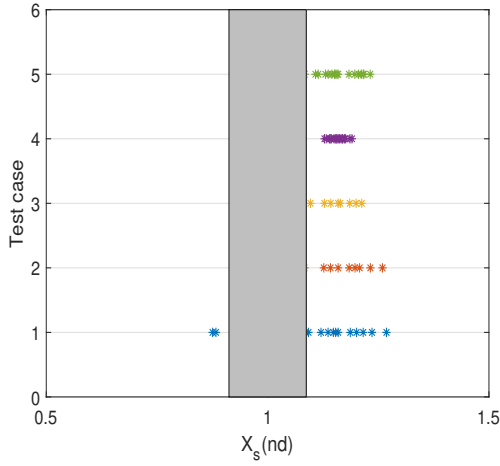


(a) Binary asteroid system at perihelion of its orbit around the Sun



(b) Binary asteroid system at aphelion of its orbit around the Sun

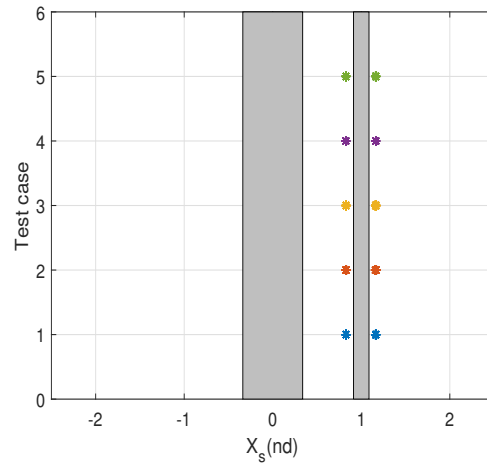
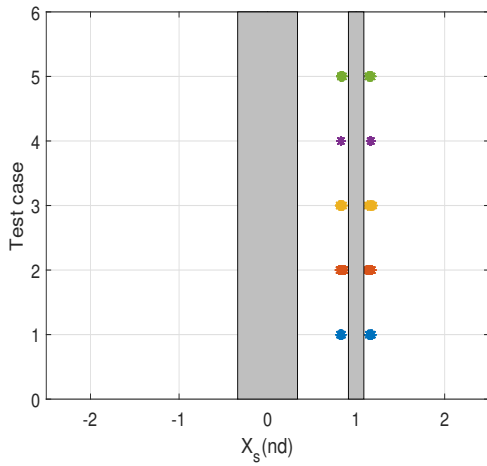
Figure 5–13: Retrograde trajectory around binary asteroid system crossing with  $X_S$ - $Z_S$  plane



(a) Binary asteroid system at perihelion of its orbit around the Sun

(b) Binary asteroid system at aphelion of its orbit around the Sun

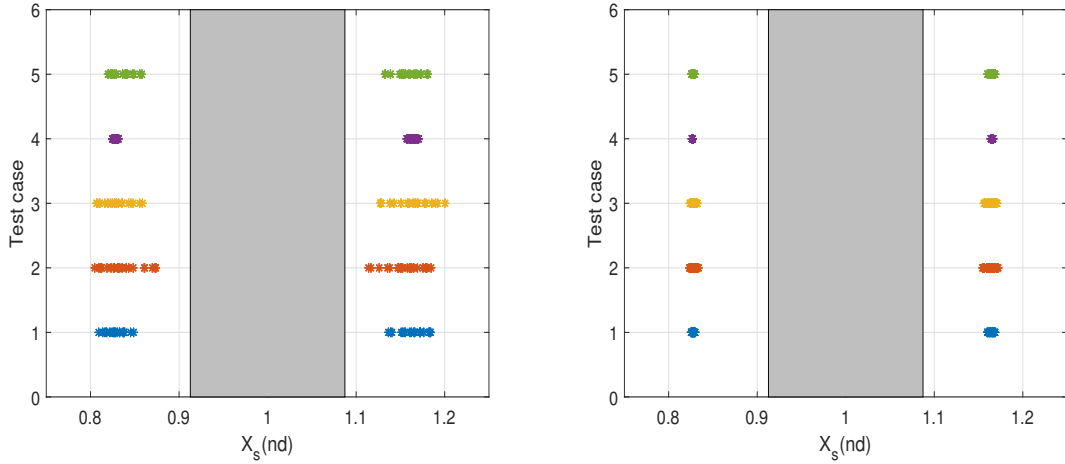
Figure 5–14: Retrograde trajectory around binary asteroid system crossing with  $X_S-Z_S$  plane zoomed around primary body 2



(a) Binary asteroid system at perihelion of its orbit around the Sun

(b) Binary asteroid system at aphelion of its orbit around the Sun

Figure 5–15: Retrograde trajectory around primary body 2 crossing with  $X_S-Z_S$  plane

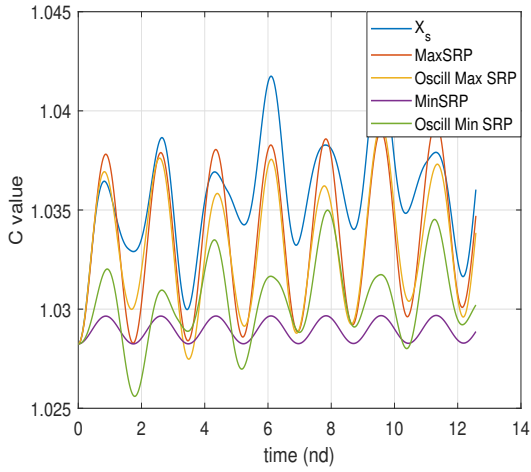


(a) Binary asteroid system at perihelion of its orbit around the Sun  
 (b) Binary asteroid system at aphelion of its orbit around the Sun

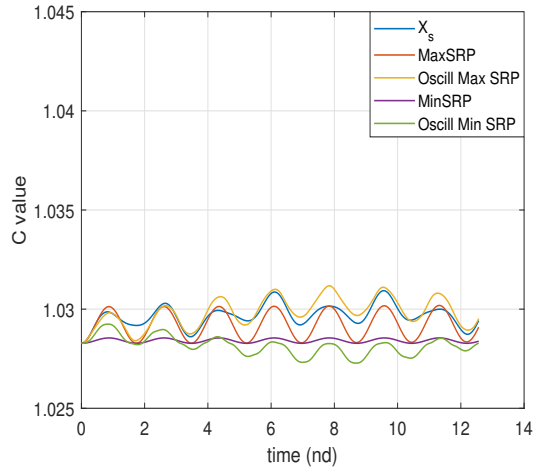
Figure 5–16: Retrograde trajectory around primary body 2 crossing with  $X_S$ - $Z_S$  plane zoomed around primary body 2

### Evolution of the C Value

As stated in section 4.2.3, when the SRP acceleration is considered, there is no Jacobi constant related to the trajectory. A  $C$  value can still be calculated, but it will change as the spacecraft is operated in the binary asteroid environment. Figures 5–17 to 5–20 show how the  $C$  value varies for the different trajectories studied. It is interesting to note that the averaged energy of the spacecraft can then be modified by using a different attitude scheme. Even if the amplitude of the variation of the  $C$  value is smaller at aphelion than at perihelion of the binary asteroid system orbit around the Sun, it is visible.

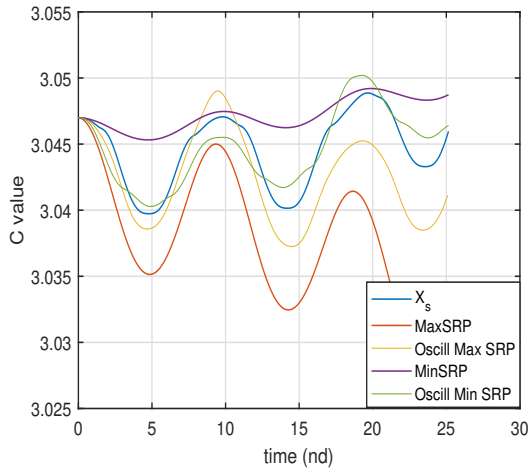


(a) Binary asteroid system at perihelion of its orbit around the Sun

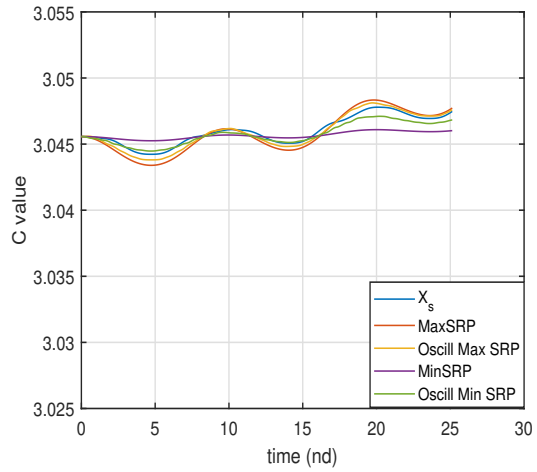


(b) Binary asteroid system at aphelion of its orbit around the Sun

Figure 5–17: Evolution of the  $C$  value for two rotations of the system for a retrograde trajectory around primary body 1

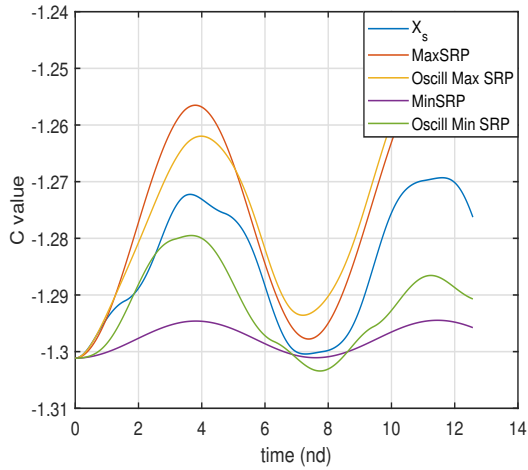


(a) Binary asteroid system at perihelion of its orbit around the Sun

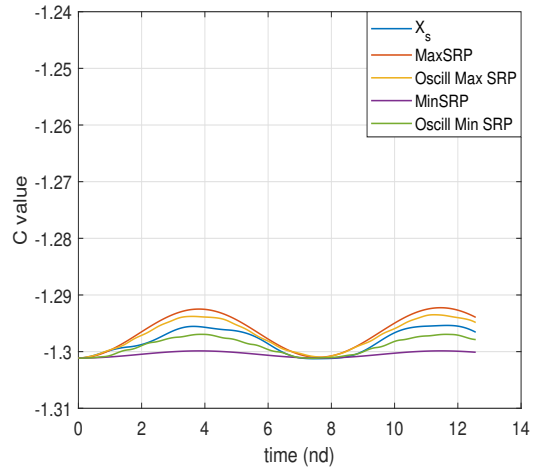


(b) Binary asteroid system at aphelion of its orbit around the Sun

Figure 5–18: Evolution of the  $C$  value for four rotations of the system for a direct trajectory around the binary asteroid system

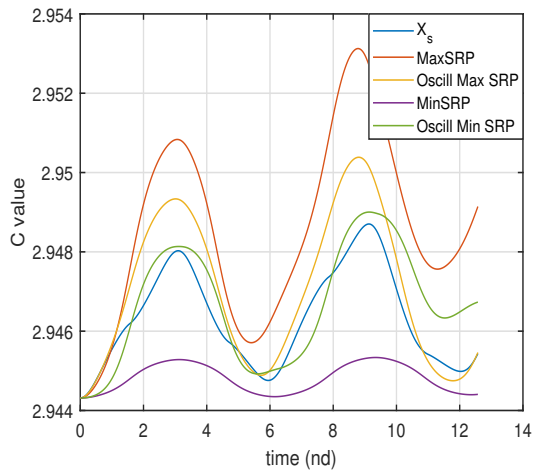


(a) Binary asteroid system at perihelion of its orbit around the Sun

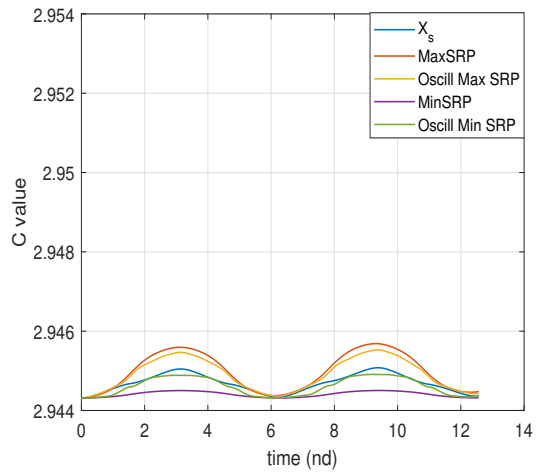


(b) Binary asteroid system at aphelion of its orbit around the Sun

Figure 5–19: Evolution of the  $C$  value for two rotations of the system for a retrograde trajectory around the binary asteroid system



(a) Binary asteroid system at perihelion of its orbit around the Sun



(b) Binary asteroid system at aphelion of its orbit around the Sun

Figure 5–20: Evolution of the  $C$  value for two rotations of the system for a retrograde trajectory around primary body 2

### Special Case: Retrograde Trajectories Around Primary Body 2 Designed with SRP Acceleration

A special case to study the possibility of having periodic trajectories in the presence of the SRP was considered. For each of the spacecraft attitude schemes a new retrograde trajectory was designed around primary body 2 using the technique presented in section 4.2.4. The initial conditions for these trajectories when the binary asteroid system is at the perihelion of its orbit around the Sun are presented in Table 5–3. Table 5–4 represent the initial conditions when the binary asteroid system is at aphelion of its orbit around the Sun.

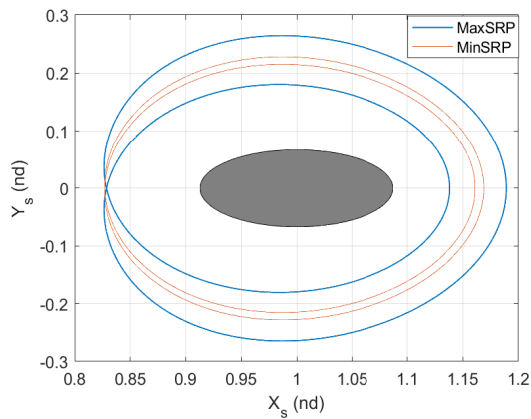
Table 5–3: Initial conditions for periodic trajectories

<i>Attitude scheme</i>	$x_0$	$vy_0$	$C$
<i>X</i>	1.17793	−0.46364	2.94267
<i>Max</i>	1.18914	−0.46953	2.94196
<i>Oscill max</i>	1.18462	−0.46733	2.94193
<i>Min</i>	1.16888	−0.45927	2.94385
<i>Oscill min</i>	1.17937	−0.46395	2.94216

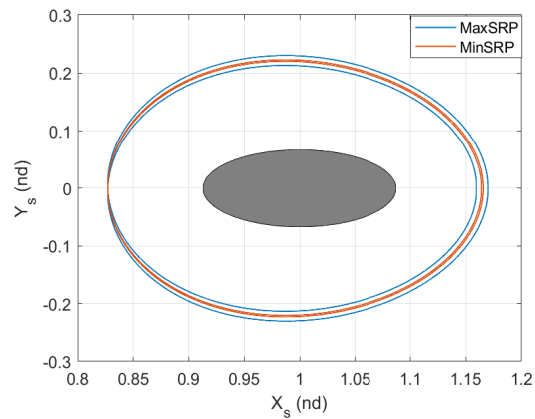
Table 5–4: Initial conditions for periodic trajectories

<i>Scheme</i>	$x_0$	$vy_0$	$C$
<i>X</i>	1.16759	−0.45880	2.94396
<i>Max</i>	1.17010	−0.45978	2.94371
<i>Oscill max</i>	1.16933	−0.45950	2.94376
<i>Min</i>	1.16577	−0.45804	2.94422
<i>Oscill min</i>	1.16748	−0.45868	2.94404

These trajectories have a period that is half of the period of rotation of the binary asteroid system. Figure 5–21 shows these trajectories over ten revolutions of the binary asteroid system for the *MaxSRP* and *MinSRP* attitude schemes for both binary asteroid system-Sun distances. Similar results are found for the other attitude scheme. It can be noted here that these trajectories are periodic and do not diverge. The dark ellipse in the middle is primary body 2. This periodicity is also visible in the evolution of the  $C$  value. Since the trajectories do not start with the same position and velocity, they all have different  $C$  curves. What is to be noticed in Fig. 5–22 is that the  $C$  values are periodic, as are the trajectories.

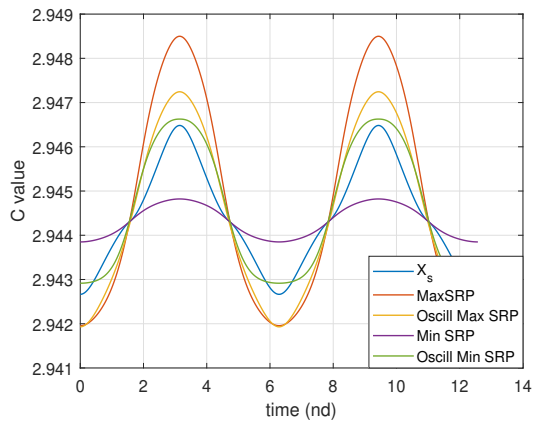


(a) Binary asteroid system at perihelion of its orbit around the Sun

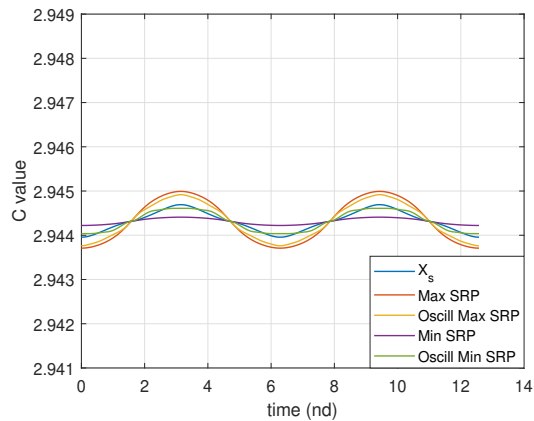


(b) Binary asteroid system at aphelion of its orbit around the Sun

Figure 5–21: Periodic trajectories over ten revolutions of the binary asteroid system shown in the synodic reference frame



(a) Binary asteroid system at perihelion of its orbit around the Sun



(b) Binary asteroid system at aphelion of its orbit around the Sun

Figure 5–22: Evolution of the  $C$  value for the periodic trajectories over two revolutions of the binary asteroid system

## 5.7 Summary

This chapter presented a full study of the effect of the SRP on the dynamics of a spacecraft in the vicinity of a binary asteroid represented in the FCRTBP. Various ways of modeling the SRP acceleration, taking into account the optical properties of the spacecraft and different attitude schemes, were studied. The results when the binary asteroid system is at perihelion and when it is at aphelion of its orbit around the Sun were also compared. It was shown that when the binary asteroid system is at perihelion, the choice of the SRP acceleration model has a direct impact on how a change in the attitude of the spacecraft is reflected in its dynamics. It was demonstrated that the only model that can correctly show how the dynamics of the spacecraft is affected by the SRP acceleration is the N-plate model.

Then, a study of the variation of the SRP acceleration and the equilibrium regions was done over one evolution of the binary asteroid system, showing the complexity of the dynamics of a spacecraft in a binary asteroid system when the SRP acceleration is taken into account. The SRP acceleration value depends on the attitude of the spacecraft with respect to the inertial reference frame and the angular position of the synodic reference frame with respect to the inertial reference frame, not on the position of the spacecraft, contrary to the acceleration due to the gravitational potential of the binary asteroid system.

A few spacecraft attitude schemes were then studied for different trajectories of the spacecraft in the binary asteroid system. Here, it was demonstrated that the

attitude scheme has a direct impact on the safety of the spacecraft in a potential mission, showing the important coupling between the attitude and the orbital dynamics in the presence of the SRP.

Finally, a special case was presented. This particular case for this specific binary asteroid system, similar to Didymos, showed that it can be possible to have periodic motion for some trajectories in the FCRTBP even when a more complex SRP acceleration model is used.

This chapter intended to demonstrate how details such as the level of complexity of the SRP acceleration model, the optical properties of the spacecraft, the attitude scheme of the spacecraft and the distance between the binary asteroid system and the Sun can affect the orbital dynamics of a spacecraft in a binary asteroid system environment.

Next chapter is studying the FRTBP. A more detailed model of the binary asteroid system, including the SRP acceleration, is used to design spacecraft trajectories.

## CHAPTER 6

### The Full Restricted Three Body Problem

The previous chapters studied the impact of the SRP on the motion of a spacecraft in the FCRTBP. In fact, the mutual motion of the primary bodies of the binary asteroid 65083 Didymos is not circular, but elliptical. The primary bodies are not tri-axial ellipsoids, but have complex irregular shapes. On top of this, body 1 has an angular velocity that is different from that of the system as a whole. This chapter is dedicated to studying how these characteristics of the system impact the way trajectories should be designed in the FRTBP and how it is possible to maintain a spacecraft as close as possible to these trajectories by using a control system designed for this purpose. This involves using a multiple-shooting correction scheme to go from a trajectory design in the classical CRTBP to one that is optimized for the FRTBP. The control system used is based on Lyapunov's stability theory, augmented with Butterworth low-pass filters. As recommended in the previous chapters, the SRP acceleration is incorporated into the dynamical model used to design the trajectories.

Here, the time frame used is still short enough to consider the barycenter of the binary asteroid system to be at an approximately fixed position in the inertial reference frame and orbits the Sun in the same plane as the mutual motion of the primary bodies of the system. The primary bodies are considered to have a uniform density.

The gravitational potential model used is the fourth-order Taylor series expansion. The inertial integrals are calculated based on a polyhedron shape model of the primary bodies, as described in Appendix C.2. The N-plates model, described in Appendix D, is chosen for the calculation of the SRP acceleration. The spacecraft is assumed to have an inertially fixed attitude, with its solar panels always facing the Sun, which corresponds to the attitude scheme *Maximum SRP acceleration* described in section 5.1.3. The motion of body 2 around the barycenter of the system is calculated using Keplerian motion, as described in section 3.3.3.

## 6.1 Equations of Motion

The equations of motion are based on the theory of the FRTBP, with the addition of the acceleration due to the SRP. In the FRTBP, the spacecraft is operated in a system where the primary bodies are orbiting their barycenter. The equations of motion are expressed in the synodic reference frame. In the FRTBP, the non-dimensional equations of motion for non-spherical bodies, including the SRP acceleration, are:

$$\begin{aligned}
 x'' &= 2\omega y' + \omega' y + U_x + a_{SRP_x} \\
 y'' &= -2\omega x' - \omega' x + U_y + a_{SRP_y} \\
 z'' &= U_z + a_{SRP_z}
 \end{aligned}
 \tag{6.1}$$

where  $x''$ ,  $y''$  and  $z''$  are the acceleration in the  $X_S$ ,  $Y_S$  and  $Z_S$  directions of the synodic reference frame;  $\omega$  is the angular velocity and  $\omega'$  is the angular acceleration due to the non-circular motion of the primaries of the binary asteroid system;  $a_{SRP_i}$  is the acceleration due to the SRP in the  $i$  direction of the synodic reference frame,

$U_i$  is the differentiation with respect to the coordinate  $i$  of the effective potential, which is the sum of the gravitational potential and the potential generated by the centripetal acceleration of the rotating binary asteroid system:

$$U = U_{grav} + \frac{1}{2}\omega^2 (x^2 + y^2) \quad (6.2)$$

## 6.2 Building Nominal Trajectories

One of the goals in this chapter is to be able to build nominal trajectories for a spacecraft operated in a binary asteroid system. Their main characteristic is that they require low control thrust to be maintained. These trajectories are built based on an initial guess calculated in the CRTBP, as explained in section 4.2.1. The initial guess trajectories are then divided into multiple segments that connect in the CRTBP, but not in the FRTBP. The goal of the multiple-shooting correction scheme is to modify the segments so that they connect in the FRTBP, creating a trajectory that is as much as possible continuous both in position and in velocity.

### 6.2.1 Multiple-shooting Correction Scheme

The multiple-shooting correction scheme used to design the trajectories is shortly described here. It is based on the work done by [50] and [12], but applied to the dynamics model defined in this chapter.

The trajectory is built based on an initial guess, calculated based on a simpler model, which is divided in  $N$  segments. At each iteration, the segments are adjusted so that the trajectory is, as much as possible, continuous in position and velocity. The modifications to the initial conditions of the segments required to achieve this goal are calculated based on the state transition matrix of each segment.

### Definition of the State Transition Matrix for One Segment

Similarly to the case of the differentiation-correction scheme presented in Chapter 4, the state transition matrix of a segment relates its final and initial state:

$$\delta \mathbf{x}(k+1) = \mathbf{\Phi}(k+1; k) \delta \mathbf{x}(k) \quad (6.3)$$

where  $k$  is the time at the beginning of a segment  $k+1$  is the time at the beginning of the next segment.  $\mathbf{\Phi}(k+1; k)$  is calculated via numerical integration, with  $\mathbf{\Phi}(k; k) = \mathbf{I}_{6 \times 6}$ , a 6x6 identity matrix as initial condition:

$$\mathbf{\Phi}'(k + \delta t; k) = \mathbf{A} \mathbf{\Phi}(k + \delta t; k) \quad (6.4)$$

where  $\delta t$  corresponds to the difference between the time at the beginning of a segment and the simulation time and  $\mathbf{A}$  is defined below.

Note that it is also possible to relate the variation of the state of node  $k$  with the variation of the state of node  $k+1$  by inverting the state transition matrix:

$$\mathbf{\Phi}(k+1; k) = \mathbf{\Phi}^{-1}(k; k+1) \quad (6.5)$$

Defining the state of the linearized system as  $\mathbf{x} = \begin{bmatrix} \delta \mathbf{r} & \delta \mathbf{r}' \end{bmatrix}$ , where  $\delta \mathbf{r}$  and  $\delta \mathbf{r}'$  are the variations of a position and its derivative around an operating position  $\mathbf{r}_0$ , it is possible to define a matrix  $\mathbf{A}$  such that:

$$\mathbf{x}' = \mathbf{A} \mathbf{x} \quad (6.6)$$

In the actual case, the  $\mathbf{A}$  matrix corresponds to:

$$\mathbf{A} = \begin{bmatrix} \mathbf{0} & \mathbf{I}_3 \\ \left. \frac{\partial^2 U}{\partial r^2} \right|_{r_0} + \boldsymbol{\omega}' & 2\boldsymbol{\omega} \end{bmatrix} \quad (6.7)$$

Note that the SRP acceleration is not included in the calculation of matrix  $\mathbf{A}$ .

$$\boldsymbol{\omega}' = \begin{bmatrix} 0 & \omega' & 0 \\ -\omega' & 0 & 0 \\ 0 & 0 & 0 \end{bmatrix}, \boldsymbol{\omega} = \begin{bmatrix} 0 & \omega & 0 \\ -\omega & 0 & 0 \\ 0 & 0 & 0 \end{bmatrix} \quad (6.8)$$

Then, to find how to modify the initial state of a segment, so that the final state is the same as the initial states of the next segment, the following equation needs to be applied:

$$\delta \mathbf{x}(k) = \boldsymbol{\Phi}^{-1}(k; k+1) \delta \mathbf{x}(k+1) \quad (6.9)$$

One needs to observe that the state transition matrix is calculated based on a linearized version of the equations of motion of the system. An iteration process is then required to achieve continuity in the trajectory. It is also possible that the correction scheme is not capable of converging into a satisfactory solution.

### Correcting Multiple Segments Simultaneously

To assure that the correction is optimized, it has to be done simultaneously on all segments. For that purpose, a state vectrix, a matrix composed of vectors, is built with the state of the spacecraft (position and velocity) at the beginning of each

segment:

$$\mathbf{X}^0 = \begin{bmatrix} \mathbf{X}_1^0 \\ \vdots \\ \mathbf{X}_{N-1}^0 \\ \mathbf{X}_N^0 \end{bmatrix} \quad (6.10)$$

Since the goal is to have the final state of a segment being equal to the initial state of the next segment, the constraint vectrix is composed of the difference between the final state of a segment and the initial state of the following segment, which corresponds to the required variation of the final state to have continuity between the segments. Note that periodicity is ensured by including the difference between the final state of the last segment and the initial state of the first segment:

$$\mathbf{F}(\mathbf{X}) = \begin{bmatrix} \mathbf{X}_1^f - \mathbf{X}_2^0 \\ \vdots \\ \mathbf{X}_{N-1}^f - \mathbf{X}_N^0 \\ \mathbf{X}_N^f - \mathbf{X}_1^0 \end{bmatrix} = \begin{bmatrix} \delta \mathbf{X}_1^f \\ \vdots \\ \delta \mathbf{X}_{N-1}^f \\ \delta \mathbf{X}_N^f \end{bmatrix} = \delta \mathbf{X}^f \quad (6.11)$$

The Jacobian matrix of the state and constraint vectrices is:

$$\mathbf{J}(\mathbf{X}) = \frac{\partial \mathbf{F}(\mathbf{X})}{\partial \mathbf{X}} = \begin{bmatrix} \frac{\partial \mathbf{X}_1^f}{\partial \mathbf{X}_1} & -\frac{\partial \mathbf{X}_2}{\partial \mathbf{X}_2} & 0 & \dots & 0 \\ 0 & \frac{\partial \mathbf{X}_2^f}{\partial \mathbf{X}_2} & -\frac{\partial \mathbf{X}_3}{\partial \mathbf{X}_3} & 0 & \dots \\ \dots & 0 & \frac{\partial \mathbf{X}_k^f}{\partial \mathbf{X}_k} & -\frac{\partial \mathbf{X}_{k+1}}{\partial \mathbf{X}_{k+1}} & \vdots \\ -\frac{\partial \mathbf{X}_1}{\partial \mathbf{X}_1} & 0 & \dots & 0 & \frac{\partial \mathbf{X}_N^f}{\partial \mathbf{X}_N} \end{bmatrix} \quad (6.12)$$

As one can see, the diagonal elements of the Jacobian matrix,  $\frac{\partial \mathbf{X}_k^f}{\partial \mathbf{X}_k}$  correspond to the state transition matrix between the end of one segment and the beginning of the same segment. The other non zero terms are the negative of 6x6 identity matrices.

The variation of the initial condition of each segment required to reduce the gap between the end of one segment and the beginning of the following one can then be calculated using the Moore-Penrose generalized inverse of the Jacobian:

$$\delta \mathbf{X}^0 = \mathbf{J}(\mathbf{X})^T \left( \mathbf{J}(\mathbf{X}) \mathbf{J}(\mathbf{X})^T \right)^{-1} \mathbf{F}(\mathbf{X}) \quad (6.13)$$

### 6.3 Control System

The trajectories built using the multiple-shooting scheme described in this chapter are unstable. For the spacecraft to be able to stay in the vicinity of the trajectories, it has to use control thrust. The design of the control system is described here.

#### 6.3.1 Lyapunov Control

The controller used in this study is based on the Lyapunov stability theory. It is used to compare the required control effort for spacecraft trajectories calculated based on the FRTBP to those calculated based on the CRTBP. The equations used are developed by [48], but they are applied to the dynamics model described earlier in this chapter. The error and control signals are calculated using the full model based on the Taylor series expansion model of the gravitational potential. The equations required for the controller are summarized here.

The error between the state of a nominal (desired) trajectory and the state of the actual trajectory of the spacecraft is defined by:

$$\mathbf{e}(t) = \mathbf{r}(t) - \mathbf{r}_d(t) \quad (6.14)$$

Considering the motion of a spacecraft in a rotating frame, where the mutual orbit of the primary bodies is circular, the acceleration of the error is then defined by:

$$\mathbf{e}'' + 2\boldsymbol{\omega}\mathbf{e}' + \boldsymbol{\omega}^2\mathbf{e} = \mathbf{F}(t)\mathbf{e} + \mathbf{u} \quad (6.15)$$

where  $\mathbf{u}$  is the control thrust vector and the matrix  $\mathbf{F}(t)$  is defined by Eq. 6.16. It is calculated at each time step of the simulation at the value of the non-dimensionalized components  $x_S, y_S, z_S$  of the position vector of the desired trajectory at that point in time:

$$\mathbf{F}(t) = \begin{bmatrix} \frac{\partial^2 U_{grav}}{\partial x^2} & \frac{\partial^2 U_{grav}}{\partial x \partial y} & \frac{\partial^2 U_{grav}}{\partial x \partial z} \\ \frac{\partial^2 U_{grav}}{\partial y \partial x} & \frac{\partial^2 U_{grav}}{\partial y^2} & \frac{\partial^2 U_{grav}}{\partial y \partial z} \\ \frac{\partial^2 U_{grav}}{\partial z \partial x} & \frac{\partial^2 U_{grav}}{\partial z \partial y} & \frac{\partial^2 U_{grav}}{\partial z^2} \end{bmatrix} \quad (6.16)$$

$\boldsymbol{\omega}$  is defined in Eq. 6.8 and  $\boldsymbol{\omega}^2$  is defined by:

$$\boldsymbol{\omega}^2 = \boldsymbol{\omega}\boldsymbol{\omega} = \begin{bmatrix} -\omega^2 & 0 & 0 \\ 0 & -\omega^2 & 0 \\ 0 & 0 & 0 \end{bmatrix} \quad (6.17)$$

The Lyapunov function,  $V$ , is given by:

$$V = \frac{1}{2} \frac{d\mathbf{e}^T}{dt} \mathbf{D}_1 \frac{d\mathbf{e}}{dt} + \frac{1}{2} \mathbf{e}^T \mathbf{D}_2 \mathbf{e} \quad (6.18)$$

where  $\mathbf{D}_1$  and  $\mathbf{D}_2$  are two constant positive definite matrices. After some algebra, the input required for a system to be asymptotically stable ( $dV/dt$  strictly negative) is:

$$\mathbf{u} = -\mathbf{Q}(\mathbf{e}') - \mathbf{P}(t)\mathbf{e} \quad (6.19)$$

where the  $\mathbf{Q}$  matrix is a constant positive definite matrix that needs to be tuned by the controller designer and  $[\mathbf{P}(t)]$  is a time-varying matrix:

$$\mathbf{P}(t) = \mathbf{Q}\boldsymbol{\omega} + \mathbf{D}_1^{-1}\mathbf{D}_2 + \mathbf{F}(t) \quad (6.20)$$

### 6.3.2 Smoothing the Control Thrust Signal

One of the issues with using a multiple-shooting scheme to design the nominal trajectories for a spacecraft is that the segments are continuous up to a certain tolerance. In the case of highly unstable trajectories, the difference between the state at the end of a segment and the state at the beginning of the following segment often reaches a plateau. This is translated in small glitches in position and velocity between the segments of the trajectory. These glitches are visible in the calculated control thrust required, which would be hard to achieve in a realistic system. An effective way to smooth out the trajectories is to introduce a low pass filter between the calculation of the error vector and the input to the Lyapunov controller and, also after the calculation of the control thrust input. This reduces the noise in the control input and the maximum control thrust required to keep the spacecraft close to its nominal trajectory. Here, low-pass fourth-order Butterworth filters, with a cutoff frequency that varies between 0.35 and 0.45 times the sampling frequency of the simulation are used. These values are tuned for each case and are chosen to reduce

the high frequency signals as much as possible, while keeping enough information to be able to control the trajectory of the spacecraft.

#### **6.4 Analysis Procedure Using the 65803 Didymos Binary Asteroid System Model**

The first step is to find initial guesses for the planned trajectories. In the present study, retrograde trajectories around body 2 have been targeted because they are planned to be used in the Hera part of the AIDA mission.  $L_1$  libration points trajectories, such as planar Lyapunov, vertical Lyapunov and halo types orbits have also been targeted because of the location of  $L_1$ , which is between the two primary bodies and permit observing them both at the same time. Initial guesses, with the binary system assumed to be composed of two point mass bodies with a circular mutual orbit, have then be designed for each of the targeted trajectory types.

The initial guess trajectories are then modified using the multiple-shooting method to fit a dynamical model based on a fourth-order Taylor series expansion of the gravitational potential of the primary bodies, with a system with primary bodies having circular mutual motion and body 1 having its own angular velocity. The final trajectory includes the SRP acceleration and the non-circular mutual motion of the primaries. For each type of trajectory, the three calculated trajectories are then used as nominal trajectories for a spacecraft operated in a fourth-order dynamical model of the FRTBP. The second and fourth-order inertia integrals are calculated based on the Didymos 65803 polyhedron shape model, used with the authorization from the author of Ref. [63]. The control effort to keep the spacecraft close to the nominal trajectory is then recorded and compared for the three nominal trajectories. Once this is done, a filter is added in the controller to smooth out the

control thrust input. The resulting trajectory and control thrust are compared with the ones without the filter.

As described earlier, the dynamical model used in this study is of the fourth order. The controller and the corrector, on the other hand, are of the second order. It reduces the computation time and the risk of numerical instability due to very small numbers produced by the second differentiation of the gravitational potential. The SRP acceleration model used in this study keeps the spacecraft in an inertially fixed attitude, with its solar panels always facing the Sun, which means maximal SRP acceleration.

Two orbits of an initial guess are used to build a nominal trajectory. The nominal trajectory is then repeated multiple times, until the binary asteroid system has made five rotations, for a total of approximately 60 hours. The control thrust results are plotted for 40 hours to make it easier to see the data.

The system used in this study is the Didymos 65803 system, with its parameters summarized in Tables 3–1 and 3–2.

## 6.5 Numerical Results

The results are presented per trajectory types. Figure 6–1 shows the trajectories in the binary asteroid system. The figures for each trajectory are zoomed on the trajectories themselves to show the details. The control thrust shown in Figures 6–4–6–19 have the following legend: blue is the thrust in the  $X_S$  direction, red is the thrust in the  $Y_S$  direction and yellow is the thrust in the  $Z_S$  direction. It represents the thrust required to control a 500 kg spacecraft.

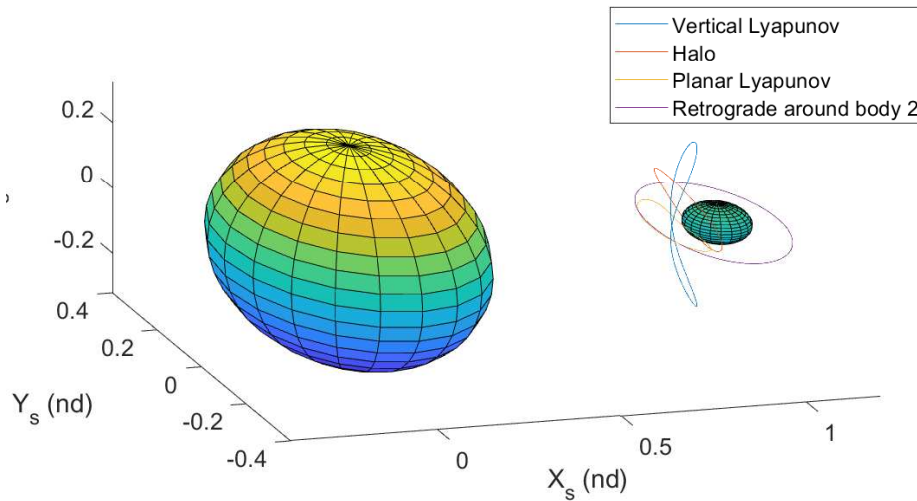


Figure 6-1: Initial guess trajectories

### 6.5.1 Retrograde Trajectory Around Body 2

The retrograde trajectory around body 2 requires 15 segments to be built. Figure 6-2 shows how it has evolved from the initial guess to the full model. Figure 6-3 shows that the spacecraft follows closely the desired trajectory. In Fig. 6-4, it is possible to see that, as mostly expected, as details are added to the model used to design the nominal trajectory, less control thrust is required to keep the spacecraft on it. The numbers being small for all nominal trajectories (less than 3 mN), and the control thrust required being cyclic, but stable, it is not absolutely necessary to use the more complex model to design the trajectory.

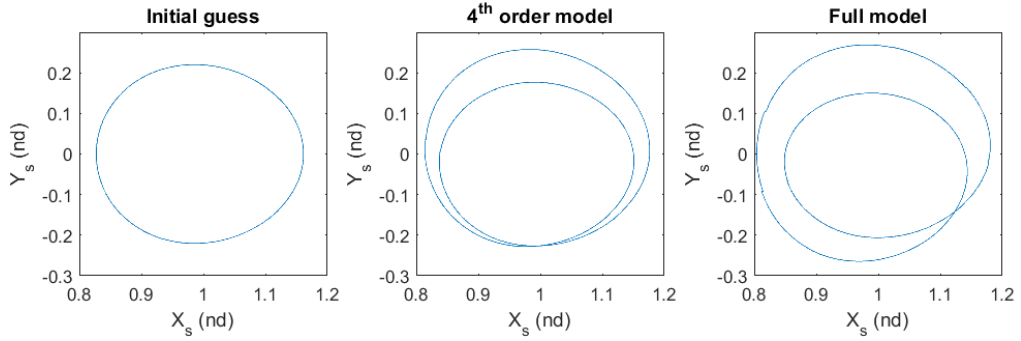


Figure 6–2: Evolution of the nominal retrograde trajectory around body 2

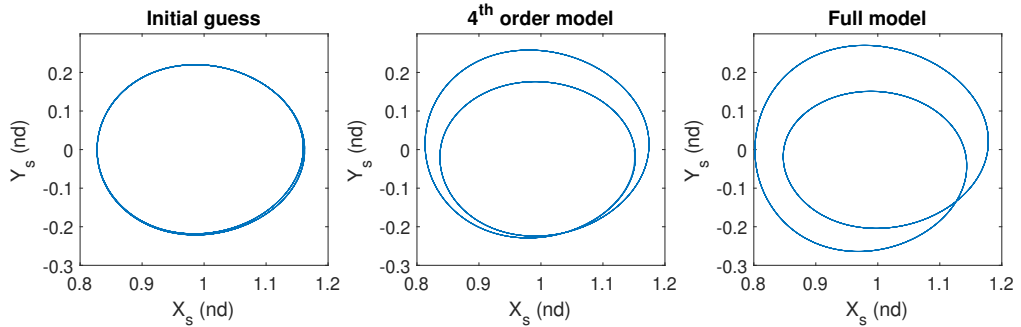


Figure 6–3: Real retrograde trajectory around body 2 followed by spacecraft

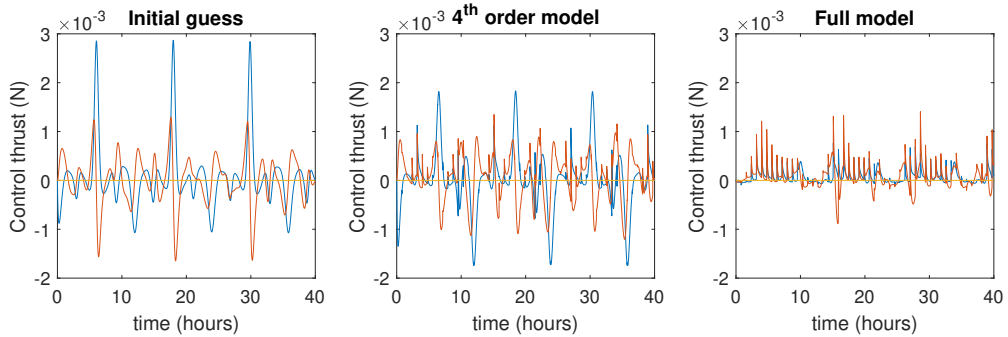


Figure 6–4: Control thrust for the retrograde trajectory around body 2

When the filter is applied to the retrograde trajectory around body 2, the oscillations in the required control thrust are reduced significantly for all nominal

trajectories, as can be seen in Fig. 6–6. On the other hand, some of the error and control signals is lost, meaning that the nominal trajectory is not followed as well, as can be seen in Fig. 6–5. In all cases, the spacecraft trajectory stays bounded. This is a trade-off that may be required between following an exact trajectory or having a control signal easier to follow.

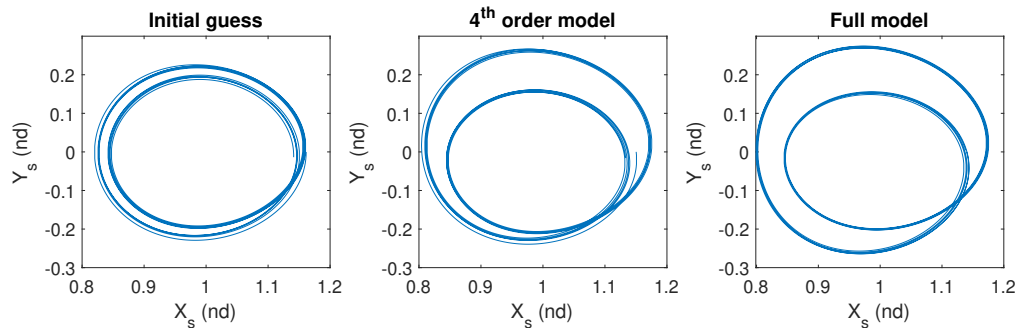


Figure 6–5: Spacecraft retrograde trajectory around body 2 when using low pass filters

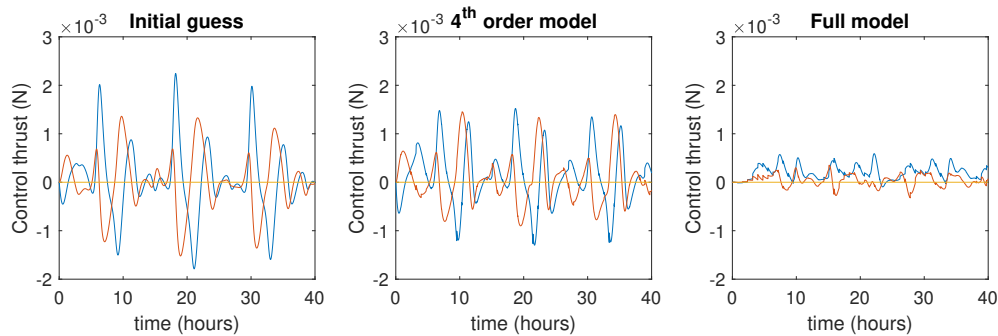


Figure 6–6: Control thrust for the retrograde trajectory around body 2 when using low pass filters

### 6.5.2 Planar Lyapunov Trajectory

The planar Lyapunov type trajectory also shows good results. It requires 15 segments to be built. Figure 6–7 shows how it has evolved from the initial guess to

the full model. In Fig. 6–8, one can see that it is quite hard for the control system to keep the spacecraft on the nominal trajectory. It is constantly a little off. In Fig. 6–9, it is possible to see that, again, as expected, as details are added to the model used to design the nominal trajectory, less control thrust is required to keep the spacecraft on it. In that case, there is significant improvement in the control thrust required to keep the spacecraft on the nominal trajectory between each of the steps.

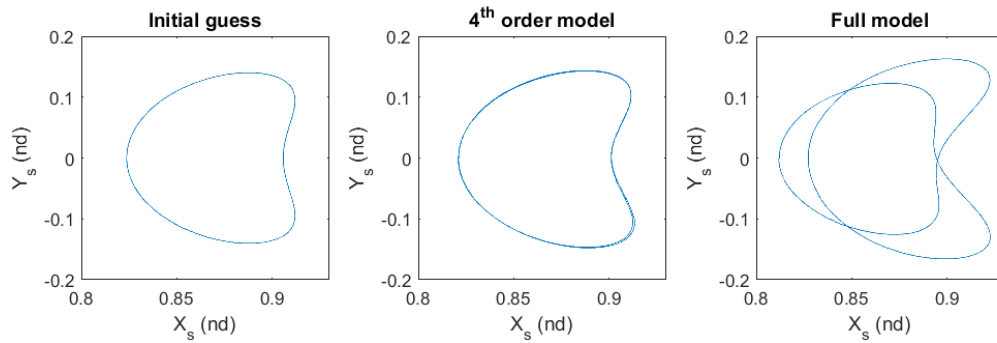


Figure 6–7: Evolution of the planar Lyapunov nominal trajectory

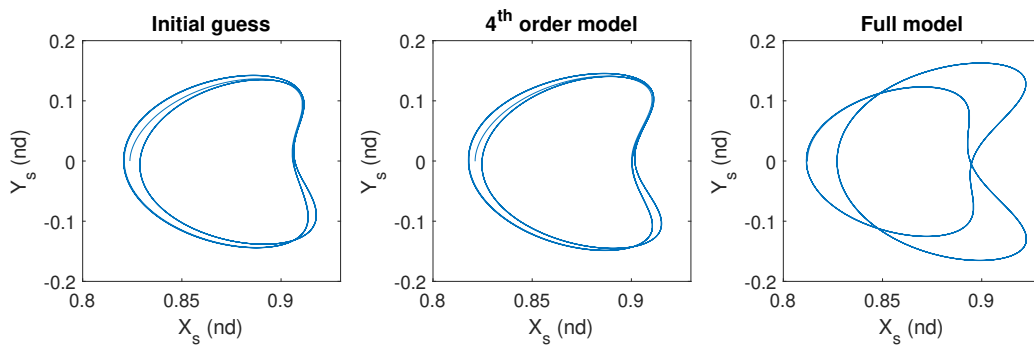


Figure 6–8: Real planar Lyapunov trajectory followed by spacecraft

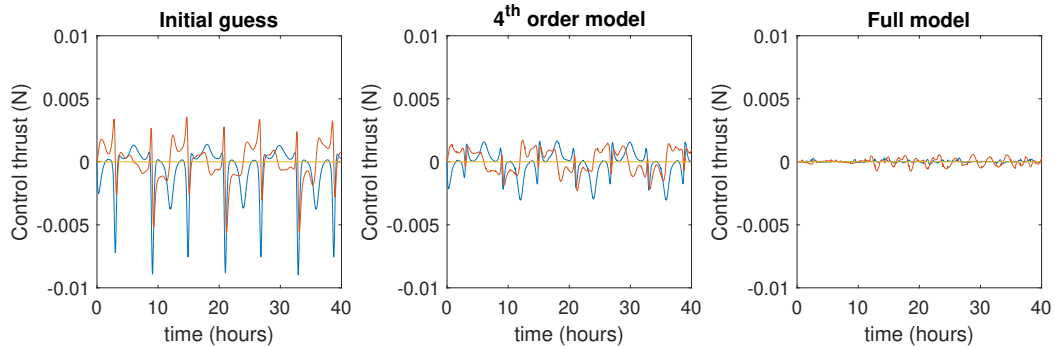


Figure 6–9: Control thrust for the planar Lyapunov trajectory

It was not possible to use the low-pass filters when the nominal trajectory is the initial guess based on the CRTBP. The control signal did not contain sufficient information for the spacecraft to keep a bounded trajectory. In the other two cases, the filtered signal was sufficient to keep the spacecraft trajectory bounded, as can be seen in Fig. 6–10. On the other hand, Fig. 6–11 does not show significant improvement in the required thrust. It may not be necessary here to use the filters.

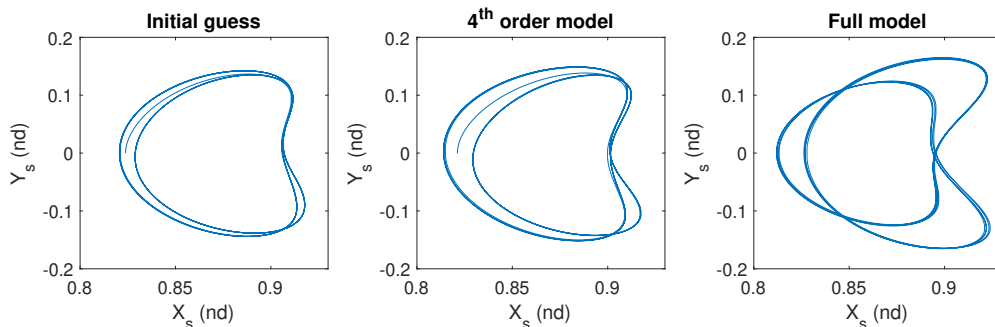


Figure 6–10: Spacecraft planar Lyapunov trajectory when using low pass filters

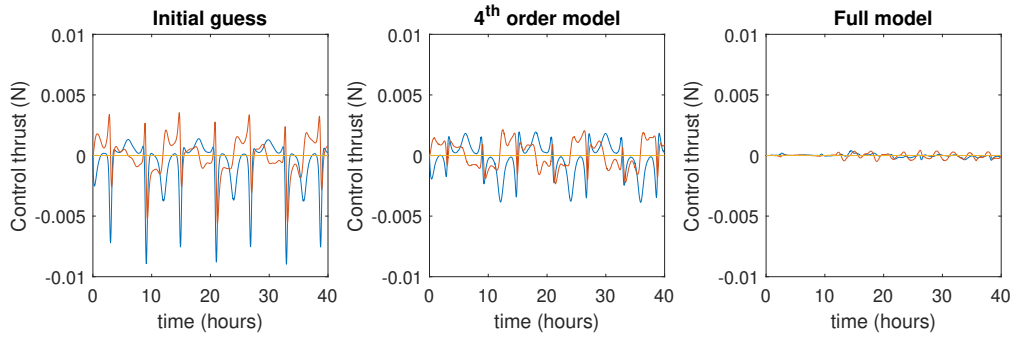


Figure 6–11: Control thrust for the planar Lyapunov trajectory when using low pass filters

### 6.5.3 Vertical Lyapunov Trajectory

The vertical Lyapunov type trajectory requires 45 segments to be built. Figure 6–12 shows how it has evolved from the initial guess to the full model. Figure 6–13 shows the actual trajectory followed by the spacecraft. In Fig. 6–14, it is possible to see that the control thrust required suddenly increases at approximately 16.5 hours, which is when the initial nominal trajectory is repeated. It means, here, that the error between the initial and final states of the nominal trajectory is too large and requires a larger control thrust to maintain the trajectory. Notice that the controller can handle the perturbation and still keep the spacecraft on the nominal trajectory. It is then preferred here, to not include the major perturbations such as the SRP acceleration and the ellipticity of the mutual orbit in the model used to build the nominal trajectory.

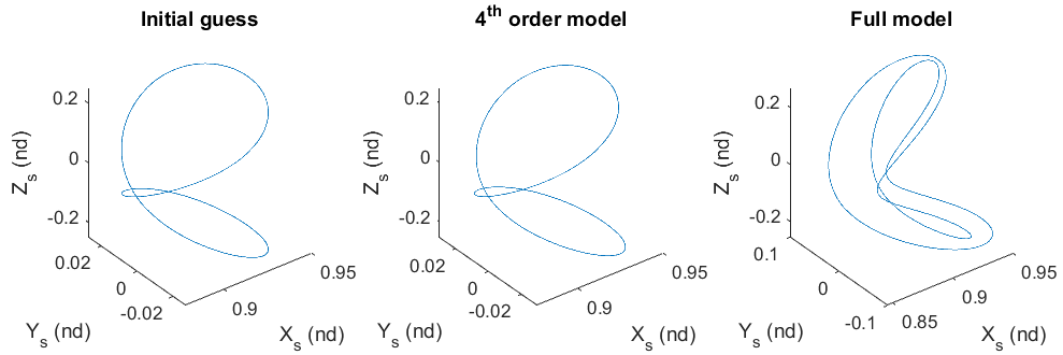


Figure 6–12: Evolution of the vertical Lyapunov nominal trajectory

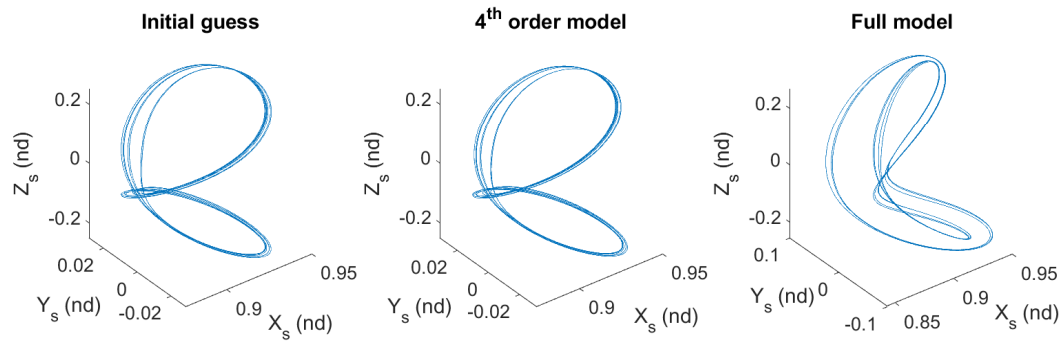


Figure 6–13: Real vertical Lyapunov trajectory followed by spacecraft

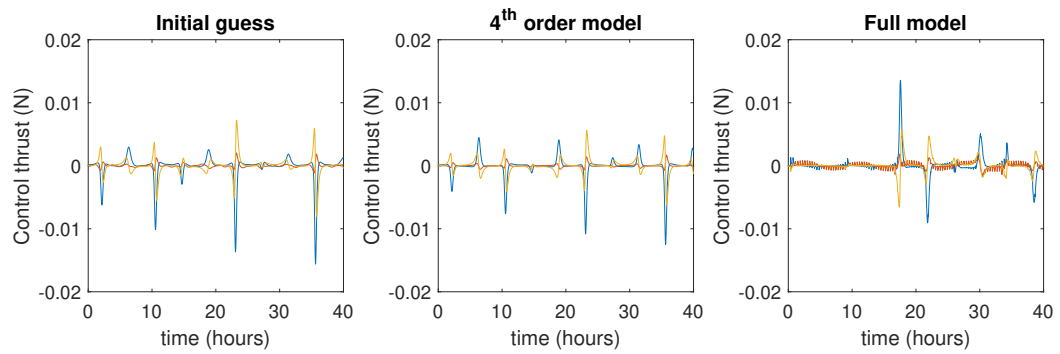


Figure 6–14: Control thrust for the vertical Lyapunov trajectory

When the filters are added to the controller, the spacecraft does not follow the nominal trajectory as well as without them, but Fig. 6–15 shows that the trajectory followed by the spacecraft is still bounded. Figure 6–16 shows that the required control thrust is significantly reduced and oscillates quite less when the filters are added.

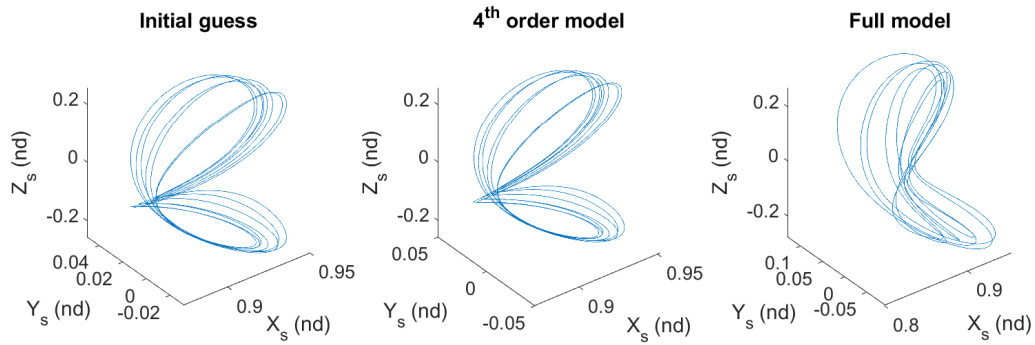


Figure 6–15: Spacecraft vertical Lyapunov trajectory when using low pass filters

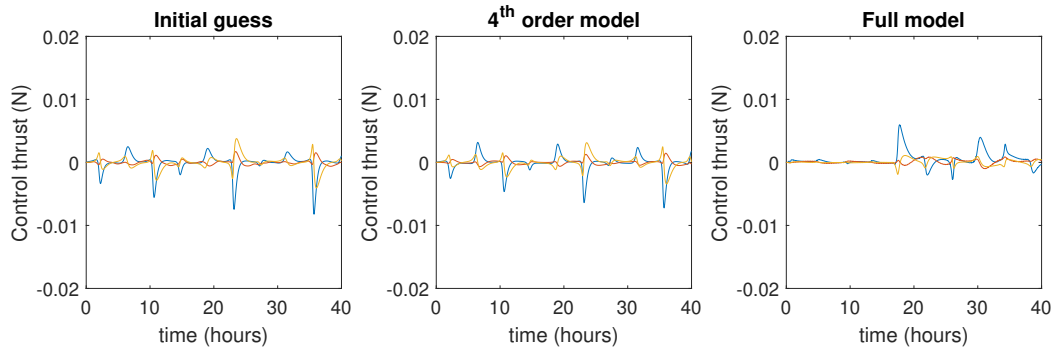


Figure 6–16: Control thrust for the vertical Lyapunov trajectory when using low pass filters

#### 6.5.4 Halo Trajectory

The halo type trajectory requires 45 segments to be built. Figure 6–17 shows how it has evolved from the initial guess to the full model. In this case, it was

not possible to build a trajectory with the ellipticity of the mutual orbit, so the "full model" is based on circular mutual motion of the primary bodies. Figure 6–18 shows the actual trajectory followed by the spacecraft. It is a little bit off the nominal trajectory, but is still bounded. In Fig. 6–19, it is possible to see that, due to the high number of segments and the small discontinuities between them in the full model, the spacecraft requires more control thrust to be kept on the full model nominal trajectory than on the other ones. In the case of trajectories which show more instability, it is then not necessary to include the major perturbations such as the SRP acceleration or the ellipticity of the mutual orbit of the primary bodies in the model used to build the nominal trajectory.

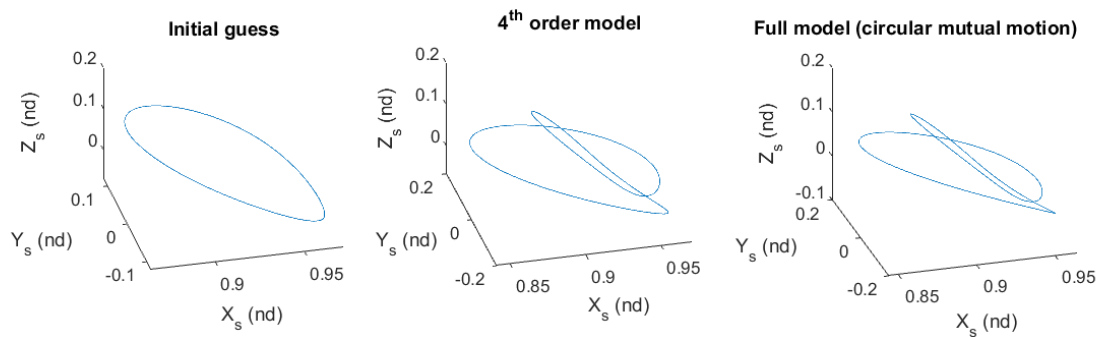


Figure 6–17: Evolution of the halo nominal trajectory

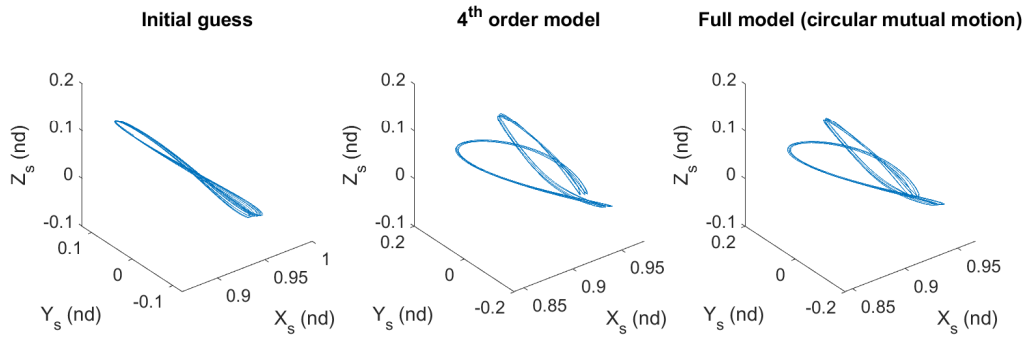


Figure 6-18: Real halo trajectory followed by spacecraft

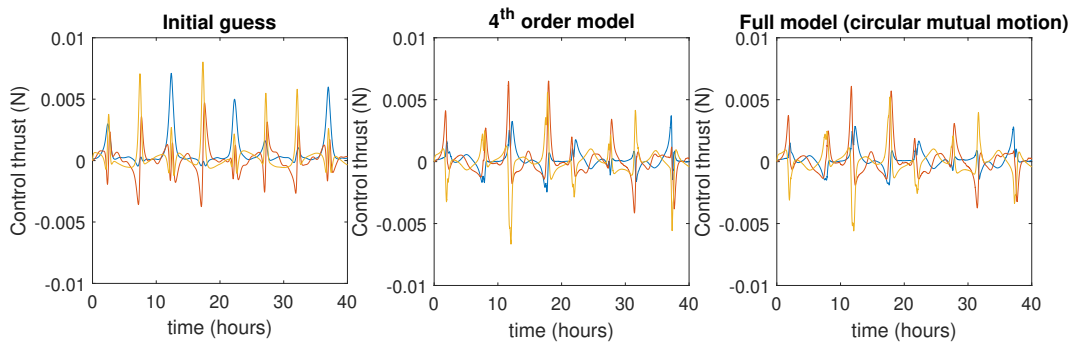


Figure 6-19: Control thrust for the halo trajectory

When the filters are added to the controller, the spacecraft does not follow the nominal trajectory as well as without them, but Fig. 6-20 shows that the trajectory followed by the spacecraft is still bounded. Figure 6-21 shows that the required control thrust is reduced when compared with the case without the filters. Here, again, there is no significant difference in the required thrust when using a more detailed model to build the nominal trajectory, but still based on a circular motion of the primary bodies. This would lead to the conclusion that the perturbation from the CRTBP that affects the nominal trajectory the most is the non-circular motion of the primary bodies around the system's barycenter.

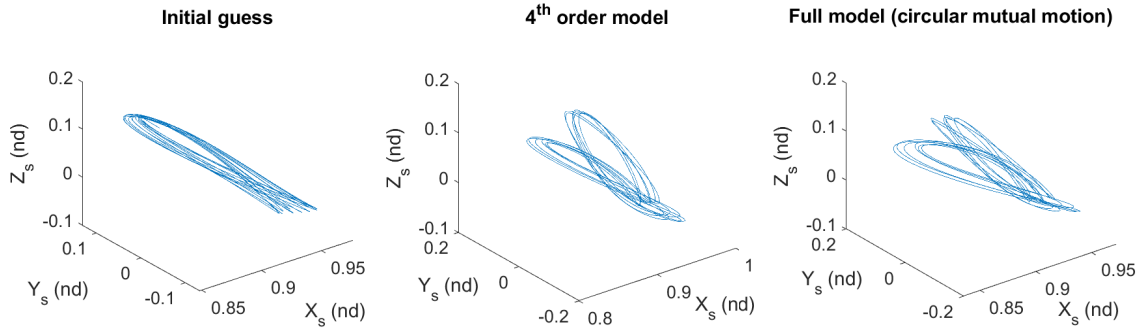


Figure 6–20: Spacecraft halo trajectory when using low pass filters

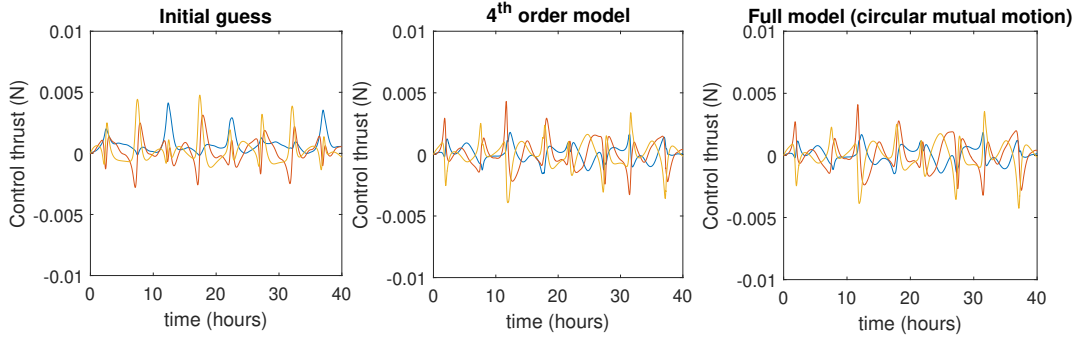


Figure 6–21: Control thrust for the halo trajectory when using low pass filters

## 6.6 Summary

In this chapter, nominal trajectories that can be maintained with low control effort were designed for a spacecraft operated in a binary asteroid system, such as Didymos 65803. The dynamical model used included a fourth-order Taylor series expansion of the gravitational potential model of the primary bodies, the specific angular velocity of body 1, the elliptical mutual motion of the primary bodies and the SRP acceleration. The second-order moments of inertia and fourth-order inertia integrals of the primary bodies required for the Taylor series expansion of the gravitational potential were calculated based on their polyhedron shape model. The

gravitational potential model is simple to implement, it does not use an excessive amount of computational power, while taking advantage of the precision of the polyhedron shape model.

It was shown that, for planar trajectories, nominal trajectories built using the full model uses less control thrust to keep a spacecraft close to the designed nominal trajectory. For 3D trajectories, which require more segments to be built or cannot fully reach periodicity, the more detailed model did not give a nominal trajectory easier to control. This is due to the higher number of discontinuities in the trajectories. It has been shown that, for most cases, adding low-pass filters in the controller reduces the amplitude and the oscillations in the required thrust signal. The downside of using it is that the nominal trajectory is followed slightly less well by the spacecraft. From the results for the halo type of trajectory, where it was not possible to build a nominal trajectory for a non-circular mutual motion of the primary bodies around the system's barycenter, it is possible to deduce that the non-circular motion of the primary bodies is the main source of perturbation with respect to the CRTBP.

For all trajectories, it is shown that it is possible to keep the spacecraft on the nominal trajectory using a reasonable amount of thrust with the appropriate Lyapunov stability theory based controller.

## **CHAPTER 7**

### **Conclusions**

This chapter presents the concluding remarks of this thesis. It summarizes the research findings of the previous chapters and then presents several suggestions for future research work that can be done in the area of the FRTBP applied to missions to binary asteroid systems.

#### **7.1 Summary of the Findings**

Binary asteroid systems are composed of two small irregular celestial bodies. Their gravitational potential needs to be calculated based on their specific shape. A gravitational model based on a fourth-order Taylor series expansion was developed and validated in chapter 2. The validation was based on the comparison of the results obtained in the thesis with those in another study using a different model. The principle of the conservation of the Hamiltonian of a spacecraft orbiting a single asteroid was used to validate the simulation code. Then, the model obtained for a single asteroid was extended to a binary asteroid system. The layered mascons model was then introduced. In the case of binary asteroids, the calculations were carried out using non-dimensionalized values to minimize numerical errors due to large variations in values. The description of the non-dimensionalization of the parameters of a binary asteroid system concluded that chapter.

The following chapter was dedicated to the study of the Full Two Body Problem (FTBP). The FTBP studies the motion of the primary bodies of a binary asteroid

system based on their specific shape, rotational motion and the distance between their centers of mass. The equations of motion were developed using Lagrangian dynamics. For that purpose, the gravitational potential energy, using the fourth-order Taylor series expansion, and the kinetic energy expressions were obtained. The FTBP included the non-circular motion and the individual rotational motion of the primary bodies. The case of circular motion of the primary bodies was also studied. These results were integrated into the analysis conducted in the later chapters. The equations of motion depend on a constant of integration related to the conservation of angular momentum of the system, which is calculated based on the initial conditions of the system. It was found that a small variation in the value of this constant of integration changes the behavior of the system significantly. A study of the 65803 Didymos binary asteroid system was also done. One of the observations was that both the layered mascons and the fourth-order Taylor series expansion models give similar gravitational potential energy results. This, again, is another reason for using the gravitational potential of an irregular small body using a fourth-order Taylor series expansion, which involves less computational effort.

Since the primary bodies of a binary asteroid have a small mass, the SRP acceleration produces a non-negligible effect on the motion of a spacecraft in its vicinity. The first task dedicated to the study of the impact of the SRP acceleration on the FCRTBP focused on the design of spacecraft trajectories that are SRP-compatible. To be SRP-compatible, a trajectory needs to have a period that is a rational fraction or a multiplier of the period of the binary asteroid system as a whole. The chosen period of the trajectories here is half the period of the binary system. A

single-shooting differential correction scheme was used to design the trajectories. A study of the stability of the trajectories showed that the shape of the primary bodies of the system has a larger impact on the stability of the trajectory than the SRP acceleration alone. It was also shown that a trajectory with a period that is only slightly different from half the period of the system is significantly more unstable than a trajectory with the right period.

To further study the effect of the SRP acceleration on the motion of a spacecraft in the FCRTBP, it was decided to compare different SRP acceleration models, optical parameters and spacecraft attitude schemes. This part of the study only concerned trajectories that were bounded for a long-term duration. The study showed that the choice of the SRP acceleration model used, including the appropriate selection of the optical parameters, may influence the safety of a mission, especially when the binary asteroid system is at the perihelion of its orbit around the Sun. Different spacecraft attitude schemes that can be used throughout a mission were examined. Here, again, the safety of the mission was linked to the attitude scheme, showing the coupling between the SRP acceleration and the attitude of the spacecraft. It demonstrated numerically the impact on the equilibrium points and the Jacobi constant of a trajectory when the SRP acceleration is added to the model. Because of the time-dependency of the system induced by the SRP, the equilibrium points become equilibrium regions and there is no Jacobi constant anymore. This completed the study of the impact of the SRP acceleration on the FCRTBP.

The last chapter was dedicated to the study of the FRTBP as a whole. It integrated the irregular shape and the rotational motion of the primary bodies, their

non-circular motion around their barycenter and the SRP acceleration. A polyhedron shape model of the 65803 Didymos binary asteroid system was used to calculate the inertia integrals of the primary bodies. This dynamic system is non-autonomous as the forces exerted on the spacecraft operating in its vicinity are time-dependent. This fact complicated the search for periodic trajectories and their maintenance. A multiple-shooting correction scheme was then used to find planar and 3D trajectories that require minimal control for maintenance. It was observed that the parameter that has the greatest effect on the trajectories is the non-circular motion of the primaries, where the distance between their centers of mass is varying. It was even impossible to add it to the halo type trajectory. A Lyapunov stability theory based controller was used to maintain the spacecraft on these trajectories. It was then observed that the small discontinuities of the trajectory noticeably affected the required thrust to maintain the trajectories. Two low-pass Butterworth filters were then added to the controller. The first one was applied to the error signal and the other one to the control thrust signal. It had the effect of reducing the need for control thrust and smoothing the control signal significantly. Finally, it was noted that the thrust required to maintain the trajectories designed never exceeded  $10\text{ mN}$  for a  $500\text{ kg}$  spacecraft. This shows that it is possible to keep a spacecraft close to a trajectory in the FRTBP with limited thrust.

## **7.2 Suggestions for Future Work**

This thesis covered a great range of subjects related to the FRTBP, but there are still more to study.

The fourth-order Taylor series expansion used for the gravitational potential model does not allow one to work with bodies having non-uniform densities. One way to overcome this would be to use the layered mascons model with variations in the density of the primary bodies. This would make the model closer to the real situation and enhance the quality of the trajectories that could be designed.

As the model of a binary asteroid system can become quite complex, using machine learning tools could lead to new trajectories that would be optimized for a particular system. This could prevent having discontinuities in the trajectories causing the glitches in the control signal seen in chapter 6.

The findings related to the effect of the SRP acceleration could be used as a foundation to design a control system that would not require the use of propellant to maintain the trajectory of a spacecraft. This, combined with the use of machine learning, would really improve the quality of the trajectory maintenance for a spacecraft in the context of the FRTBP.

## APPENDIX A

### Reference Frames Used in the Thesis

Various reference frames are used to understand the dynamics of a spacecraft in the vicinity of a binary asteroid system. Here is a description of the ones used in this thesis. They are also illustrated in Fig.A-1.

#### **Inertial Reference Frame ( $X_I; Y_I; Z_I$ )**

This reference frame is centered at the Sun. Its axes are fixed in the inertial space. Because the calculations are done in a time frame short enough to consider the barycenter of the binary asteroid system to be at an approximately fixed position in the inertial space, the inertial reference frame can also be located at the barycenter  $C$  of the binary asteroid system.

#### **Synodic Reference Frame ( $X_S; Y_S; Z_S$ )**

This reference frame is centered at the barycenter  $C$  of the system. Its  $X_S$  axis is aligned with the line joining the center of masses of primary body 1 and primary body 2. Its  $Z_S$  axis is aligned with the angular momentum vector of the system. The  $Y_S$  axis completes the right-handed reference frame. This reference frame rotates at the same rate as primary bodies 1 and 2 are rotating around their barycenter.

#### **Primary Bodies 1 and 2 Body Fixed Reference Frames ( $X_1; Y_1; Z_1$ and $X_2; Y_2; Z_2$ )**

These reference frames are aligned with the principal moments of inertia of their corresponding primary body. The  $X_i$  axis is directed towards the minimum moment

of inertia axis of body  $i$ , the  $Z_i$  axis is directed towards the maximum moment of inertia axis of body  $i$  and the  $Y_i$  axis completes the right-handed system. This reference frame also applies to a single asteroid as being the body fixed reference frame.

### Plates Reference Frame ( $X_P; Y_P; Z_P$ )

This reference frame refers to the orientation of the vectors normal to the plates involved in the calculation of the SRP. Its  $X_P$  axis is the vector normal to the surface of the spacecraft including the solar panels, its  $Y_P$  axis is aligned with the solar panels, and its  $Z_P$  axis completes the right-handed system.

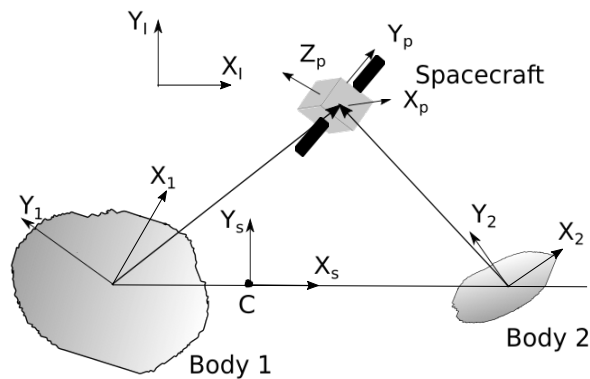


Figure A-1: Reference frames

**APPENDIX B**  
**Development of the Expression of the Gravitational Potential of an Asteroid**

The calculation of the gravitational potential of an asteroid based on the Taylor series expansion of Eq. 2.2 requires to integrate each of the terms of Eq. 2.6. Because the body fixed reference frame has its origin at the center of mass of the asteroid and has its axes along the principal moments of inertia of the asteroid, the  $(\hat{\mathbf{u}}_R \cdot \boldsymbol{\delta})$ ,  $\delta^2 (\hat{\mathbf{u}}_R \cdot \boldsymbol{\delta})$  and  $(\hat{\mathbf{u}}_R \cdot \boldsymbol{\delta})^3$  terms of Eq. 2.6 vanish when integrated over the entire mass distribution of the asteroid. The remaining terms are integrated individually for clarity.

Zeroth-order term:

$$U_{grav,0th} = \int \frac{G}{R} dm = \frac{MG}{R} \quad (\text{B.1})$$

where  $M$  is the total mass of the asteroid.

Second-order terms:

$$U_{grav,2nd} = \int \frac{G}{R^3} \left[ \frac{3}{2} (\hat{\mathbf{u}}_R \cdot \boldsymbol{\delta})^2 - \frac{1}{2} \delta^2 \right] dm = \frac{3G}{2R^3} \left[ \frac{1}{3} tr [I_a] - \{\hat{\mathbf{u}}_R\}^T [I_a] \{\hat{\mathbf{u}}_R\} \right] \quad (\text{B.2})$$

where  $\{\hat{\mathbf{u}}_R\}$  is a column matrix containing the components of the  $\hat{\mathbf{u}}_R$  unit vector expressed in the body fixed reference frame and  $[I_a]$  is the inertia matrix of the asteroid. Since the body fixed reference frame is aligned with the principal moments

of inertia, it is represented by:

$$[I_a] = \begin{bmatrix} I_{xx} & 0 & 0 \\ 0 & I_{yy} & 0 \\ 0 & 0 & I_{zz} \end{bmatrix} \quad (\text{B.3})$$

Considering that the components of the unit vector are equivalent to the component of the full size vector divided by the length of the vector and considering the inertia matrix presented above, the expression for the contribution of the second-order terms to the gravitational potential is as follow:

$$U_{grav,2^{nd}} = \frac{3G}{2R^3} \left[ \frac{1}{3} (I_{xx} + I_{yy} + I_{zz}) - \frac{1}{R^2} (X^2 I_{xx} + Y^2 I_{yy} + Z^2 I_{zz}) \right] \quad (\text{B.4})$$

where  $X$ ,  $Y$  and  $Z$  are the components of the position vector of point P with respect to the center of mass of the asteroid expressed in the asteroid body fixed reference frame.

Fourth-order terms:

$$U_{grav,4^{th}} = \int \frac{G}{R^5} \left[ \frac{3}{8} \delta^4 - \frac{15}{4} \delta^2 (\hat{\mathbf{u}}_{\mathbf{R}} \cdot \boldsymbol{\delta})^2 + \frac{35}{8} (\hat{\mathbf{u}}_{\mathbf{R}} \cdot \boldsymbol{\delta})^4 \right] dm \quad (\text{B.5})$$

The integration of the fourth-order terms will be done one term at a time for more clarity. Let us start by defining:

$$\delta^2 = \delta_x^2 + \delta_y^2 + \delta_z^2 \quad (\text{B.6})$$

where  $\delta_x$ ,  $\delta_y$  and  $\delta_z$  are the  $x$ ,  $y$  and  $z$  components of the position vector of the mass element  $dm$  relative to the center of mass of the asteroid and

$$\hat{\mathbf{u}}_{\mathbf{R}} \cdot \boldsymbol{\delta} = \hat{u}_{Rx}\delta_x + \hat{u}_{Ry}\delta_y + \hat{u}_{Rz}\delta_z \quad (\text{B.7})$$

where  $\hat{u}_{Rx}$ ,  $\hat{u}_{Ry}$  and  $\hat{u}_{Rz}$  are the  $x$ ,  $y$  and  $z$  components of the unit vector  $\hat{\mathbf{u}}_{\mathbf{R}}$  in the asteroid body fixed reference frame.

The integration of the first fourth-order term,  $\delta^4$  is then:

$$\begin{aligned} \int \delta^4 dm &= \int (\delta_x^2 + \delta_y^2 + \delta_z^2)^2 dm \\ &= \int [\delta_x^4 + \delta_y^4 + \delta_z^4 + 2(\delta_x^2\delta_y^2 + \delta_y^2\delta_z^2 + \delta_z^2\delta_x^2)] dm \end{aligned} \quad (\text{B.8})$$

The integration of the second fourth-order term gives:

$$\begin{aligned} \int \delta^2 (\hat{\mathbf{u}}_{\mathbf{R}} \cdot \boldsymbol{\delta})^2 dm &= \int \left[ (\delta_x^2 + \delta_y^2 + \delta_z^2) (\hat{u}_{Rx}\delta_x + \hat{u}_{Ry}\delta_y + \hat{u}_{Rz}\delta_z)^2 \right] dm \\ &= \int \left[ (\delta_x^2 + \delta_y^2 + \delta_z^2) ((\hat{u}_{Rx}\delta_x)^2 + (\hat{u}_{Ry}\delta_y)^2 + (\hat{u}_{Rz}\delta_z)^2) \right. \\ &\quad + (\delta_x^2 + \delta_y^2 + \delta_z^2) \left( 2(\hat{u}_{Rx}\delta_x)(\hat{u}_{Ry}\delta_y) + 2(\hat{u}_{Ry}\delta_y)(\hat{u}_{Rz}\delta_z) \right. \\ &\quad \left. \left. + 2(\hat{u}_{Rz}\delta_z)(\hat{u}_{Rx}\delta_x) \right) \right] dm \end{aligned} \quad (\text{B.9})$$

The second line of the integration gives terms in  $\delta_x^3\delta_y$ ,  $\delta_x^2\delta_y\delta_z$ ,  $\delta_x^3\delta_z\dots$  which vanish when integrated over the entire mass distribution of the asteroid. Keeping

only the first line and rearranging, the integral is then:

$$\begin{aligned}
& \int \delta^2 (\hat{\mathbf{u}}_{\mathbf{R}} \cdot \boldsymbol{\delta})^2 dm = \\
& \int \left[ \hat{u}_{Rx}^2 \delta_x^4 + \hat{u}_{Ry}^2 \delta_y^4 + \hat{u}_{Rz}^2 \delta_z^4 \right. \\
& \left. + (\hat{u}_{Rx}^2 + \hat{u}_{Ry}^2) \delta_x^2 \delta_y^2 + (\hat{u}_{Ry}^2 + \hat{u}_{Rz}^2) \delta_y^2 \delta_z^2 + (\hat{u}_{Rz}^2 + \hat{u}_{Rx}^2) \delta_z^2 \delta_x^2 \right] dm
\end{aligned} \tag{B.10}$$

Finally, the last fourth-order term:

$$\begin{aligned}
& \int (\hat{\mathbf{u}}_{\mathbf{R}} \cdot \boldsymbol{\delta})^4 dm \\
& = \int (\hat{u}_{Rx} \delta_x + \hat{u}_{Ry} \delta_y + \hat{u}_{Rz} \delta_z)^4 dm \\
& = \int \left[ (\hat{u}_{Rx} \delta_x)^2 + (\hat{u}_{Ry} \delta_y)^2 + (\hat{u}_{Rz} \delta_z)^2 + 2 (\hat{u}_{Rx} \delta_x) (\hat{u}_{Ry} \delta_y) \right. \\
& \left. + 2 (\hat{u}_{Ry} \delta_y) (\hat{u}_{Rz} \delta_z) + 2 (\hat{u}_{Rz} \delta_z) (\hat{u}_{Rx} \delta_x) \right]^2 dm
\end{aligned} \tag{B.11}$$

Here again, when multiplying, terms in  $\delta_x^3 \delta_y$ ,  $\delta_x^2 \delta_y \delta_z$ ,  $\delta_x^3 \delta_z \dots$  appear. When integrated, they vanish. Considering this and after some algebra, the final expression for the last fourth-order term is:

$$\begin{aligned}
& \int (\hat{\mathbf{u}}_{\mathbf{R}} \cdot \boldsymbol{\delta})^4 dm \\
& = \int \left[ (\hat{u}_{Rx} \delta_x)^4 + (\hat{u}_{Ry} \delta_y)^4 + (\hat{u}_{Rz} \delta_z)^4 + 6 (\hat{u}_{Rx} \hat{u}_{Ry})^2 \delta_x^2 \delta_y^2 \right. \\
& \left. + 6 (\hat{u}_{Ry} \hat{u}_{Rz})^2 \delta_y^2 \delta_z^2 + 6 (\hat{u}_{Rz} \hat{u}_{Rx})^2 \delta_z^2 \delta_x^2 \right] dm
\end{aligned} \tag{B.12}$$

Inserting the resulting fourth-order terms in Eq. B.5, the integral for the calculation of the contribution of the fourth-order terms to the gravitational potential

gives:

$$\begin{aligned}
& \int \frac{G}{R^5} \left[ \frac{3}{8} \delta^4 - \frac{15}{4} (\hat{\mathbf{u}}_{\mathbf{R}} \cdot \boldsymbol{\delta})^2 + \frac{35}{8} (\hat{\mathbf{u}}_{\mathbf{R}} \cdot \boldsymbol{\delta})^4 \right] dm \\
&= \frac{G}{8R^5} \left\{ [35\hat{u}_{Rx}^4 - 30\hat{u}_{Rx}^2 + 3] \int \delta_x^4 dm + [35\hat{u}_{Ry}^4 - 30\hat{u}_{Ry}^2 + 3] \int \delta_y^4 dm \right. \\
&+ [35\hat{u}_{Rz}^4 - 30\hat{u}_{Rz}^2 + 3] \int \delta_z^4 dm \\
&+ 6 [35\hat{u}_{Rx}^2 \hat{u}_{Ry}^2 - 5(\hat{u}_{Rx}^2 + \hat{u}_{Ry}^2) + 1] \int \delta_x^2 \delta_y^2 dm \\
&+ 6 [35\hat{u}_{Ry}^2 \hat{u}_{Rz}^2 - 5(\hat{u}_{Ry}^2 + \hat{u}_{Rz}^2) + 1] \int \delta_y^2 \delta_z^2 dm \\
&\left. + 6 [35\hat{u}_{Rz}^2 \hat{u}_{Rx}^2 - 5(\hat{u}_{Rz}^2 + \hat{u}_{Rx}^2) + 1] \int \delta_z^2 \delta_x^2 dm \right\} \tag{B.13}
\end{aligned}$$

The remaining expressions needing to be integrated are giving the fourth-order inertia integrals that will be used in the expressions for the gravitational potential of an asteroid represented by any arbitrary shape:

$$\begin{aligned}
& \int \delta_x^4 dm = J_{xxxx} \\
& \int \delta_y^4 dm = J_{yyyy} \\
& \int \delta_z^4 dm = J_{zzzz} \\
& \int \delta_x^2 \delta_y^2 dm = J_{xxyy} \\
& \int \delta_y^2 \delta_z^2 dm = J_{yyzz} \\
& \int \delta_z^2 \delta_x^2 dm = J_{zzxx}
\end{aligned} \tag{B.14}$$

Rearranging Eq. B.13, the contribution of the fourth-order terms to the gravitational potential is:

$$\begin{aligned}
U_{grav,4^{th}} = \frac{G}{8R^5} & \left[ \frac{35}{R^4} \left( X^4 J_{xxxx} + Y^4 J_{yyyy} + Z^4 J_{zzzz} \right. \right. \\
& + 6 \left( (XY)^2 J_{xxyy} + (YZ)^2 J_{yyzz} + (XZ)^2 J_{zzxx} \right) \\
& - \frac{30}{R^2} \left( X^2 J_{xxxx} + Y^2 J_{yyyy} + Z^2 J_{zzzz} \right. \\
& + (X^2 + Y^2) J_{xxyy} + (Y^2 + Z^2) J_{yyzz} + (Z^2 + X^2) J_{zzxx} \\
& \left. \left. + 3(J_{xxxx} + J_{yyyy} + J_{zzzz}) + 6(J_{xxyy} + J_{yyzz} + J_{zzxx}) \right] \quad (B.15)
\end{aligned}$$

The force exerted by the gravitational potential of an asteroid by a unit mass can be calculated as per Eq. 2.9. After some algebra, the expressions for the force components exerted on a unit mass by an asteroid are as follow:

$$\begin{aligned}
F_{grav_x} = & \left\{ -\frac{MG}{R^3} - \frac{3G}{2R^5} \left[ (3I_{xx} + I_{yy} + I_{zz}) - \frac{5}{R^2} (X^2 I_{xx} + Y^2 I_{yy} + Z^2 I_{zz}) \right] \right. \\
& + \frac{G}{8R^7} \left[ \frac{-315}{R^4} (X^4 J_{xxxx} + Y^4 J_{yyyy} + Z^4 J_{zzzz} \right. \\
& + 6((XY)^2 J_{xxyy} + (YZ)^2 J_{yyzz} + (XZ)^2 J_{zzxx}) \\
& + \frac{70}{R^2} (5X^2 J_{xxxx} + 3Y^2 J_{yyyy} + 3Z^2 J_{zzzz} \\
& + 3(X^2 + 3Y^2) J_{xxyy} + 3(Y^2 + Z^2) J_{yyzz} + 3(X^2 + 3Z^2) J_{zzxx}) \\
& \left. \left. - 15(5J_{xxxx} + J_{yyyy} + J_{zzzz}) - 30(3J_{xxyy} + J_{yyzz} + 3J_{zzxx}) \right] \right\} X
\end{aligned} \tag{B.16}$$

$$\begin{aligned}
F_{grav_y} = & \left\{ -\frac{MG}{R^3} - \frac{3G}{2R^5} \left( (I_{xx} + 3I_{yy} + I_{zz}) - \frac{5}{R^2} (X^2 I_{xx} + Y^2 I_{yy} + Z^2 I_{zz}) \right) \right. \\
& + \frac{G}{8R^7} \left[ \frac{-315}{R^4} (X^4 J_{xxxx} + Y^4 J_{yyyy} + Z^4 J_{zzzz} \right. \\
& + 6((XY)^2 J_{xxyy} + (YZ)^2 J_{yyzz} + (XZ)^2 J_{zzxx}) \\
& + \frac{70}{R^2} (3X^2 J_{xxxx} + 5Y^2 J_{yyyy} + 3Z^2 J_{zzzz} \\
& + 3(3X^2 + Y^2) J_{xxyy} + 3(Y^2 + 3Z^2) J_{yyzz} + 3(X^2 + Z^2) J_{zzxx}) \\
& \left. \left. - 15(J_{xxxx} + 5J_{yyyy} + J_{zzzz}) - 30(3J_{xxyy} + 3J_{yyzz} + J_{zzxx}) \right] \right\} Y
\end{aligned} \tag{B.17}$$

$$\begin{aligned}
F_{grav_y} = & \left\{ -\frac{MG}{R^3} - \frac{3G}{2R^5} \left( (I_{xx} + I_{yy} + 3I_{zz}) - \frac{5}{R^2} (X^2 I_{xx} + Y^2 I_{yy} + Z^2 I_{zz}) \right) \right. \\
& + \frac{G}{8R^7} \left[ \frac{-315}{R^4} (X^4 J_{xxxx} + Y^4 J_{yyyy} + Z^4 J_{zzzz} \right. \\
& + 6 ((XY)^2 J_{xxyy} + (YZ)^2 J_{yyzz} + (XZ)^2 J_{zzxx}) \\
& + \frac{70}{R^2} (3X^2 J_{xxxx} + 3Y^2 J_{yyyy} + 5Z^2 J_{zzzz} \\
& + 3(X^2 + Y^2) J_{xxyy} + 3(3Y^2 + Z^2) J_{yyzz} + 3(3X^2 + Z^2) J_{zzxx}) \\
& \left. \left. - 15(J_{xxxx} + J_{yyyy} + 5J_{zzzz}) - 30(J_{xxyy} + 3J_{yyzz} + 3J_{zzxx}) \right] \right\} Z
\end{aligned}
\tag{B.18}$$

## APPENDIX C

### Fourth-order Inertia Integrals of an Arbitrarily Shaped Body

#### C.1 Fourth-order Inertia Integrals of an Ellipsoid

The ellipsoid for which the calculation of the fourth-order inertia integrals are calculated here has uniform density and semi-axes of  $a$ ,  $b$ , and  $c$ . The expressions of the fourth-order inertia integrals are calculated based on the integration over the entire body of the ellipsoid of  $x^4$ ,  $y^4$ ,  $z^4$ ,  $x^2y^2$ ,  $y^2z^2$ ,  $z^2x^2$ . In the case of  $J_{zzzz}$ , the calculation is done as explained in this appendix and is based in the method described in [62] for the second-order moments of inertia of an ellipsoid.

First, let us define the integral to calculate:

$$J_{zzzz} = \int_M z^4 dm = \rho \int_V z^4 dx dy dz \quad (\text{C.1})$$

where  $\rho$  is the density of the ellipsoid,  $M$  is the total mass of the ellipsoid,  $dm$  is a mass element of the ellipsoid and  $V$  is the volume of the ellipsoid. We know that the surface curve of the ellipsoid is defined by the equation:

$$\frac{x^2}{a^2} + \frac{y^2}{b^2} + \frac{z^2}{c^2} = 1 \quad (\text{C.2})$$

A change of variables transforms the ellipsoid into a sphere:

$$\begin{aligned}
 x &= au \Rightarrow dx = a du \\
 y &= bv \Rightarrow dy = b dv \\
 z &= cw \Rightarrow dz = c dw
 \end{aligned}
 \tag{C.3}$$

We now have:

$$J_{zzzz} = \rho \int_{V_{sphere}} c^4 w^4 abc \, dudvdw = \rho abc^5 \int_{V_{sphere}} w^4 \, dudvdw
 \tag{C.4}$$

Transforming into spherical coordinates:

$$\begin{aligned}
 u &= r \cos \theta \sin \phi \\
 v &= r \sin \theta \cos \phi \\
 w &= r \cos \phi
 \end{aligned}
 \tag{C.5}$$

and using the Jacobian of:

$$\left| \frac{\partial (u, v, w)}{\partial (r, \theta, \phi)} \right| = r^2 \sin \phi
 \tag{C.6}$$

then:

$$dudvdw = r^2 \sin \phi \, dr d\theta d\phi
 \tag{C.7}$$

and:

$$J_{zzzz} = abc^5 \rho \int_0^\pi \int_0^{2\pi} \int_0^1 r^6 \cos^4 \phi \sin \phi \, dr d\theta d\phi
 \tag{C.8}$$

After some algebra:

$$J_{zzzz} = \frac{4}{35} abc^5 \pi \rho
 \tag{C.9}$$

where:

$$\rho = \frac{M}{\frac{4}{3}\pi abc} \quad (\text{C.10})$$

so the final expression for  $J_{zzzz}$  is:

$$J_{zzzz} = \frac{3Mc^4}{35} \quad (\text{C.11})$$

Similarly:

$$\begin{aligned} J_{xxxx} &= \frac{3Ma^4}{35} \\ J_{yyyy} &= \frac{3Mb^4}{35} \end{aligned} \quad (\text{C.12})$$

A similar method can be used to find the coupled inertia integrals:

$$\begin{aligned} J_{xxyy} &= \frac{3Ma^2b^2}{105} \\ J_{yyzz} &= \frac{3Mb^2c^2}{105} \\ J_{zzxx} &= \frac{3Mc^2a^2}{105} \end{aligned} \quad (\text{C.13})$$

## C.2 Calculating Inertia Integrals from a Polyhedron Shape Model

The inertia integrals of an arbitrary shape can be calculated based on its polyhedron shape model. Dobrovolski developed a method to calculate the inertia integrals of the second order based on a polyhedron shape model [37]. A few concepts described in Ref. [37] are first summarized. The technique required to calculate the fourth-order inertia integrals are then be explained.

A polyhedron shape model is composed of tetrahedrons having their triangular face composing the external shape of the body. Each face is described by the coordinates of the vertices composing it, named here  $\mathbf{D}$ ,  $\mathbf{E}$  and  $\mathbf{F}$  as in Fig. C-1. The

edges  $\mathbf{G}$  and  $\mathbf{H}$  are defined as follow:

$$\begin{aligned}\mathbf{G} &= \mathbf{E} - \mathbf{D} \\ \mathbf{H} &= \mathbf{F} - \mathbf{D}\end{aligned}\tag{C.14}$$

All of the vertices coordinate of the model are defined with respect with the origin  $\mathbf{O}$  which does not necessarily correspond to the center of mass of the arbitrarily shaped body.

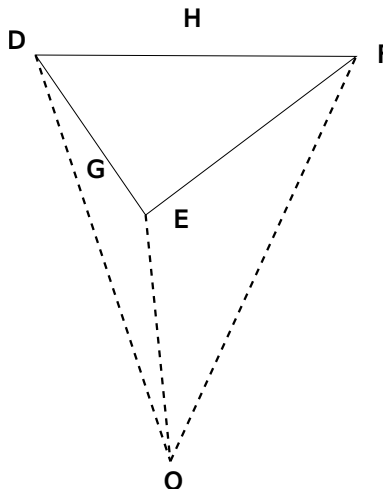


Figure C-1: Facet with vertices and edges

The first things to define are the area of a facet, the volume of a tetrahedron and the center of mass of the body modeled using a polyhedron shape.

The area of a facet,  $\Delta S$  is the norm of the cross product of the edges  $\mathbf{G}$  and  $\mathbf{H}$  divided by 2:

$$\begin{aligned}\mathbf{N} &= \mathbf{G} \times \mathbf{H} \\ \Delta S &= N/2\end{aligned}\tag{C.15}$$

The total surface of the body is then the sum of all the  $\Delta S$ s.

The volume of a tetrahedron is 1/3 its height multiplied by the surface of its facet:

$$\Delta V = \mathbf{D}/3 \cdot (\mathbf{G} \times \mathbf{H})/2 \quad (\text{C.16})$$

Here again, the total volume of the body is the sum of the  $\Delta V$ s.

Considering the body has uniform density  $\rho$ , each tetrahedron can be considered having a mass of  $\Delta M = \rho \Delta V$ . The centroid of a tetrahedron is calculated by:

$$\Delta \mathbf{R} = (\mathbf{D} + \mathbf{E} + \mathbf{F} + \mathbf{O})/4 \quad (\text{C.17})$$

The center of mass  $\mathbf{R}$  of the body as a whole is calculated as follow:

$$\mathbf{R} = \sum \Delta M \Delta \mathbf{R} / M = \sum \Delta V \Delta \mathbf{R} / V \quad (\text{C.18})$$

### C.2.1 Second-order Inertia Integrals

The calculation of the second-order inertia integrals is well described in Ref. [37] and will be summarized here. The second-order moments of inertia can be represented in the inertia matrix of the body:

$$[I] = \begin{bmatrix} I_{xx} & I_{xy} & I_{xz} \\ I_{xy} & I_{yy} & I_{yz} \\ I_{xz} & I_{yz} & I_{zz} \end{bmatrix} \quad (\text{C.19})$$

since  $I_{jk} = I_{kj}$ , there are only six values to calculate to get the full inertia matrix.

Each term of the inertia matrix can be calculated are follow:

$$\begin{aligned}
 I_{xx} &= J_{yy} + J_{zz} \\
 I_{yy} &= J_{xx} + J_{zz} \\
 I_{zz} &= J_{yy} + J_{xx} \\
 I_{xy} &= -J_{xy} \\
 I_{yz} &= -J_{yz} \\
 I_{zx} &= -J_{zx}
 \end{aligned}
 \tag{C.20}$$

where:

$$J_{jk} = \rho \int \int \int jk \, dV
 \tag{C.21}$$

is the inertia integral. The triple integral in  $x$ ,  $y$ , and  $z$  is done over the volume of the body with a uniform density  $\rho$ .

In Ref. [37], the volume integral is simplified using Gauss' theorem stating that the integral of a value  $q = \text{div}\mathbf{Q}$  over a closed volume  $V$  is equal to the integral of  $\mathbf{Q}$  over its boundary  $S$ :

$$\int \int \int q dV = \int \int \mathbf{Q} \cdot d\mathbf{S}
 \tag{C.22}$$

Here,  $d\mathbf{S}$  is a vector in the direction normal to the surface  $S$  with a magnitude equal to the element of area  $dS$ . Taking the vector  $\mathbf{Q}$  parallel to the radius vector  $\mathbf{r}$  going from the origin of the tetrahedron to the center of the external surface ( $\mathbf{r} = \mathbf{D} + \mathbf{G} + \mathbf{H}$ ) assures that only the external surface contribute to the integral.

The simplest choice of  $\mathbf{Q}$  is then  $jk\mathbf{r}/5$ . The products of inertia then become:

$$J_{jk} = \frac{\rho}{5} \int \int jk\mathbf{r} \cdot d\mathbf{S} \quad (\text{C.23})$$

Considering that:

$$\mathbf{r} \cdot d\mathbf{S} = (\mathbf{r} \cdot \mathbf{N}/N) dS = (6\Delta V/N) dS \quad (\text{C.24})$$

the integral to evaluate is then:

$$\Delta J_{jk} = \rho \frac{6}{5} \frac{\Delta V}{N} \int \int jk dS \quad (\text{C.25})$$

To simplify the integral, let us define dimensionless coordinates  $(g, h)$  in the plane of the facet  $\mathbf{D}$ ,  $\mathbf{E}$ ,  $\mathbf{F}$  such that:

$$\mathbf{r} = \mathbf{D} + g\mathbf{G} + h\mathbf{H} \quad (\text{C.26})$$

We then have:

$$\begin{aligned} x &= D_x + gG_x + hH_x \\ y &= D_y + gG_y + hH_y \\ z &= D_z + gG_z + hH_z \end{aligned} \quad (\text{C.27})$$

The element of area  $dS$  then becomes  $Ndgdh$ . Inserting the last results into C.25 gives:

$$\begin{aligned}
\Delta J_{jk} &= \frac{6}{5}\rho\Delta V \int \int jk \, dgdh \\
&= \frac{6}{5}\rho\Delta V \int \int (D_j + gG_j + hH_j)(D_k + gG_k + hH_k) \, dgdh \\
&= \frac{6}{5}\rho\Delta V \int \int \left[ D_j D_k + g^2 G_j G_k + h^2 H_j H_k + g(D_j G_k + D_k G_j) \right. \\
&\quad \left. + h(D_j H_k + D_k H_j) + gh(G_j H_k + G_k H_j) \right] dgdh
\end{aligned} \tag{C.28}$$

With the limit of integration being either  $0 < g < 1 - h, 0 < h < 1$  or  $0 < h < 1 - g, 0 < g < 1$ , it can be calculated that:

$$\begin{aligned}
\int \int dgdh &= \frac{1}{2} \\
\int \int g \, dgdh &= \int \int h dgdh = \frac{1}{6} \\
\int \int g^2 \, dgdh &= \int \int h^2 dgdh = \frac{1}{12} \\
\int \int gh \, dgdh &= \frac{1}{24}
\end{aligned} \tag{C.29}$$

Substituting in Eq. C.28 and applying  $\mathbf{G} = \mathbf{E} - \mathbf{D}$  and  $\mathbf{H} = \mathbf{F} - \mathbf{D}$ , gives the final result:

$$\Delta J_{jk} = \frac{\rho\Delta V}{20} [2D_j D_k + 2E_j E_k + 2F_j F_k + D_j E_k + D_k E_j + D_j F_k + D_k F_j + E_j F_k + E_k F_j] \tag{C.30}$$

As previously,  $J_{jk}$  is the sum of the  $\Delta J_{jk}$ s.

At this point, the inertia matrix is populated, but the origin of the reference frame used to define the position of the vertices is not necessarily the center of mass of the body and the reference frame is not necessarily aligned with the principal

moments of inertia of the body. One of the assumption made in the development of the fourth-order Taylor series expansion gravitational potential model is that the body fixed reference frame is aligned with the principal moments of inertial of the body. It is then necessary to modify the polyhedron shape model to use it to calculate the inertia integrals required for the gravitational potential model. First, let us use the parallel axis theorem to calculate the equivalent moments and products of inertia for a reference frame having its origin at the center of mass of the body. By using the previously calculated center of mass of the body with coordinates  $X$ ,  $Y$  and  $Z$ :

$$\mathbf{I}' = \mathbf{I} - M \begin{bmatrix} Y^2 + Z^2 & -XY & -XZ \\ -XY & X^2 + Z^2 & -YZ \\ -XZ & -YZ & X^2 + Y^2 \end{bmatrix} \quad (\text{C.31})$$

Because the inertia matrix is composed of real numbers and is symmetric, its eigenvalues and also real numbers and its eigenvectors are orthogonal. The direction cosine matrix (DCM) describing the orientation of the actual reference frame relative to reference frame aligned with the principal axes is then the matrix composed of the eigenvectors of the inertia matrix with the reference frame aligned with the center of mass of the body. Transposing it gives the DCM describing the reference frame aligned with the principal axes of the body relative to the original reference frame. Knowing that, it is then possible to calculate the coordinates of each vertices into the reference frame aligned with the principal moments of inertia of the body and having its origin at the center of mass of the body. Applying Eq. C.30 to the modified coordinates show that the products of inertia have now negligible values

compared to the principal moments of inertia. These modified coordinates will be used to calculate the fourth-order inertia integrals of the body.

### C.2.2 Fourth-order Inertia Integrals

Using the modified coordinates for the calculation of the fourth-order inertia integrals permits to only calculate the following six values, the other ones being null:  $J_{xxxx}, J_{yyyy}, J_{zzzz}, J_{xxyy}, J_{yyzz}, J_{zzxx}$ . The same method than the one described in [37] is used here. In the case of the fourth order,  $\mathbf{Q}$  is  $(jk)^2 \mathbf{r}/7$ . The integrals that need to be evaluated are:

$$\begin{aligned}
\Delta J_{jjkk} &= \frac{6}{7} \rho \Delta V \int \int jjkk \, dgdh \\
&= \frac{6}{7} \rho \Delta V \int \int (D_j + gG_j + hH_j)^2 (D_k + gG_k + hH_k)^2 \, dgdh \\
&= \frac{6}{7} \rho \Delta V \int \int \left[ D_j^2 D_k^2 + g(2D_j^2 D_k G_k + 2D_j G_j D_k^2) + g^2 (D_j^2 G_k^2 + 4D_j G_j D_k G_k + D_k^2 G_j^2) \right. \\
&\quad + g^3 (2G_j^2 D_k G_k + 2D_j G_j G_k^2) + g^4 (G_j^2 G_k^2) + h(2D_j^2 D_k H_k + 2D_j H_j D_k^2) \\
&\quad + h^2 (D_j^2 H_k^2 + 4D_j H_j D_k H_k + D_k^2 H_j^2) + h^3 (2H_j^2 D_k H_k + 2D_j H_j H_k^2) + h^4 (H_j^2 H_k^2) \\
&\quad + gh(2D_j^2 G_k H_k + 4D_j G_j D_k G_k + 4D_j H_j D_k G_k + 2G_j H_j D_k^2) \\
&\quad + g^2 h(2G_j^2 D_k H_k + 4D_j G_j G_k H_k + 4G_j H_j D_k G_k + 2D_j H_j G_k^2) \\
&\quad + g^2 h^2 (G_j^2 H_j^2 + 4G_j H_j G_k H_k + G_k^2 H_k^2) + g^3 h(2G_j^2 G_k H_k + 2G_j H_j G_k^2) \\
&\quad + gh^3 (2H_j^2 G_k H_k + 2G_j H_j H_k^2) \\
&\quad \left. + gh^2 (2D_j G_j H_k^2 + 4D_j H_j G_k H_k + 4G_j H_j D_k H_k + 2H_j^2 D_k G_k) \right] dgdh
\end{aligned} \tag{C.32}$$

The required extra integrals for the calculation of the fourth-order inertia integrals are then:

$$\begin{aligned}
\int \int g^3 dgdh &= \int \int h^3 dgdh = \frac{1}{20} \\
\int \int g^4 dgdh &= \int \int h^4 dgdh = \frac{1}{30} \\
\int \int gh^2 dgdh &= \int \int g^2h dgdh = \frac{1}{60} \\
\int \int gh^3 dgdh &= \int \int g^3h dgdh = \frac{1}{120} \\
\int \int g^2h^2 dgdh &= \frac{1}{180}
\end{aligned} \tag{C.33}$$

Substituting these results into Eq. C.32 and after some algebra, the resulting calculation of the fourth-order inertia integrals is:

$$\begin{aligned}
\Delta J_{jjkk} &= \frac{6}{7} \rho \Delta V \left[ \frac{1}{2} D_j^2 D_k^2 + \frac{1}{12} (D_j^2 (G_k^2 + H_k^2) + 4D_j D_k (G_j G_k + H_j H_k) + D_k^2 (G_j^2 + H_j^2)) \right. \\
&\quad + \frac{1}{3} (D_j^2 D_k (G_k + H_k) + D_j D_k^2 (G_j + H_j)) \\
&\quad + \frac{1}{10} (D_k (G_j^2 G_k + H_j^2 H_k) + D_j (G_j G_k^2 + H_j H_k^2)) \\
&\quad + \frac{1}{30} (G_j^2 G_k^2 + H_j^2 H_k^2) + \frac{1}{12} (D_j^2 G_k H_k + 2D_j G_j D_k H_k + 2D_j H_j D_k G_k + G_j H_j D_k^2) \\
&\quad + \frac{1}{30} (D_k (G_j^2 H_k + H_j^2 G_k + 2G_j H_j G_k + 2G_j H_j H_k) \\
&\quad + D_j (H_j G_k^2 + G_j H_k^2 + 2G_j G_k H_k + 2H_j G_k H_k)) \\
&\quad \left. + \frac{1}{60} (H_j G_j (G_k^2 + H_k^2) + H_k G_k (G_j^2 + H_j^2)) + \frac{1}{180} (G_j^2 H_k^2 + H_j^2 G_k^2 + 4G_j H_j G_k H_k) \right]
\end{aligned} \tag{C.34}$$

### C.2.3 Validation of the Fourth-order Inertia Integrals Calculated from a Polyhedron Shape Model

The validation of the calculation of the fourth-order inertia integrals has been done using a polyhedron shape of an ellipsoid with a mass of  $4.8631492e09 \text{ kg}$  and size of semi-axes of  $a = 103 \text{ m}$ ,  $b = 79 \text{ m}$  and  $c = 66 \text{ m}$ , which are the mass and dimensions of the smallest body of the 65803 Didymos binary asteroid system [59]. As demonstrated previously, the equations for the fourth-order gravitational potential of an ellipsoid based on the volume integral are:

$$\begin{aligned} J_{xxxx} &= \frac{3M}{35}a^4; J_{yyyy} = \frac{3M}{35}b^4; J_{zzzz} = \frac{3M}{35}c^4 \\ J_{xxyy} &= \frac{3M}{105}a^2b^2; J_{yyzz} = \frac{3M}{105}b^2c^2; J_{zzxx} = \frac{3M}{105}a^2c^2 \end{aligned} \quad (\text{C.35})$$

Table C–1 compares the values obtained using the expressions of Eq. C.35 with the values calculated using the polyhedron shape model.

Table C–1: Fourth-order inertia integrals of an ellipsoid

<i>M. of Inertia</i>	<i>Integral</i>	<i>Polyhedron</i>
$J_{xxxx}$	4.69159e16	4.61936e16
$J_{yyyy}$	1.62360e16	1.59861e16
$J_{zzzz}$	7.90945e15	7.93842e15
$J_{xxyy}$	9.19980e15	9.05805e15
$J_{yyzz}$	3.77739e15	3.74709e15
$J_{zzxx}$	6.42114e15	6.36964e15

The values are similar and show that the equations are good to be used for a polyhedron shape model. The difference between the values from the volume

integral and from the polyhedron shape are due to the shape model not being an exact ellipsoid. It is composed of facets that are flat and not following the exact external shape of the ellipsoid.

## APPENDIX D

### Solar Radiation Pressure

The information contained here comes mainly from [52] and [51]. The SRP acceleration is created by the impact of photons emitted by the Sun hitting the spacecraft [51]. When calculating the SRP acceleration, two unit vectors are considered. The first one,  $\hat{\mathbf{u}}$  is the unit vector representing the direction of the solar radiation. In the synodic reference frame, the components of the  $\hat{\mathbf{u}}$  vector are represented as:  $\begin{bmatrix} \cos \theta & -\sin \theta & 0 \end{bmatrix}$  where  $\theta$  is the angle between the direction of sunlight ( $X_I$  axis of the inertial reference frame) and the  $X_S$  axis of the synodic reference frame. The second unit vector,  $\hat{\mathbf{n}}$ , represents the unit vector of the normal to the reflecting surface of the spacecraft. Both vectors are shown in Fig. D-1.

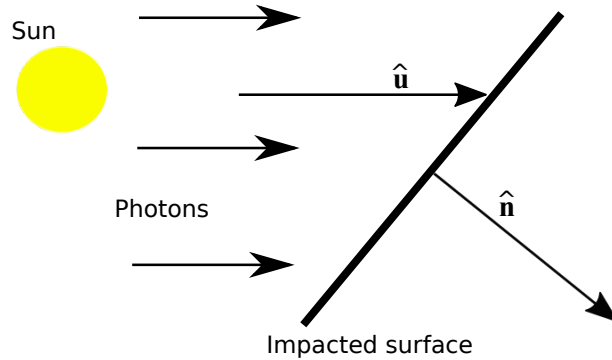


Figure D-1: Geometry used to describe the solar radiation pressure acceleration

Another aspect to be considered in the model of the SRP acceleration is the optical properties of the spacecraft, which can go from perfectly reflective, as in the

case of an ideal solar sail, to mainly absorptive, as in the case of a solar panel. The optical properties of the spacecraft are the specular reflectivity, the absorptivity and the diffusive reflectivity of the surface. The absorptivity generates an acceleration that is in the same direction as the vector  $\hat{\mathbf{u}}$ . The specular reflectivity generates an acceleration that is in the direction of the  $\hat{\mathbf{n}}$  vector. The diffusive reflectivity generates a force that is somewhere in between as it is not possible to know where exactly the photons are diffused. It is then visible in both the  $\hat{\mathbf{n}}$  and in the  $\hat{\mathbf{u}}$  directions in the equation of the acceleration due to the SRP.

These aspects are reflected in the generic equation for the SRP acceleration:

$$\mathbf{a}_{SRP} = \frac{P_{SRP}}{B} \left[ \langle \hat{\mathbf{u}}, \hat{\mathbf{n}} \rangle (1 - r_s) \hat{\mathbf{u}} + 2 \left( r_s \langle \hat{\mathbf{u}}, \hat{\mathbf{n}} \rangle^2 + \frac{r_d}{3} \right) \hat{\mathbf{n}} \right] \quad (\text{D.1})$$

where  $\mathbf{a}_{SRP}$  is the vector of the acceleration due to the SRP,  $r_s$  and  $r_d$  are the specular and diffusive reflectivity of the spacecraft, respectively,  $B$  is the mass to area ratio of the spacecraft and  $P_{SRP}$  is a measure of the pressure exerted by the solar radiation on a spacecraft and is calculated as follows [51]:

$$P_{SRP} = \frac{P_0}{c} \left( \frac{D_0}{D} \right)^2 \quad (\text{D.2})$$

where  $P_0$  ( $1367W/m^2$ ) is the solar flux at 1 Astronomical Unit(AU),  $c$  is the speed of light ( $2.998e08m/s$ ),  $D_0$  is the Sun-Earth distance ( $1.495e11m$ ) and  $D$  is the distance between the spacecraft and the Sun [52]. In the case of a spacecraft operated in the vicinity of a binary asteroid system, the distance  $D$  is calculated between the barycenter of the binary asteroid system and the Sun.

It is important to note that the absorptivity of the spacecraft is considered here. Since the sum of the specular reflectivity, the diffusive reflectivity and the absorptivity is 1, then only two of the parameters are required for the equation. The absorptivity is then included, along with the diffuse reflectivity, in the  $(1 - r_s)$  term of Eq. D.1. As one can see in Eq. D.1, if a spacecraft is not perfectly reflective, it is accelerated by the SRP in more than one direction: partially in the direction of the  $\hat{\mathbf{u}}$  vector, and partially in the direction of the  $\hat{\mathbf{n}}$  vector. This creates another level of complexity to the dynamics of a spacecraft in this kind of environment.

The coming subsections present different types of models that can be used to calculate the SRP acceleration. It goes from the simplest one, the cannonball model, to a much more complex one, the N-plates model, that considers the attitude of the spacecraft with respect to the inertial reference frame and some aspects of the shape of the spacecraft. The models were derived from the information found in [52].

### **Cannonball Model**

The cannonball model is the simplest way to model the SRP acceleration. This is the model used in Ref. [59]. It considers the spacecraft as a sphere, so the attitude of the spacecraft is not part of the model. The  $\hat{\mathbf{n}}$  vector is then always parallel to the  $\hat{\mathbf{u}}$  vector, making the SRP acceleration always at its maximum possible value. Most of the time, the spacecraft is also considered as purely reflecting.

For these conditions, the SRP acceleration is given by:

$$\mathbf{a}_{SRP} = \frac{2P_{SRP}}{B} \hat{\mathbf{u}} \tag{D.3}$$

### **Flat Plate Model**

The flat plate model is commonly used for the calculation of the SRP acceleration. It has the advantage of taking into consideration the orientation of the main surface of the spacecraft exposed to the SRP. For this model, the spacecraft is considered as a flat surface with uniform optical properties and area to mass ratio throughout the surface. It uses Eq. D.1 for the calculation of the acceleration due to the SRP.

### **Multi-body Flat Plate Model**

This model considers the main surface of the spacecraft exposed to the SRP as being built from bodies with different properties. Most of the time, it is an addition of the solar panel and of the satellite bus. These bodies may have different reflectivity and absorptivity values. The values of the parameters are calculated based on the ratio of the surface of the bodies. For example, for a spacecraft where 25% of the surface exposed to the SRP is the satellite bus and 75% the solar panels, the final absorptivity would be:  $0.25abs_{bus} + 0.75abs_{SP}$ . The equation to use would then be the same as for the flat plate model.

### **N-plates Model**

The N-plates model sums the effect of the SRP on all surfaces of the spacecraft affected by the SRP. For example, if the spacecraft is not perfectly aligned with the  $\hat{\mathbf{u}}$  vector, there would be more than one surface where the photons would hit. For each plate, the reflectivity is calculated based on the multi-body flat plate model. Each plate also has its own mass to area ratio,  $B$ . In Fig. 3,  $\hat{\mathbf{n}}_1$  is aligned with the  $X_P$

axis of the plates reference frame,  $\hat{\mathbf{n}}_2$  is aligned with  $Y_P$  axis of the plates reference frame and  $\hat{\mathbf{n}}_3$  is aligned with the  $Z_P$  axis of the plates reference frame.

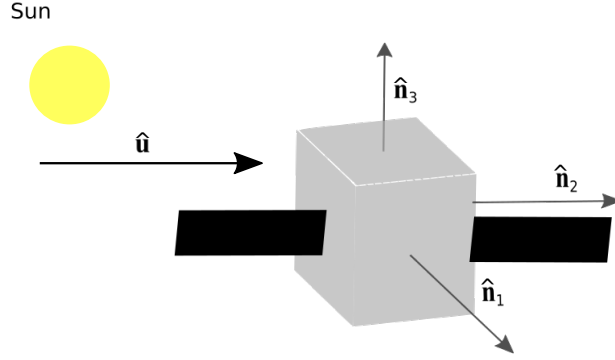


Figure D–2: Graphical representation of the  $\hat{\mathbf{n}}$  vectors involved in the N-plates model

In this case the total acceleration due to the SRP is the sum of the accelerations due to the impact of the photons on each surface exposed to the SRP:

$$\mathbf{a}_{SRP} = \sum_{i=1}^3 \frac{P_{SRP}}{B_i} \left[ \langle \hat{\mathbf{u}}, \hat{\mathbf{n}}_i \rangle (1 - r_{s_i}) \hat{\mathbf{u}} + 2 \left( r_{s_i} \langle \hat{\mathbf{u}}, \hat{\mathbf{n}}_i \rangle^2 + \frac{r_{d_i}}{3} \right) \hat{\mathbf{n}}_i \right] \quad (\text{D.4})$$

## REFERENCES

- [1] L. Prockter, S. Murchie, A. Cheng, S. Krimigis, R., Farquhar, A., Santo, The NEAR Shoemaker mission to asteroid 433 Eros, *Acta Astronautica*, Vol. 51:491-500, 2002, DOI: 10.1016/S0094-5765(02)00098-X.
- [2] M. Yoshikawa, A. Fujiwara, J. Kawaguchi, Hayabusa and its adventure around the tiny asteroid Itokawa, *International Astronomical Union*, 2007, DOI: 10.1017/S174392130701085X.
- [3] R.S. Park, A.T. Vaughan, A.S. Konopliv, A.I. Ermakov, N. Mastrodemos, J.C. Castillo-Rogez, S.P. Joy, A. Nathues, C.A. Polansjey, M.D. Rayman, J.E. Riedel, C.A. Raymons, C.T. Russell, M.T. Zuber, High-resolution shape model of Ceres from stereophotoclinometry using Dawn imaging data, *Icarus*, 319:812-827, 2019, DOI: 10.1016/j.icarus.2018.10.024.
- [4] C.D. Grimm, J.T. Grundmann, J., Hendrikse, C. Lange, C. Ziach, T. Ho, From idea to flight - A review of the Mobile Asteroid Surface Scout (MASCOT) development and a comparison to historical fast-paced space programs, *Progress in Aerospace Sciences*, 104:20-39, 2018, DOI: 10.1016/j.paerosci.2018.11.001.
- [5] B.V. Sarli, Y. Tsuda, Hayabusa 2 extension plan: Asteroid selection and trajectory design, *Acta Astronautica*, 138:225-232, 2017, DOI: 10.1016/j.actaastro.2017.05.016.
- [6] D.S. Lauretta, S.S. Balram-Knuston, E. Beshore et al., OSIRIS-REx: Sample return from asteroid (101955) Bennu, *Space Science Reviews*, 212:925-984, 2017, DOI: 10.1007/s11214-017-0405-1.
- [7] J.-L. Margot, M.C. Nolan, L.A.M. Benner, S.J. Ostro, R.F. Jurgens, J.D. Giorgini, M.A. Slade, D.B. Campbell, Binary asteroids in the near-Earth object population, *Science*, 296:1445-1448, 2002, DOI: 10.1126/science.1072094.
- [8] A.F. Cheng, A.S. Rivkin, P. Michel, J. Atchison, O. Barnouin, L. Benner, N.L. Chabot, C. Ernst, E.G. Fahnestock, M. Kueppers, P. Pravec, E. Rainey, D.C. Richardson, A.M. Stickle, C. Thomas, AIDA DART asteroid deflection test:

- Planetary defence and science objective, *Planetary and Space Science*, 157:104-115, 2018, DOI: 10.1016/j.pss.2018.02.015.
- [9] P. Michel, et al., European component of the AIDA mission to a binary asteroid: Characterization and interpretation of the impact of the DART mission, *Advances in Space Research*, 62:2261-2272, 2018, DOI: 10.1016/j.asr.2017.12.020.
- [10] J. Bellerose, D.J. Scheeres General dynamics in the restricted full three body problem, *Acta Astronautica*, 62:563-576, 2008, DOI: 10.1016/j.actaastro.2008.01.018.
- [11] P. Woo, A.K. Misra, M. Keshmiri On the planar motion in the full two-body problem with inertial symmetry, *Celestial Mechanics and Dynamical Astronomy*, 117:263-277, 2013, DOI: 10.1007/s10569-013-9512-9.
- [12] A. Capannolo, F. Ferrari, M. Lavagna, Families of bounded orbits near binary asteroid 65803 Didymos, *Journal of Guidance, Control, and Dynamics*, 42:189-198, 2019, DOI:10.2514/1.G003437.
- [13] Y. Shi, Y. Wang, S. Xu, Equilibrium points and associated periodic orbits in the gravity of binary asteroid systems: (66391) 1999 KW4 as an example, *Celestial Mechanics and Dynamical Astronomy*, 130:32, 2018, DOI: 10.1007/s10569-018-9827-7.
- [14] P. Pravec et al., Photometric survey of binary near-Earth asteroids *Icarus*, 181:63-93, 2006, DOI:10.1016/j.icarus.2005.10.014.
- [15] P. Michel, et al., Science case for the Asteroid Impact Mission (AIM): A component of the Asteroid Impact & Deflection Assessment (AIDA) mission, *Advances in Space Research*. Vol.57, 2016, pp. 2529-2547. DOI: 10.1016/j.asr.2016.03.031
- [16] V.G. Szebehely, *Theory of Orbits: The Restricted Problem of Three Bodies*, Academic Press, 1967.
- [17] A. McInnes, *An Introduction to Libration Point Orbits*, 2009.
- [18] R.W. Farquhar, *The control and use of libration-point satellites*, NASA technical report, 1970.
- [19] M. Henon, M., Numerical exploration of the restricted problem. I-V, *Astronomy and Astrophysics 1*, 1965-1970.

- [20] R.W. Farquhar, A.A. Kamel, Quasi-periodic orbits about the translunar libration point, *Celestial Mechanics*, 7:458-473, 1973, DOI: 10.1007/BF01227511.
- [21] J.V. Breakwell, J. V. Brown, The Halo family of 3-dimensional periodic orbits in the Earth-Moon restricted 3-body problem, *Celestial Mechanics*, 20:389-404, 1979, DOI: 10.1007/BF01230405.
- [22] K.C Howell, Three-dimensional, periodic, halo orbits, *Celestial Mechanics*, 32:53-71, 1984, DOI: 10.1007/BF01358403.
- [23] K.C Howell, J.V. Breakwell, Almost rectilinear halo orbits, *Celestial Mechanics* 32:29-52, 1984, DOI: 10.1007/BF01358402.
- [24] K.C. Howell, Families of orbits in the vicinity of the collinear libration points, *The Journal of the Astronautical Sciences*, 49:107-125, 1998, DOI: 10.2514/6.1998-4465.
- [25] D.C. Folta, T. Pavlak, A. Haapala, K.C. Howell, M. Woodward, Earth-Moon libration stationkeeping: theory, modeling and operations, *Acta Astronautica*, 94:421-433, 2014, DOI: 10.1016/j.actaastro.2013.01.022.
- [26] D.J. Grebow, M.T. Ozimek, K.C. Howell, D.C. Folta, Multi-body architecture for lunar south pole coverage, *Journal of Spacecraft and Rockets*, 45:344-358, 2008, DOI: 10.2514/1.28738.
- [27] R. Whitley, R. Martinez, Options for staging Orbits in cislunar space, *IEEE Aerospace Conference Proceedings*, IEEE Aerospace Conference, Big Sky, USA, March 5-12 2016, DOI:10.1109/AERO.2016.7500635.
- [28] D.C. Davis, K.C. Howell, Long term evolution of trajectories near the smaller primary in the restricted problem, *Advances in the Astronautical Sciences*, Vol. 136, AAS 10-184, 2010.
- [29] D.C Davis, K.C. Howell, Characterization of trajectories near the smaller primary in the restricted problem for applications, *Journal of Guidance, Control and Dynamics*, 35:116-129,2012, DOI: 10.2514/1.53871.
- [30] E.J. Doedel et al., Computation of periodic solutions of conservative systems with application to the 3-body problem, *International Journal of Bifurcation and Chaos*, 13:1353-1381, 2003, DOI:10.1142/S0218127403007291.

- [31] E.J. Doedel et al., Elemental periodic orbits associated with the libration points in the circular restricted 3-body problem, *International Journal of Bifurcation and Chaos*, 17:2625-2677, 2007, DOI: 10.1142/S0218127407018671.
- [32] D.J. Scheeres, *Orbital Motion in Strongly Perturbed Environments*, Springer-Praxis, 1<sup>st</sup> edition, 2012, DOI:10.1007/978-3-642-03256-1
- [33] R.S. Hudson, S.J. Ostro, Shape of asteroid 4760 Castalia (1989 PB) from inversion of radar images, *Science*, 263:940-943, 1994, DOI: 10.1126/science.263.5149.940
- [34] R.S. Hudson, S.L. Ostro, Shape and non-principal axis spin state of asteroid 4179 Toutatis, *Science*, 270:84-86, DOI:10.1126/science.270.5233.84
- [35] R.A. Werner, D.J. Scheeres, Exterior gravitation of a polyhedron derived and compared with harmonic and mascon gravitation representations of asteroid 4760 Castalia, *Celestial Mechanics and Dynamical Astronomy*, 65:313-344, 1996, DOI:10.1007/BF00053511
- [36] D.J. Scheeres et al. Dynamics of orbits close to asteroid 4179 Toutatis, *Icarus*, 132:53-79, 1998, DOI:10.1006/icar.1997.5870.
- [37] A.R. Dobrovolskis, Inertia of any polyhedron, *Icarus*, 124:698-704, 1996, DOI: 10.1006/icar.1996.0243.
- [38] Y. Wang, S. Xu. M. Zhu, Stability of relative equilibria of the full spacecraft dynamics around an asteroid with orbit-attitude coupling, *Advances in Space Research*, 53:1092-1107, 2014, DOI:10.1016/j.asr.2013.12.040
- [39] S. Kikuchi et al. Orbit-attitude coupled motion around small Bodies: Sun-synchronous orbits with Sun-tracking attitude motion, *Acta Astronautica*, 140:34-48, 2017, DOI: 10.1016/j.actaastro.2017.07.043.
- [40] F.C.F. Venditti, *Manobras Orbitais ao Redor de Corpos Irregulares*, Ph.D. Thesis, INPE-Brazil, 2013, <http://mtc-m16d.sid.inpe.br/col/sid.inpe.br/mtc-m19/2013/11.12.19.30/doc/publicacao.pdf>
- [41] F.C.F Venditti, E.M. Rocco, Modeling asteroids to assist in orbiting and landing missions, *Advances in the Astronautical Sciences*. Vol. 162, 2018, pp.2041-2060.

- [42] T.G.G. Chanut, S. Aljbaae, V. Carruba, Mascon gravitational model using a polyhedral source, *Monthly Notices of the Royal Astronomical Society*, 450:3742-3749, 2015, DOI: 10.1093/mnras/stv845
- [43] J. Bellerose, D.J. Scheeres, Stability of equilibrium points in the restricted full three body problem, *Acta Astronautica*, 60:141-152, 2007, DOI:10.1016/j.actaastro.2006.07.009.
- [44] D.J. Scheeres, Stability of the planar full 2-Body Problem, *Celestial Mechanics and Dynamical Astronomy*, 104:103-128, 2009, DOI: 10.1007/s10569-009-9184-7.
- [45] X. Hou, D.J. Scheeres, X. Xin, Mutual potential between two rigid bodies with arbitrary shapes and mass distribution, *Celestial Mechanics and Dynamical Astronomy*, 127:369-395, 2017, DOI:10.1007/s10569-016-9731-y.
- [46] Y. Shi, Y. Wang, S. Xu, Mutual gravitational potential force, and torque of a homogeneous polyhedron and an extended body: an application to binary asteroids, *Celestial Mechanics and Dynamical Astronomy*, 129:307-320, 2017, 10.1007/s10569-017-9776-6.
- [47] S.P. Naidu, J.-L. Margot, "Near-Earth asteroid satellite spins under spin-orbit coupling.", *The Astronomical Journal*. Vol.149, 2015, pp.80-91. DOI:10.1088/0004-6256/149/2/80
- [48] P. Woo, A.K. Misra, Bounded trajectories of a spacecraft near an equilibrium point of a binary asteroid system, *Acta Astronautica*, 110:313-323, 2015, DOI: 10.1016/j.actaastro.2014.11.001.
- [49] X. Li, D. Qiao, P. Li, Bounded trajectory design and self-adaptive maintenance control near non-synchronized binary systems comprised of small irregular bodies, *Acta Astronautica*, 152:768-781, 2018, DOI: 10.1016/j.actaastro.2018.09.028.
- [50] F. Ferrari, M. Lavagna, Periodic motion around libration points in the Elliptic Restricted Three-Body Problem, *Nonlinear Dynamics*. 93:453-462, 2018, DOI: 10.1007/s11071-018-4203-4.
- [51] C.R. McInnes, *Solar Sailing, Technology, Dynamics and Mission Application* (2<sup>nd</sup> edition), Springer-Praxis, Germany, 2004, ISBN 978-1-85233-102-3.
- [52] A. Farrés, D. Folta, C. Webster, Using spherical harmonics to model solar radiation pressure accelerations, *Advances in the Astronautical Sciences*, 162:3365-3383, 2018.

- [53] Misra, G., Izadi, M., Sanyal, A., Scheeres, D.J., Coupled orbit-attitude dynamics and relative state estimation of spacecraft near small solar system bodies, *Advances in Space Research*, 57:pp.1747-1761, 2016, DOI: 10.1016/j.asr.2015.05.023.
- [54] X. Xin, D.J. Scheeres, X. Hou, Forced periodic motions by solar radiation pressure around uniformly rotating asteroids, *Celestial Mechanics and Dynamical Astronomy*, 126:405-432, 2016, DOI: 10.1007/s10569-016-9701-4.
- [55] M. Giancotti, S. Campagnola, Y. Tsuda, J. Kawaguchi, Families of periodic orbits in Hills problem with solar radiation pressure: application to Hayabusa 2, *Celestial Mechanics and Dynamical Astronomy*, 120:269-286, 2014, DOI: 10.1007/s10569-014-9564-5.
- [56] E. Morrow, D.J. Scheeres, D. Lubin, Solar Sail Operations at Asteroids, *Journal of Spacecraft and Rockets*, 38:279-286, 2001 DOI: 10.2514/2.3682.
- [57] J. Heiligers, D.J. Scheeres, Solar sail orbital motion about asteroids and binary asteroid systems, *Journal of Guidance, Control, and Dynamics*, 41:1947-1962, 2018, DOI:10.2514/1.G003235.
- [58] D. García Yárnoz, D.J. Scheeres, C.R. and McInnes, On the a and g families of orbits in the Hill problem with solar radiation pressure and their application to asteroid orbiters, *Celestial Mechanics and Dynamical Astronomy*, 12:365-38, 2015. DOI: 10.1007/s10569-015-9604-9.
- [59] L. Dell'Elce, N. Baresi, S.P. Naidu, L.A.M. Benner, D.J. Scheeres, Numerical investigation of the dynamical environment of 65803 Didymos, *Advances in Space Research*, 59:1304-1320, 2017, DOI: 10.1016/j.asr.2016.12.018.
- [60] J. Heiligers, M. Ceriotti, Orbital dynamics of an oscillating sail in the Earth-Moon system, *Fourth International Symposium on Solar Sailing*, Kyoto, Japan, 2017
- [61] J. Heiligers, M. Macdonald, J.S. Parker, Extension of Earth-Moon libration point orbits with solar sail propulsion, *Astrophysics and Space Sciences*, 361:241, 2016. DOI: 10.1007/s10509-016-2783-3.
- [62] [https://en.wikiversity.org/wiki/Advanced\\_Classical\\_Mechanics/Rigid\\_Bodies#Moment\\_of\\_Inertia](https://en.wikiversity.org/wiki/Advanced_Classical_Mechanics/Rigid_Bodies#Moment_of_Inertia)

- [63] S. Naidu et al, Observations and characterization of binary near-Earth asteroid 65803 Didymos, the target of the AIDA mission, *American Geophysical Union, Fall General Assembly 2016*. abstract id.P52B-02, December 2016.<http://adsabs.harvard.edu/abs/2016AGUFM.P52B..02N>
- [64] C. Lange, J. Biele, S. Ulamec, C. Krause, B. Cozzoni, O. Küchemann, S. Tardivel, T. Ho, C. Grimm, J.T. Grundmann, E. Wejmo, S. Schröder, M. Lange, J. Reill, A. Hérique, Y. Rogez, D. Plettemeier, I. Carnelli, A. Galvez, C. Philippe, M. Küppers, B. Grieger, J.G. Fernandez, J. Grygorczuk, M. Tokarz, C. Ziach, MASCOT2- A small body lander to investigate the interior of 65803 Didymos' moon in the frame of the AIDA/AIM mission, *Acta Astronautica*, 149:25-34, 2018. DOI: 10.1016/j.actaastro.2018.05.013.